5-1-2010

Travertine from Egypt's Western Desert: a terrestrial record of North African paleohydrology and paleoclimate during the late Pleistocene

Gloria Jimenez

Gloria Jimenez
Candidate

Earth and Planetary Sciences
Department

This thesis is approved, and it is acceptable in quality and form for publication:

Approved by the Thesis Committee:

Dr. Laura Crossey, Chairperson

Dr. Karl Karlstrom

Dr. Yemane Asmerom

Dr. Peter Fawcett

TRAVERTINE FROM EGYPT'S WESTERN DESERT: A TERRESTRIAL RECORD OF NORTH AFRICAN PALEOHYDROLOGY AND PALEOCLIMATE DURING THE LATE PLEISTOCENE

BY

GLORIA JIMENEZ

B.A., Geology, Carleton College, 2007

M.S., Earth and Planetary Sciences, University of New Mexico, 2014

THESIS

Submitted in Partial Fulfillment of the
Requirements for the Degree of

Master of Science
Earth and Planetary Sciences

The University of New Mexico
Albuquerque, New Mexico

May, 2014

ACKNOWLEDGMENTS

I thank my advisor and committee chair, Dr. Laura Crossey, for her encouragement and unflagging positivity from the moment we "met" over email. Her patient advice and compassion have been invaluable to me as I navigated the sometimes unexpectedly turbulent waters of my M.S., and her excitement about the natural world and genuine interest in mentoring has been an inspiration. I also thank my committee members: Dr. Karl Karlstrom provided numerous insights into structural geology and tectonics, passed on the unforgettable pi rule, and maintained good humor while providing comments on endless thesis drafts. Dr. Yemane Asmerom challenged me to do nothing less than my best in any endeavor—while steadfastly insisting that my best was sky-high. Dr. Peter Fawcett, in one of the best graduate courses I have taken, introduced me to major questions in paleoclimatology, many of which underpin this manuscript.

I owe thanks to numerous people for making my M.S. work possible: Drs. Crossey and Karlstrom gave me the opportunity to go to Egypt. Along with April Tafoya, Jason Ricketts, Abdel Mohammed, and Tarek Anan, they guided me in fieldwork, and Khaled Ahmed and Gabriela Lory of Desert Arrow provided safe transport and guiding. Dr. Victor Polyak provided hours of assistance with U/Th and $^{87}Sr/^{86}Sr$ methods and mass spectrometer runs, as well as general wisdom. Zach LaPointe and Ryan Crow also assisted me in the radiogenic isotope laboratory. Dr. Viorel Atudorei guided me in stable isotopic analyses, with laboratory help from Rebecca Wacker.

Finally, I appreciate the help of many others. Dr. Gary Weissmann gave hydrology assistance in the early stages of this project; Dr. Jay Quade at the University of Arizona consulted on U/Th isochrons; the members of the Urbino Summer School in Paleoclimatology (2013) lent nuance to my understanding of paleoclimate; many graduate students at UNM and UA offered help and advice over the last two and a half years. Cindy Jaramillo and the EPS office staff greatly facilitated my M.S. work. Finally, I would not have gotten far without the support of friends and family: special thanks to Violeta Jimenez, Robert Voloshin, Scott Jasechko, and Shelley Leiphart. This work is supported by NSF grant #1004276 from International Programs and Hydrologic Sciences to Drs. Crossey and Karlstrom, and I gratefully acknowledge the support of UNM's EEE Black Fellowship, and a NSF Graduate Research Fellowship.

TRAVERTINE FROM EGYPT'S WESTERN DESERT: A TERRESTRIAL RECORD OF NORTH AFRICAN PALEOHYDROLOGY AND PALEOCLIMATE DURING THE LATE PLEISTOCENE

by

Gloria Jimenez

Coauthors to include:

Crossey, L.J., Karlstrom, K.E., Polyak, V. and Asmerom, Y.

B.A., Geology, Carleton College, 2007

M.S., Earth and Planetary Sciences, University of New Mexico, 2014

ABSTRACT

The "Green Sahara" pluvial phases that alternated with North African hyper-aridity during the Pleistocene are well recognized in tropical and Mediterranean marine records. However, comparatively few studies have investigated the terrestrial expression of these pluvials, in part because of the paucity of paleohydrologic archives in the desert. In this study, we show that the travertine record of Egypt's Western Desert constitutes a promising terrestrial proxy for North African paleohydrology. Integrating our reconnaissance sampling of travertine and modern groundwaters from five important oasis areas with data from previously published studies, we combine high-precision U/Th dating, geologic characterization, and stable isotope and $^{87}Sr/^{86}Sr$ geochemistry to contribute to a record of Egyptian pluvial periods for the last ~650 ka. We show that changing hydrologic head controlled voluminous travertine deposition and dictated its landscape position, and that major depositional episodes were largely synchronous across the Western Desert, suggesting a regional signal. We confirm previous findings that large volume deposition occurred across oasis areas at ~125 ka, as well as constraining major deposition from ~450-600 ka. We also show that at least some lacustrine deposits at Dahkla Oasis associated with paleolithic artifacts are 300-350 ka rather than ~130 ka. A comparison of travertine geochemistry with modern groundwater chemistry suggests that a consistent Nubian groundwater source has fed travertine deposition over the last half million years. Dakhla Oasis has an enriched $^{87}Sr/^{86}Sr$ signature in both modern groundwater (0.7170-0.7211) and travertine (~0.7098), reflecting water circulation through radiogenic basement rocks; higher $^{87}Sr/^{86}Sr$ in modern waters is interpreted to be due to deeper tapping of modern pumped waters relative to past artesian conditions. Travertine stable isotopic signatures from Dahkla also differ from the other oases and are interpreted to reflect its lacustrine rather than spring-mound depositional environment. These observations lead to a depositional model in which travertine accumulations around paleo-oasis springs reflect episodes of enhanced spring discharge deriving from high hydrologic head in the Nubian aquifer system. Increased head in the artesian system, in turn, is interpreted as a response to greater precipitation in southern groundwater recharge areas. Importantly, discharge from these travertine-depositing springs includes significant upward flux of deeply-derived carbonic fluids through faults in paleo-oasis areas. Thus, in this model, large-scale travertine accumulations serve as an archive of wet intervals in the Ethiopian-Sudan recharge region, which are then expressed in oasis springs following the short (<10 ka) lapse time it takes for transmission of high head pressure from the highlands to the oasis springs. This idea is supported by the fact that peak times of large volume travertine deposition are associated, roughly, with sapropels, indicating response to major regional pluvial episodes. However, our data do not show a coherent correlation to glacial cycles, suggesting that previous emphasis on travertine's association with glacial forcings should be scrutinized. In summary, our study reveals that travertine deposition in broadly synchronous regional episodes across the Western Desert is consistent with the pluvial events recognized in marine records. Subject to further testing, we interpret large volume travertine deposition in Egypt's Western Desert to be a pluvial indicator ultimately responding to orbital forcing.

TABLE OF CONTENTS

LIST OF FIGURES

LIST OF TABLES

INTRODUCTION

The "Green Sahara" pluvial (rainy) phases that overprinted North African aridity during the Pleistocene are well recognized in tropical and Mediterranean marine records (Larrasoaña et al., 2003; deMenocal, 2004; Tzedakis, 2007; Trauth et al., 2009). These high insolation/high monsoon intervals have been linked to minima in the orbital precession index (Lourens et al., 2001; Larrasoaña et al., 2003; Trauth et al., 2009), and indeed there is evidence that precessional forcing of North African climate has been pervasive for at least the last 12 Ma (deMenocal, 2004). Thus, most authors consider the primary control on the region's hydrological cycle to be insolation-driven change in the strength of the ITCZ (Intertropical Convergence Zone) and therefore the intensity and northward extent of the African boreal summer monsoon (Rossignol-Strick, 1985; Tuenter et al., 2003; Rohling et al., 2002; Trauth et al., 2009; Blome et al., 2012).

Recent work emphasizing the heterogeneity of Pleistocene climate in North Africa suggests, though, that terrestrial climate may be out of phase with marine records, particularly showing little response to MIS (Marine Isotope Stage) boundaries or North Atlantic SSTs (sea surface temperatures) (Blome et al., 2012). Thus, key questions about the nature of Green Sahara pluvials have remained unanswered: what was the spatial extent of monsoonal rains across North Africa, and particularly, how far north did they penetrate? What moisture sources fed monsoonal rains, and were these consistent across North Africa? Marine records integrating a large regional signal have not been able to address these questions, while terrestrial records offer tantalizing evidence for the effects of past wet periods on local paleohydrology. For example, buried drainage channels in Egypt imply large amounts of water at the surface over the Tertiary and possibly later in the Quaternary (McCauley et al., 1982), while paleo-lacustrine deposits from Egypt's Dakhla Oasis have been calculated to require at least some direct precipitation (Kieniewicz and Smith, 2009).

Despite the potential of terrestrial studies to improve our understanding of Green Sahara episodes, comparatively fewer terrestrial records have been established, and thus the expression of pluvials across the North African land surface remains enigmatic. The Western Desert of Egypt is an ideal area in which to examine the terrestrial record of pluvial episodes (see Fig. 1a). A relatively large number of workers have investigated paleohydrology in the Western Desert, in large part because of abundant evidence of hominid use during past pluvial periods (Caton-Thompson and Gardner, 1932; Smith et al., 2004b; Smith et al., 2004a; Kleindienst et al., 2008). These studies show abundant evidence for profoundly altered hydroclimate over the late Pleistocene, through proxies including travertine (Crombie et al., 1997; Smith et al., 2004a; Smith et al., 2007),

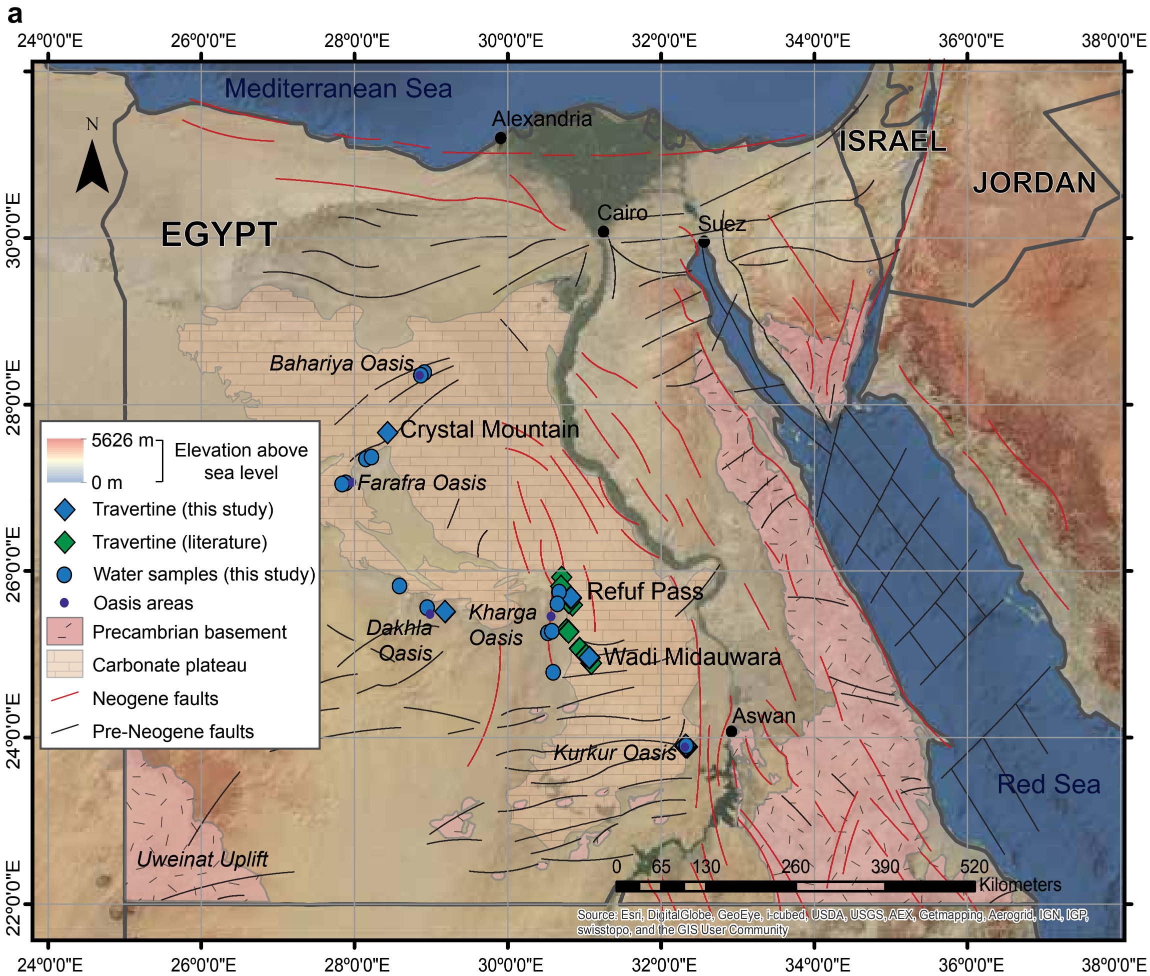

Figure 1. Geographic and geologic setting of oasis areas in Egypt's Western Desert. a) Index map of travertine and water samples from Egypt's Western Desert. Data from this study is colored blue; travertine samples are diamonds and water samples are circles. U/Th dated travertine samples from previous studies are shown in green (see Appendix 1). Purple dots indicate modern oasis areas; with the exception of Kurkur Oasis, no paleo-oasis area (where travertine samples were taken) currently has artesian flow, so water samples could not be taken from these areas themselves. Faults with Neogene or younger offset (shown in red) are commonly associated with areas of travertine deposition. b) Generalized geologic map of Egypt (after Said, 1990); symbology follows a). Note position of oasis areas at the margins of carbonate units.

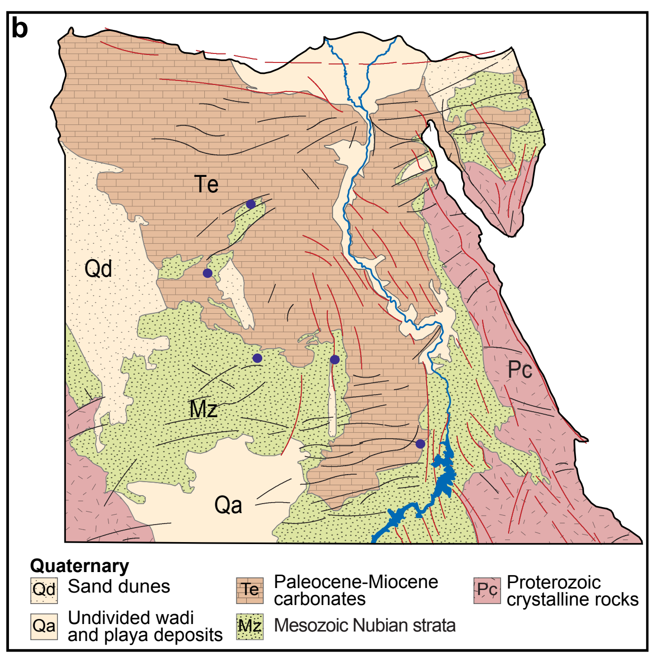

groundwaters (Sultan et al., 1997), speleothems (Dabous and Osmond, 2000; Brook et al., 2002; Railsback et al., 2002; Holzkamper, 2004), and secondary ore precipitates (Osmond and Dabous, 2004).

To date, however, terrestrial evidence for Western Desert pluvial timing and drivers has been equivocal or contradicted the conclusions of marine studies. While studies have shown evidence for increased moisture between ~80 and 300 ka, there is little agreement on the precise timing of wet periods, with the exception of a well-documented episode from ~115-135 ka (MIS6/5e; e.g. Crombie et al., 1997; Smith et al., 2004a; Smith et al., 2007). Second, many authors posit a correlation between observed wet times and interglacials (e.g. Szabo et al., 1995; Smith et al., 2004b; Smith et al., 2007), and some explicitly suggest the operation of glacial forcings (e.g. Crombie et al., 1997; Kieniewicz and Smith, 2009), in contrast to the consensus of orbital cycle/tropical insolation control on moisture in the marine proxy-based paleoclimate literature.

The moisture sources of pluvial episodes in the Western Desert also remain a topic of debate. Several Western Desert studies have used the carbon and oxygen stable isotopic signatures of travertine to infer the moisture sources that fed travertine-depositing springs, but have reached distinct conclusions. Many authors suggest that isotopic depletion in travertine $\delta^{18}O$ (approximately -8 to -14 ‰ relative to VPDB) indicates a distant Atlantic precipitation source, which (e.g., Crombie et al., 1997; Sultan et al., 1997); Sultan et al. (1997) specifically suggested that westerly winds might have propelled Atlantic precipitation towards Egypt, subjecting it to extensive fractionation as it crossed the continent. In contrast, Kieniewicz and Smith (2007) argued that an isotopically heavy source water such as the Indian monsoon was necessary to produce the depleted $\delta^{18}O$ values they observed in carbonate silts at Kharga Oasis (again, -12 to -8 ‰). Smith et al. (2004b) also invoked the influence of the Indian monsoon, suggesting that the Western Desert could represent a mixing zone between Indian monsoon precipitation and westerly-derived moisture (after Sultan et al., 1997).

In general, these studies of travertine suggest that pluvial episodes increased local precipitation to oasis areas, thus enhancing spring flow; that is, that “greening” of the Western Desert resulted from direct recharge of shallow aquifers (Crombie et al., 1997; Kleindienst et al., 1999; Kieniewicz and Smith, 2009). Some specifically dismiss the possibility of a deep groundwater (Nubian aquifer) component feeding springs in oasis areas (e.g., Kieniewicz and Smith, 2009). However, given that travertine in arid regions often has a significant groundwater component (see following section), the relative importance of local precipitation over Western Desert oases versus enhanced spring flow from the Nubian aquifer system (fed by distant precipitation in recharge regions) needs further examination.

In this study, we use a comprehensive analysis of the travertine depositional record from Egypt's Western Desert to address persistent uncertainties regarding the terrestrial expression of pluvial episodes:

1) Does the timing of wet periods in the Western Desert align with large-scale pluvial episodes established by marine records, and can we therefore assume that these wet periods had the same climatic drivers?

2) Did Western Desert moisture during past wet periods derive from local precipitation or distant groundwater recharge? Where did the precipitation come from (the Atlantic or Indian monsoons, paleowesterly winds, etc.)?

3) Do Western Desert travertines record incision of the landscape or changing hydrologic head?

We test the idea that travertine deposition depended not on local recharge to shallow aquifers, but remote recharge to deeper portions of the Nubian aquifer. That is, we propose that Western Desert travertine deposits when precipitation falls in remote southern groundwater recharge areas, increasing head throughout the confined Nubian aquifer. This increases groundwater flow up fault conduits, causing discharge and travertine accumulation at paleo-oasis springs over the duration of the pluvial episode (Fig. 2).

An important contribution of this paper is 25 new, high-precision, geologically well-constrained U/Th ages on travertine, and our results also highlight the importance of a stratigraphically-based sampling scheme that ensures an age represents a significant episode of deposition correlating to a pluvial. We synthesize our data with previously published U/Th ages on Western Desert travertines, and combine this geochronology with stable isotope and $^{87}Sr/^{86}Sr$ geochemistry, and modern Nubian groundwater hydrochemistry, in order to investigate the terrestrial expression of Green Sahara pluvial events in North Africa. This record constitutes a promising terrestrial proxy for North African pluvial periods for the last ~650 ka.

Travertine as a paleohydrologic indicator

Travertine, defined inclusively after Pentecost (2005), encompasses a wide range of chemically-precipitated carbonates while avoiding genetic or morphological implications. These groundwater discharge deposits form when CO_2-rich groundwaters acquire solutes by dissolving limestone bedrock, then upon reaching the surface, degas and precipitate $CaCO_3$ (Crossey et al., 2011). Thus, travertine precipitation requires inputs of both CO_2 and water. The CO_2 in travertine-depositing systems is derived from vegetation, soil, and/or carbonate rocks, and often has a significant tectonic or "endogenic" CO_2 component, sourced via faults or other structural features that act as conduits for deep groundwater (Zhang et al., 2008; Crossey et al., 2009; Crossey et al., 2011). Travertine occurrence is also generally water-limited, such that high volumes form during times of high hydrologic head, or humid conditions in the recharge area (Crombie et al., 1997; Auler and Smart, 2001; Darling et al., 2005).

Travertine's utility as a record of pluvials is based, first, on its potential to impose a useful temporal constraint. With modern techniques, these carbonates can be well-resolved through U/Th dating to ~650 ka, and less precisely to over 2 Ma, using $d^{234}U$ model ages (e.g. Neymark, 2011). Travertine should also reflect pluvial timing fairly well, as travertine deposits represent times of high groundwater flow at a given site, which presumably reflects enhanced recharge to the aquifer. Thus, a date on travertine reflects a time of high inputs somewhere in the aquifer system, with some lag between recharge and increased head, depending on the geographic separation between a site and recharge area (Fig. 2). Secondly, travertine deposition can, to a first-order estimate, imply pluvial magnitude. Large volumes of travertine deposition reflect large amounts of water at a site, and therefore significant aquifer recharge. Finally, travertines also record the geochemical signature of the water they precipitated from and so can provide information about source water, precipitation temperature, and groundwater flow paths via stable carbon and oxygen isotopes and $^{87}Sr/^{86}Sr$ (cf., respectively, Talbot, 1990; Andrews, 2006; and Li et al., 2008b; Carucci et al., 2012).

Geologic setting of Western Desert oases

There are several major oasis areas in the Western Desert that hosted large-scale travertine deposition in the past: Farafra, Dakhla, Kharga, and Kurkur (Fig. 1a), though no active deposition occurs now. A Paleocene to Eocene-age limestone plateau surrounds shale-floored depressions that host the oases, and travertine deposits are located along the edges of the plateau at breaches in the confining shale layers (Hermina, 1990; Luo et al., 1997). Modeling studies suggests that the depressions that host the larger paleo-oases were formed by a combination of groundwater sapping and fluvial erosion (Luo et al., 1997).

Egypt's Western Desert is underlain by the Dakhla Basin of the Nubian aquifer, a 2 million km^2 system which is hosted in Cretaceous sandstone units that vary from 1000 m thick in southern Egypt to over 2500 m thick near Farafra Oasis (Fig. 1b, Fig. 2; Hesse

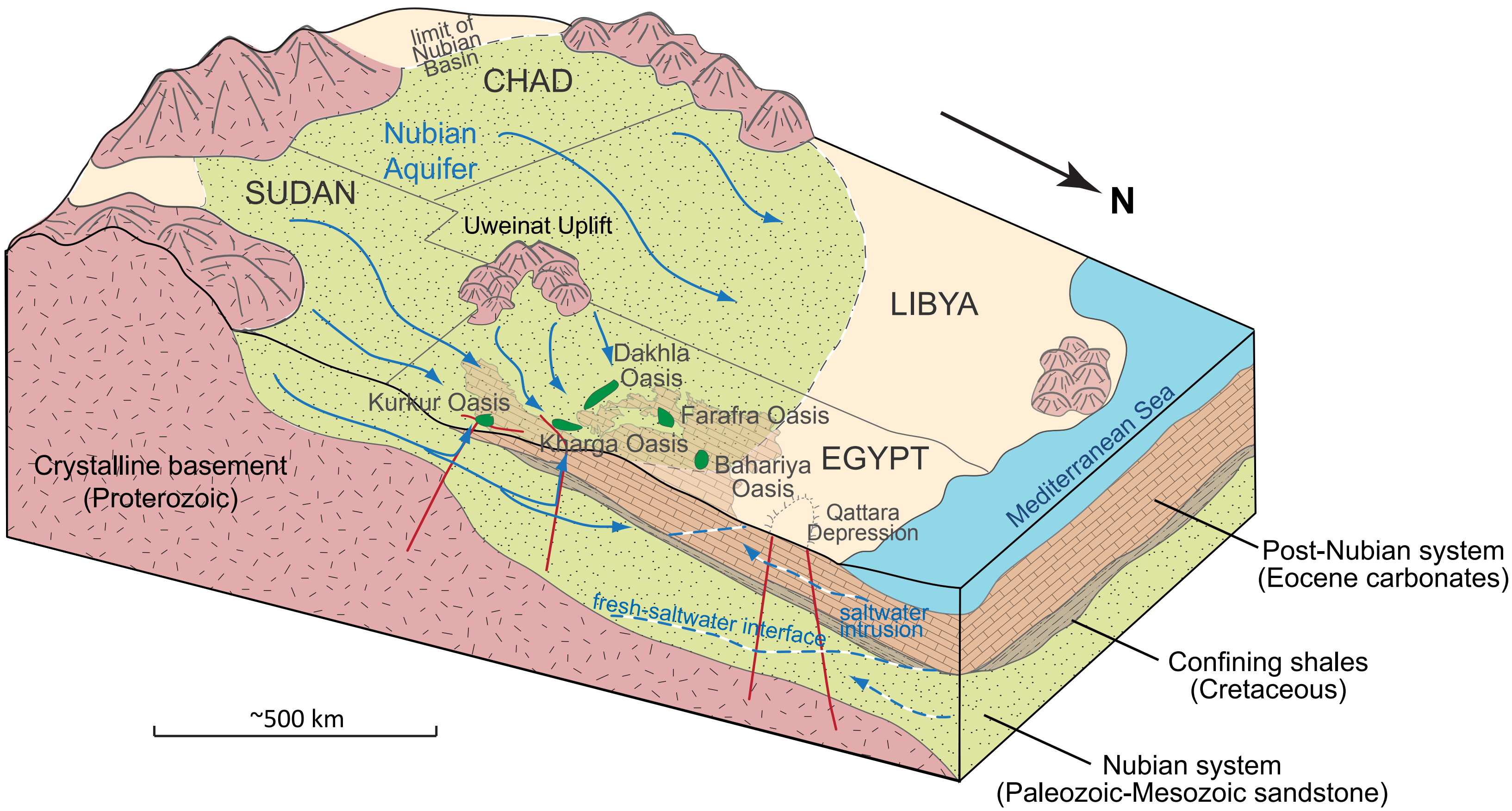

Figure 2. Simplified box model of the hydrological setting of Western Desert oasis areas in Egypt (modified from Salem and Pallas, 2004; geological information from Hesse et al., 1987; Hermina, 1990; Luo et al., 1997; Patterson et al., 2005). At the surface, the Nubian Aquifer is shown in green, the carbonate plateau in orange, and oasis areas in dark green. In cross-section, major aquifer and confining units are indicated; blue arrows show subsurface flow from southern recharge areas, and dashed blue arrows show saltwater intrusion from the Mediterranean Sea to the north. Faults, inferred to serve as conduits allowing subsurface flow to discharge at oasis areas, are shown schematically in red.

et al., 1987). The Nubian Aquifer rests on Proterozoic granite basement and is covered by Paleocene shale and Eocene limestones above (Thorweihe, 1990). Modern and paleo-oasis areas are formed where confining shales have eroded to allow artesian discharge (Salem and Pallas, 2004). Travertine in these areas generally forms where artesian springs emerge, creating mounds and large platforms (Caton-Thompson and Gardner, 1932).

The Western Desert is currently hyper-arid, receiving 5-20 mm of rainfall annually (Patterson et al., 2005); past pluvial episodes caused surface recharge to the Nubian Aquifer, primarily in uplifted areas such as the crystalline Gebel Uweinat complex in the southwest and the Bir Safsaf and Aswan complexes in the southeast (Hesse et al., 1987). In general, deep groundwaters of the Nubian aquifer show flowpaths moving in a northwest direction from these southern recharge areas, with groundwater velocities of 0.5-3.5 m/yr and residence times up to 1.3 Ma (Sturchio, 2004; Patterson et al., 2005).

METHODS

Field sampling and stratigraphic designations

We identified sites in the Western Desert with large-volume travertine deposits based on the results of previous studies: Crystal Mountain (Holzkamper, 2004), Dakhla Oasis (Kleindienst et al., 1999; Kieniewicz and Smith, 2009), Refuf Pass (Caton-Thompson and Gardner, 1932; Smith et al., 2004b; Kieniewicz and Smith, 2007; Kleindienst et al., 2008) and Wadi Midauwara (Smith et al., 2007; both in Kharga Oasis and hereafter referred to by their specific site names only), and Kurkur Oasis (Crombie et al., 1997). Using aerial photography, we divided these deposits into large, aggregate "levels" that approximated depositional periods, based on consistent elevation and appearance. In the field, we used these photographs to help us identify travertine accumulations that represented significant (representing a large-scale pluvial episode) and continuous travertine deposition.

Using a laser range finder, we determined the relative elevation of each level above modern base level so as to correlate deposition at a given relative elevation for spatially-separated travertine accumulations. We took samples from the bottom and top of each level to estimate the duration of deposition, as well as additional samples from features of interest such as dissolution caves or vein deposits, and determined the location of each sample with a handheld GPS device. We gave each sample a stratigraphic context designation that reflected its relative landscape elevation, as well as whether it represented the chronological onset or end of a depositional episode.

Artesian springs no longer exist at most of the paleo-oasis areas we studied, with the exception of a low-volume seep at Kurkur Oasis. We sampled modern groundwaters from pumped and artesian wells at nearby modern oasis areas, determining their GPS locations as above. We collected two samples at each site; one, with no head space, was analyzed for stable isotopes. A second, which was filtered to 0.45 microns and acidified with HNO_3, was used for $^{87}Sr/^{86}Sr$ analysis. Water samples were refrigerated and analyzed at the University of New Mexico.

Geochronology and geochemistry

All samples were analyzed for $\delta^{13}C$ and $\delta^{18}O$, and a subset was selected for U/Th dating based on the chronological control they represented, as well as their suitability for dating; all dated samples were also analyzed for $^{87}Sr/^{86}Sr$. For all analyses, field samples were cut into slabs, and sample layers were drilled based on characteristics that were likely to yield good U/Th dates: continuity, cohesiveness, lack of inclusions, and white, yellow, or gray color (see Placzek et al., 2006).

U/Th analysis was performed at the University of New Mexico's Radiogenic Isotope Laboratory. Analytical procedures follow Asmerom et al. (2010): for each sample, ~100 mg of drilled powder was spiked with a mixed $^{229}Th/^{233}U/^{236}U$ solution and progressively dissolved in 15N HNO_3 and $HClO_4$ to attack all sample components. U and Th were purified from the sample solutions using anion exchange columns. Samples were analyzed on a Finnigan Neptune multicollector ICP-MS with 10^{11} and 10^{12} Ω resistors connected to seven Faraday cups and a secondary electron multiplier. Since most samples had low initial Th contamination, with $^{230}Th/^{232}Th$ activity > 20 (see Table 1 and Bischoff and Fitzpatrick, 1991), a simple correction of $4.4*10^{-6} \pm 50\%$ was made to correct for initial ^{230}Th.

Given current analytical techniques and very precise half-life measurements, the current upper limit of the U/Th technique exceeds 600 ka (Cheng et al., 2000; Edwards et al., 2003; Andersen et al., 2008). For those samples that were undatable because their age exceeded this approximate limit (that is, which gave ages indistinguishable from infinity), we calculated a $\delta^{234}U$ model age. Estimating an initial value for $\delta^{234}U_{initial}$ via successful samples from the same site, we solved for t using the $\delta^{234}U$ age equation (cf. Neymark, 2011):

$$\delta^{234}U_{measured} = (\delta^{234}U_{initial})*e^{-\lambda 234*t}$$

Analysis of $^{87}Sr/^{86}Sr$ of travertines was done at the University of New Mexico's Radiogenic Isotope Laboratory, using either powders for U/Th analysis, or powders drilled from an adjacent spot in the same layer. ~25 mg of each sample powder was dissolved in 15N HNO_3 and spiked with 1g of NBS 987 spike, then Sr was purified on anion exchange columns. For water samples, 15-25 mL of water was spiked, dried down, then redissolved in 0.5 mL 3N HNO_3 (because of the high Sr concentration at the Kurkur Oasis seep, only 5 mL was used); thereafter the water samples followed the same method as travertine samples. All samples were analyzed on the same system as for U/Th.

~1 mg of powder drilled for U/Th or $^{87}Sr/^{86}Sr$ analysis was used to determine stable isotopic signatures for travertine samples, and 1 mL was used analyzed for each water sample. Samples were placed in borosilicate vials, flushed with He gas, and reacted with H_3PO_4 for 24 hours at 25ºC to evolve CO_2 gas. CO_2 isotope ratios were measured by continuous flow isotope ratio mass spectrometry using an automated CombiPal-Gas Bench system coupled to a Thermo Finnigan Delta Plus mass spectrometer in the Stable Isotope Laboratory at the University of New Mexico. Results were corrected against laboratory standards and are reported in standard delta notation, with travertines versus VPDB and waters versus VSMOW. Reproducibility of laboratory standards exceeded 0.1‰. $\delta^{13}C$ information is unavailable for Kurkur Oasis given the small volume of water collected.

Synthesis of literature geochronology and stable isotope geochemistry

We compiled a database of previously published U/Th dates from the Western Desert for analysis of pluvial episode timing. We selected ages based on four characteristics:

1) Geographic location in Egypt's Western Desert. In order to minimize uncertainties caused by the geographical separation of sites (which could be significant, for example, if paleowesterly winds were responsible for at least some of the moisture feeding travertine precipitation—e.g. Sultan et al., 1997), we excluded studies from other locations.

2) Consistency in depositional process. While proxies such as speleothems (Brook et al., 2002; Dabous et al., 2002; Holzkamper, 2004) and secondary uranium mobilization (Osmond et al., 1999; Osmond and Dabous, 2004) certainly reflect locally wet conditions, it is difficult to evaluate whether they respond to the same major, groundwater-based forcings as we presume that travertine does. We therefore discuss these separately.

3) Individual samples' stratigraphic context. Again, since our model focuses on large-scale pluvial episodes rather than small or local precipitation episodes, we attempted to select only samples reflective of large-scale deposition (cf. Smith, 2012). Unfortunately, this information was unclear from many

studies; we excluded samples whose depositional context likely reflected only minor wet episodes (such as reprecipitated rinds), but otherwise erred on the side of inclusivity, assuming that the majority of samples would fall within a pluvial episode.

4) Precision and reliability of U/Th dates. In order to make useful paleoclimatic correlations, a reasonable amount of precision is required. U/Th dates from older studies were often generated with alpha counting and had large errors. We thus removed dates that had errors over 20% of the stated age.

Application of these criteria resulted in a database solely consisting of travertine samples (64 in total, including 39 samples from previous studies; see Appendix 1). We stress that, while samples from studies we did not include may provide useful points of comparison, we were aiming to compile a group of samples which was internally consistent with respect to depositional mechanism, stratigraphy, and location (and hence likely paleoclimate forcing).

We restricted our comparison of geochemical data to other analyses of carbonates, given the complexities inherent in comparing the geochemistry of different proxy systems. This yielded a stable isotope database consisting of 157 samples (travertine and lacustrine carbonate silts, including 100 literature samples; see Appendix 2). To our knowledge, no previous studies have reported $^{87}Sr/^{86}Sr$ on Western Desert carbonates, so we report solely data from this study (34 samples).

RESULTS

We collected 57 travertine samples from Egypt's Western Desert. In Table 1, we report 25 new U/Th ages and 8 $\delta^{234}U$ model ages, showing U/Th geochronology for each sample, as well as location, facies, and stratigraphic context. We show stable isotope analyses for all 57 samples, and $^{87}Sr/^{86}Sr$ analyses for 34 samples, in Table 2. We report the same geochemical data for 8 modern water samples in Table 3. The geochronology and geochemistry data from previously published studies that we used in our analyses is compiled in Appendices 1 and 2.

Travertine facies and geochronology

The environments represented by each paleo-oasis area vary greatly. Figure 3 shows representative photographs of Western Desert travertine facies: dissolution caves with "groundwater speleothems," lacustrine deposits, drapes from a perched springline setting, paludal developments characterized by phytohermal textures and stick casts,

Table 1
Geochronology and stratigraphic context of travertine samples from the study

Sample ID	Latitude	Longitude	Elevation (m ABSL)	Sample facies	Stratigraphic level*	Corrected U/Th age	+/- error	Uncorrected U/Th age	+/- error	238U (ppb)	+/- error	232Th (ppt)	+/- error	230/232	+/- error	230/238	+/- error	$d^{234}U_m$	+/- error	$d^{234}U_i$	+/- error
Crystal Mountain																					
K11E-CRYS-4	27.66112	28.43120	239	flowstone--outer bands	E2	523339	29793	525587	30401	608.54	0.25	61393.19	40.96	33.12	0.07	1.0933	0.0022	72.77	1.07	320.61	29.10
K11E-CRYS-4B	*27.66112*	*28.43120*	*239*	*flowstone--inner bands*	*B2*	*1396978*	*181479*	---	---	*1883.62*	*1.15*	*61247.78*	*47.54*	*95.24*	*0.20*	*1.0133*	*0.0021*	*7.16*	*1.01*	---	---
K11E-CRYS-7A	*27.66053*	*28.43194*	*238*	*micrite*	*B3*	*1013991*	*119370*	---	---	*83.90*	*0.05*	*13784.58*	*59.85*	*19.41*	*0.09*	*1.0437*	*0.0023*	*19.20*	*1.02*	---	---
Dakhla Oasis																					
K12E-DAK-17	25.51423	29.17847	147	micrite	E1	349012	6053	351716	6038	841.49	0.32	98617.27	236.22	28.51	0.09	1.0932	0.0024	103.04	1.10	277.95	5.63
K12E-DAK-18B	25.50798	29.18239	136	micrite	B1	292297	4751	299476	3344	609.27	0.24	208507.18	1264.33	10.42	0.07	1.1670	0.0024	188.13	1.19	437.95	4.99
Kharga Oasis: Refuf Pass																					
K12E-KHAR-31	25.67835	30.82167	270	micrite drape	E1	449554	10520	449741	10537	479.60	0.22	3884.13	47.80	409.63	5.06	1.0855	0.0012	74.68	1.07	265.65	8.88
K12E-KHAR-30	25.67781	30.82120	264	stick casts	B1	600220	63819	600573	64053	709.62	0.29	11894.34	30.61	199.63	0.65	1.0949	0.0022	70.06	1.07	381.40	75.77
K12E-KHAR-21	25.67981	30.81280	251	stick cast	E2	128545	552	128759	542	1276.95	0.52	13470.12	21.80	270.71	0.70	0.9344	0.0019	299.20	1.30	430.27	1.98
K12E-KHAR-20	25.67980	30.81276	250	stick cast	B2	123996	583	124945	343	1081.19	0.38	49850.32	41.81	60.73	0.08	0.9162	0.0010	295.97	1.30	421.07	1.89
K12E-KHAR-32	25.67891	30.82203	277	porous micrite	E2	130652	741	131626	565	1652.86	0.76	79280.56	46.88	60.52	0.13	0.9498	0.0020	304.08	1.30	440.83	2.02
K12E-KHAR-34	25.68303	30.82195	311	micrite	E3	543885	35391	543986	35424	360.33	0.21	1802.53	65.27	687.51	24.94	1.1254	0.0024	94.49	1.09	438.52	46.37
K12E-KHAR-33	25.68288	30.82212	297	micrite	B3	429895	9565	430963	9640	264.09	0.11	12735.77	42.65	70.30	0.25	1.1093	0.0016	95.13	1.10	320.92	9.59
K12E-KHAR-37	25.68440	30.82250	322	spar	E4	448057	13928	448066	13929	3386.90	1.99	1463.27	24.81	8062.50	137.64	1.1398	0.0024	114.81	1.11	406.47	16.76
K12E-KHAR-36	25.68440	30.82250	322	root cast	4	496495	21382	496645	21411	3620.93	1.12	26822.64	40.97	469.04	1.18	1.1369	0.0023	106.60	1.11	432.85	27.33
K12E-KHAR-35	25.68443	30.82245	320	micrite	B4	645793	60676	646253	60946	2960.25	1.83	77227.70	41.10	134.40	0.15	1.1473	0.0014	105.57	1.11	653.79	122.86
Kharga Oasis: Wadi Midauwara																					
K12E-MIDA-48	24.95987	31.06233	275	flowstone--outer bands	E1	179102	1560	179444	1556	1625.04	0.99	22308.31	59.94	202.19	0.85	0.9082	0.0030	102.89	1.10	170.70	1.98
K12E-MIDA-48C	24.95987	31.06233	275	flowstone--inner bands	B1	158949	870	159335	851	1646.66	1.00	24183.01	43.80	173.41	0.47	0.8333	0.0017	70.93	1.07	111.19	1.70
K12E-MIDA-40	24.96077	31.06057	275	micrite	B1	103412	402	103511	399	954.04	0.44	3694.44	39.10	538.85	5.80	0.6828	0.0014	100.22	1.10	134.21	1.48
K12E-MIDA-47B	24.96034	31.06488	314	botryoidal coating	E2	565518	50194	565556	50213	888.81	0.55	1410.05	45.22	2032.72	65.31	1.0552	0.0022	43.27	1.04	213.40	32.89
K12E-MIDA-47	24.96034	31.06488	314	stick cast	B2	600050	74659	600124	74721	794.32	0.72	2543.29	37.55	1015.33	15.13	1.0637	0.0023	48.01	1.05	261.02	61.52
K12E-MIDA-46	*24.95964*	*31.06535*	*305*	*groundwater speleothem*	*2*	*728223*	*120378*	*700842*	*5426593*	*545.90*	*0.72*	*985.61*	*23.75*	*1715.84*	*41.49*	*1.0137*	*0.0024*	*10.70*	*1.01*	*77.33*	---
K12E-MIDA-45	*24.95826*	*31.06991*	*352*	*stick cast*	*E3*	*914822*	*119591*	---	---	*637.10*	*0.23*	*1603.35*	*23.88*	*1243.96*	*19.70*	*1.0244*	*0.0055*	*15.14*	*1.01*	---	---
K12E-MIDA-43	*24.95846*	*31.07010*	*353*	*micrite*	*B3*	*790853*	*119591*	---	---	*364.13*	*0.14*	*4545.51*	*26.19*	*257.35*	*1.57*	*1.0512*	*0.0022*	*21.07*	*1.02*	---	---
Kurkur Oasis																					
K12E-KUR-63	23.90621	32.32439	325	stick cast	B1	126513	949	128082	545	1495.03	0.76	110915.05	368.36	37.40	0.15	0.9079	0.0019	269.67	1.27	387.06	1.92
K12E-KUR-65	23.90621	32.32439	325	stick cast	E1	76749	635	77915	257	2082.77	0.93	108336.89	31.13	38.12	0.08	0.6488	0.0013	245.16	1.24	305.44	1.57
K12E-KUR-52	23.89226	32.32240	308	laminated spar	1	143756	763	144997	451	1052.73	0.49	64046.82	38.34	49.57	0.06	0.9867	0.0011	289.02	1.29	435.11	2.02
K12E-KUR-58	23.89816	32.32496	314	stick cast	B2	245825	2665	249261	2102	2445.10	1.73	414329.27	168.72	20.92	0.04	1.1597	0.0025	227.71	1.23	460.06	3.69
K12E-KUR-53	23.89235	32.32598	359	stick cast	B3	514337	29730	515437	30044	521.63	0.19	22965.14	40.92	72.65	0.20	1.0466	0.0021	39.93	1.04	170.95	15.76
K12E-KUR-59	*23.90587*	*32.32511*	*337*	*botryoidal coating*	*B3*	*610146*	*119416*	---	---	*568.00*	*0.27*	*226870.68*	*503.02*	*8.31*	*0.02*	*0.9079*	*0.0019*	*50.31*	*1.05*	---	---
K12E-KUR-60	*23.90587*	*32.32511*	*337*	*laminated micrite*	*B3*	*844384*	*119416*	---	---	*758.36*	*0.35*	*147259.33*	*77.30*	*16.37*	*0.03*	*1.0404*	*0.0022*	*26.43*	*1.03*	---	---
K12E-KUR-55	23.89196	32.32640	361	laminated micrite vein	3	191583	3445	198098	1316	597.54	0.26	141355.99	125.14	11.50	0.03	0.8903	0.0018	51.07	1.05	89.31	1.87
K12E-KUR-62	*23.90567*	*32.32529*	*343*	*stick cast*	*E3*	*1024327*	*119416*	---	---	*515.26*	*0.19*	*420463.34*	*107.63*	*3.88*	*0.01*	*1.0371*	*0.0021*	*16.29*	*1.02*	---	---
K12E-KUR-56	23.89196	32.32640	361	micrite	E3	145803	894	147199	569	395.36	0.19	21178.50	46.23	46.38	0.12	0.8129	0.0012	82.25	1.08	124.59	1.65

Notes:

*Stratigraphic level designations are as follows: numbers reflect a deposit's landscape level relative to modern base level, with 1 being the lowest-elevation deposit. B indicates that a sample represents the chronological beginning of deposition; E indicates chronological end of deposition.

-Samples in italics have ages modeled using the $\delta^{234}U$ equation.

-Ages are reported as years before present, where present is AD 2012. Ratios denote activity, and all errors are 2σ of the mean. $\delta^{234}U_m$ and $\delta^{234}U_i$ are measured and initial values, in per mil. Sample powder sizes ranged from 100-210 mg.

Table 2
Geochemistry of travertine samples from the study

Sample ID	Latitude	Longitude	Sample facies	$\delta^{13}C$ (‰)	$\delta^{18}O$ (‰)	Sr (ppm)	Sr error (ppm)	$^{87}Sr/^{86}Sr$	$^{87}Sr/^{86}Sr$ error
Crystal Mountain									
K11E-CRYS-3	27.661122	28.431196	groundwater speleothem	-0.09	-11.07	---	---	---	---
K11E-CRYS-4	27.661122	28.431196	flowstone--outer bands	-0.93	-10.87	74.68	0.01	0.70821	1.49E-05
K11E-CRYS-4B	27.661122	28.431196	flowstone--inner bands	-2.59	-11.27	203.27	0.01	0.70821	1.00E-05
K11E-CRYS-5	27.660527	28.431939	spar	-11.47	-10.76	18.67	0.00	0.70844	1.10E-05
K11E-CRYS-6	27.660527	28.431939	micrite	-10.77	-10.75	---	---	---	---
K11E-CRYS-7A	27.662097	28.439826	micrite	-10.20	-11.45	17.80	0.00	0.70859	1.38E-05
K11E-CRYS-7B	27.016077	27.918767	micrite	-8.24	-12.37	---	---	---	---
Dakhla Oasis									
K12E-DAK-14	26.335662	27.781254	carbonate vein	-4.72	-10.28	---	---	---	---
K12E-DAK-15A	26.335808	27.780994	root cast	-4.30	-10.31	---	---	---	---
K12E-DAK-15B	26.335808	27.780994	vein	-4.43	-10.11	---	---	---	---
K12E-DAK-17	25.475119	29.110658	micrite	-5.92	-9.17	624.26	0.11	0.71038	1.00E-05
K12E-DAK-18A	25.475119	29.110658	micrite	-5.47	-7.59	---	---	---	---
K12E-DAK-18B	25.474572	29.111047	micrite	-5.47	-7.77	237.92	0.03	0.71076	1.00E-05
Kharga Oasis: Refuf Pass									
K12E-KHAR-20	25.474572	29.111047	stick cast	-5.15	-10.77	378.88	0.09	0.70787	1.01E-05
K12E-KHAR-21	25.656772	28.995129	stick cast	-4.95	-10.74	368.96	0.05	0.70786	1.00E-05
K12E-KHAR-22	25.514230	29.178466	stick cast	-3.21	-8.64	---	---	---	---
K12E-KHAR-23	25.507979	29.182392	semi-micritic	-3.82	-9.84	---	---	---	---
K12E-KHAR-24	25.507979	29.182392	porous, clay-rich micrite	-2.81	-10.07	---	---	---	---
K12E-KHAR-30	25.679802	30.812764	stick casts	-1.79	-9.95	288.99	0.07	0.70789	1.00E-05
K12E-KHAR-31	25.679802	30.812764	micrite drape	-2.60	-10.02	207.68	0.03	0.70789	1.24E-05
K12E-KHAR-32	25.679811	30.812803	porous micrite	-3.07	-10.55	477.86	0.10	0.70790	1.00E-05
K12E-KHAR-33	25.680063	30.816365	micrite	-3.47	-10.75	154.85	0.01	0.70786	1.00E-05
K12E-KHAR-34	25.678450	30.817719	micrite	-4.32	-10.94	140.40	0.01	0.70788	1.00E-05
K12E-KHAR-35	25.676673	30.818389	micrite	-2.10	-10.47	824.61	0.17	0.70784	1.00E-05
K12E-KHAR-36	25.677807	30.821197	root cast	-0.92	-10.06	824.97	0.17	0.70784	1.00E-05
K12E-KHAR-37	25.678347	30.821665	spar	-2.90	-11.01	631.36	0.18	0.70785	1.00E-05
Kharga Oasis: Wadi Midauwara									
K12E-MIDA-40	25.678912	30.822033	micrite	-2.11	-9.06	1055.94	0.15	0.70782	1.00E-05
K12E-MIDA-41	25.682876	30.822121	groundwater speleothem	-1.65	-10.43	---	---	---	---
K12E-MIDA-42	25.683026	30.821949	laminated micrite	-1.95	-9.15	---	---	---	---
K12E-MIDA-43	25.684433	30.822451	micrite	-1.42	-9.47	295.78	0.02	0.70788	1.00E-05
K12E-MIDA-44	25.684398	30.822501	micrite	-1.59	-9.17	---	---	---	---
K12E-MIDA-45	25.684398	30.822501	stick cast	-1.62	-9.79	360.47	0.04	0.70785	1.00E-05
K12E-MIDA-46	24.960771	31.060566	groundwater speleothem	-1.29	-11.47	341.37	0.06	0.70785	1.00E-05
K12E-MIDA-47	24.958262	31.068934	stick cast	-0.69	-9.35	701.95	0.13	0.70787	1.00E-05
K12E-MIDA-47B	24.958170	31.069520	botryoidal coating	-0.86	-7.59	860.71	0.38	0.70787	1.00E-05
K12E-MIDA-48	24.958458	31.070100	flowstone--outer bands	-1.69	-6.59	1117.47	0.44	0.70784	1.00E-05
K12E-MIDA-48C	24.958206	31.070163	flowstone--inner bands	-2.36	-10.26	1223.99	0.40	0.70784	1.00E-05
Kurkur Oasis									
K12E-KUR-50	24.958257	31.069914	laminated spar	-0.69	-12.44	---	---	---	---
K12E-KUR-51	24.959642	31.065347	micrite	-0.42	-11.40	---	---	---	---
K12E-KUR-52	24.960340	31.064881	laminated spar	-4.02	-13.42	568.62	0.10	0.70784	1.00E-05
K12E-KUR-53	24.960340	31.064881	stick cast	-2.86	-11.03	137.54	0.01	0.70788	1.02E-05
K12E-KUR-54	24.959873	31.062333	stick cast	-2.80	-9.65	---	---	---	---
K12E-KUR-55	24.959873	31.062333	laminated micrite vein	-3.51	-11.17	97.16	0.01	0.70795	1.49E-05
K12E-KUR-56	23.888176	32.323048	micrite	-1.41	-8.55	94.03	0.01	0.70799	1.00E-05
K12E-KUR-58	23.888304	32.323420	stick cast	-2.86	-10.94	764.92	0.28	0.70783	1.00E-05
K12E-KUR-59	23.892264	32.322398	botryoidal coating	-2.21	-8.96	203.81	0.01	0.70789	1.00E-05
K12E-KUR-60	23.892352	32.325983	laminated micrite	-2.26	-9.48	425.06	0.07	0.70794	1.00E-05
K12E-KUR-61	23.892352	32.325983	stick cast	-2.94	-10.77	---	---	---	---
K12E-KUR-62	23.891957	32.326397	stick cast	-3.30	-10.54	147.86	0.01	0.70786	1.00E-05
K12E-KUR-63	23.891957	32.326397	stick cast	-4.53	-12.86	368.34	0.07	0.70787	1.00E-05
K12E-KUR-64	23.892111	32.326485	groundwater speleothem	-2.49	-11.02	---	---	---	---
K12E-KUR-65	23.898155	32.324960	stick cast	-4.00	-12.91	730.67	0.19	0.70789	1.00E-05
K12E-KUR-65B	23.905869	32.325107	micrite	-2.39	-8.16	---	---	---	---
K12E-KUR-66	23.905869	32.325107	micrite	-2.02	-8.63	---	---	---	---
K12E-KUR-67	23.905617	32.325226	micrite	-2.26	-8.96	---	---	---	---
K12E-KUR-68	23.905671	32.325295	clay-rich micrite	-1.49	-8.26	---	---	---	---
K12E-KUR-69	23.906209	32.324388	laminated micrite	-1.16	-12.05	---	---	---	---

Notes:
-Stable isotopic ratios are reported relative to VPDB.
-$^{87}Sr/^{86}Sr$ ratios denote activity, and all errors are 2σ of the mean.

Table 3
Geochemistry of water samples from the study

Sample ID	Name	Water source	Latitude	Longitude	Temperature (°C)	$\delta^{13}C$ (‰, PDB)	$\delta^{18}O$ (‰, SMOW)	calcite equivalent $\delta^{13}C$ (‰, PDB)	+/- error	calcite equivalent $\delta^{18}O$ (‰, PDB)	+/- error	Sr (ppm)	Sr error (ppm)	$^{87}Sr/^{86}Sr$	$^{87}Sr/^{86}Sr$ error
Farafra Oasis															
LC11E-FAR-1	Bir Regwa	artesian spring	27.34628	28.14676	27.7	-13.90	-10.44	-4.45	-1.18	-11.04	-1.01	0.3576	3.88E-05	0.70830	1.00E-05
LC11E-FAR-2	Bir 400	pumped well	27.05860	27.88128	44.1	-15.00	-10.39	-5.56	-1.18	-11.00	-1.01	0.0481	4.02E-06	0.71325	1.00E-05
LC11E-FAR-3	Bir 19	artesian well	27.04711	27.83554	43.2	-17.00	-10.53	-7.58	-1.18	-11.14	-1.01	0.0474	3.71E-06	0.71573	1.00E-05
LC11E-FAR-4	Ain Khadra	artesian spring	27.37114	28.22071	27.4	-15.00	-7.27	-5.56	-1.18	-7.88	-1.01	0.3787	5.34E-05	0.70807	1.00E-05
Dakhla Oasis															
LC11E-DAK-1	Ashra Well 10	artesian well	25.81889	28.58635	45	-12.80	-11.04	-3.34	-1.18	-11.64	-1.01	0.1042	1.55E-05	0.71715	1.00E-05
LC11E-DAK-2	El Dohous	pumped well	25.56216	28.94830	41.6	-17.50	-11.07	-8.09	-1.18	-11.68	-1.01	0.1558	7.16E-06	0.72186	1.00E-05
Kharga Oasis															
LC12E-KHAR-1	Um Elqusor	pumped well	25.74925	30.66805	29.8	-13.50	-10.83	-4.05	-1.18	-11.44	-1.01	0.1080	3.65E-05	0.70745	1.00E-05
LC12E-KHAR-2	Bir 36	pumped well	25.60577	30.64584	37.4	-11.20	-10.89	-1.73	-1.19	-11.50	-1.01	0.2535	3.31E-05	0.70710	1.00E-05
LC12E-KHAR-3	Nasser Well #1	pumped well	25.25679	30.52458	32.3	-16.30	-10.77	-6.88	-1.18	-11.38	-1.01	0.3977	7.44E-05	0.71154	1.00E-05
LC12E-KHAR-4	Bir 7	pumped well	25.27691	30.57499	41	-13.30	-10.57	-3.85	-1.18	-11.18	-1.01	0.2489	1.87E-05	0.70778	1.00E-05
LC12E-KHAR-5	Bir 34	pumped well	24.78313	30.59151	33.4	-12.90	-10.36	-3.44	-1.18	-10.97	-1.01	0.4329	2.19E-05	0.70743	1.00E-05
Kurkur Oasis															
LC12E-KUR-1	Kurkur Oasis	seep	23.90034	32.32730	---	---	-9.39	---	---	---	---	8.3057	2.60E-03	0.70783	1.00E-05

Notes:
-$^{87}Sr/^{86}Sr$ ratios denote activity, and all errors are 2σ of the mean.
-Outflow at Kurkur Oasis was too low to allow sampling of a sufficient quantity of water to determine $\delta^{13}C$.
-Calcite equivalent $\delta^{13}C$ and $\delta^{18}O$ are calculated after Romanek et al. (1992) and Demény et al. (2010), respectively, over a temperature range of 15-25°C.

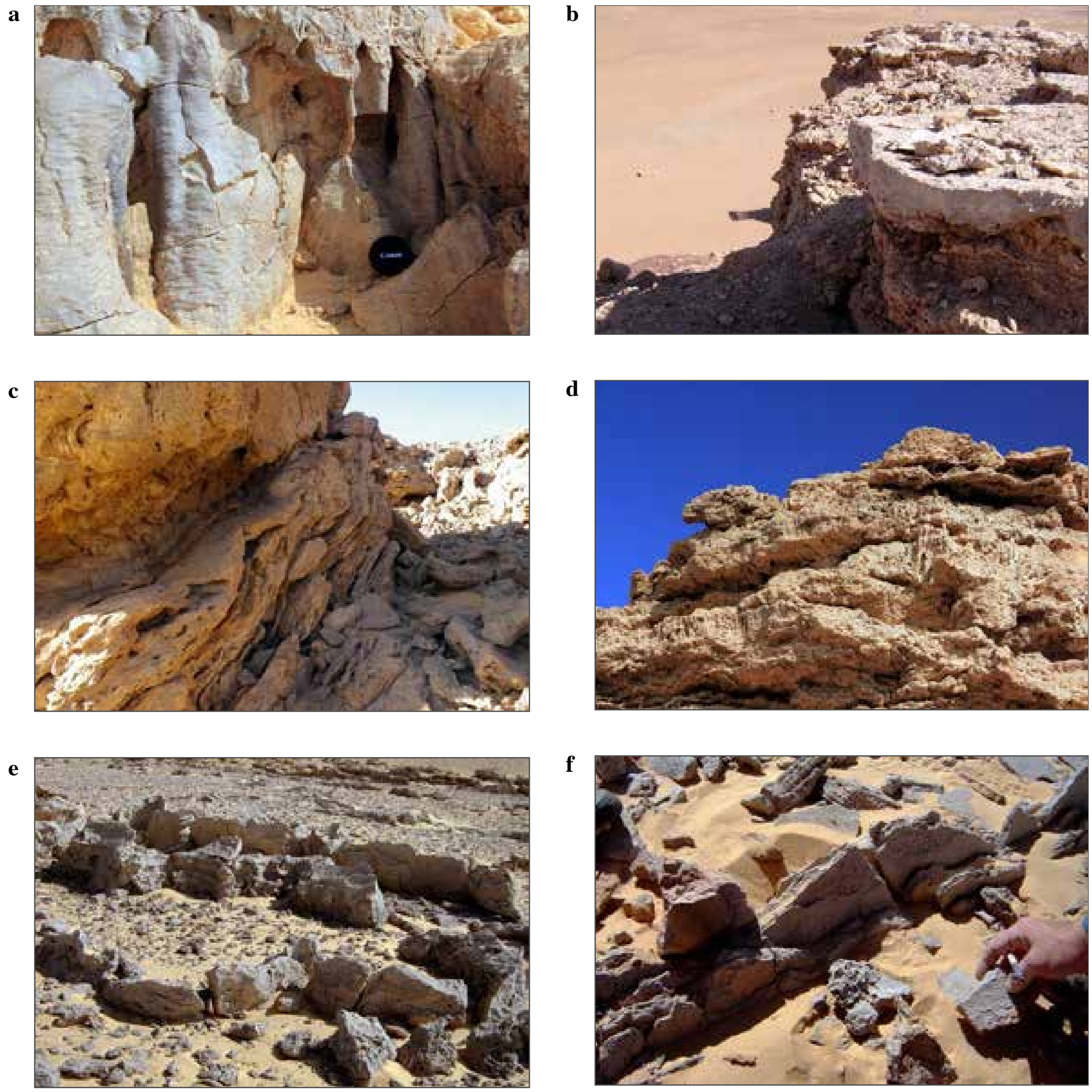

Figure 3. Travertine facies from Western Desert paleo-oasis areas. a) Groundwater speleothem facies from a dissolution cave at Crystal Mountain. b) Microdetrital mud at the top of a lake bed at Dakhla Oasis. c) Drape at Refuf Pass. d) Paludal facies at Refuf Pass, with abundant stick casts, vegetated textures, and gastropods. e) Fluvial barrage/rimstone dams at Wadi Midauwara. f) Fissure ridge formed by a vertical vein at Kurkur Oasis. g) Paludal facies with phytohermal layers and very large palm casts; broken pieces draped by later deposition suggests that fluvial action modified the deposit after initial formation.

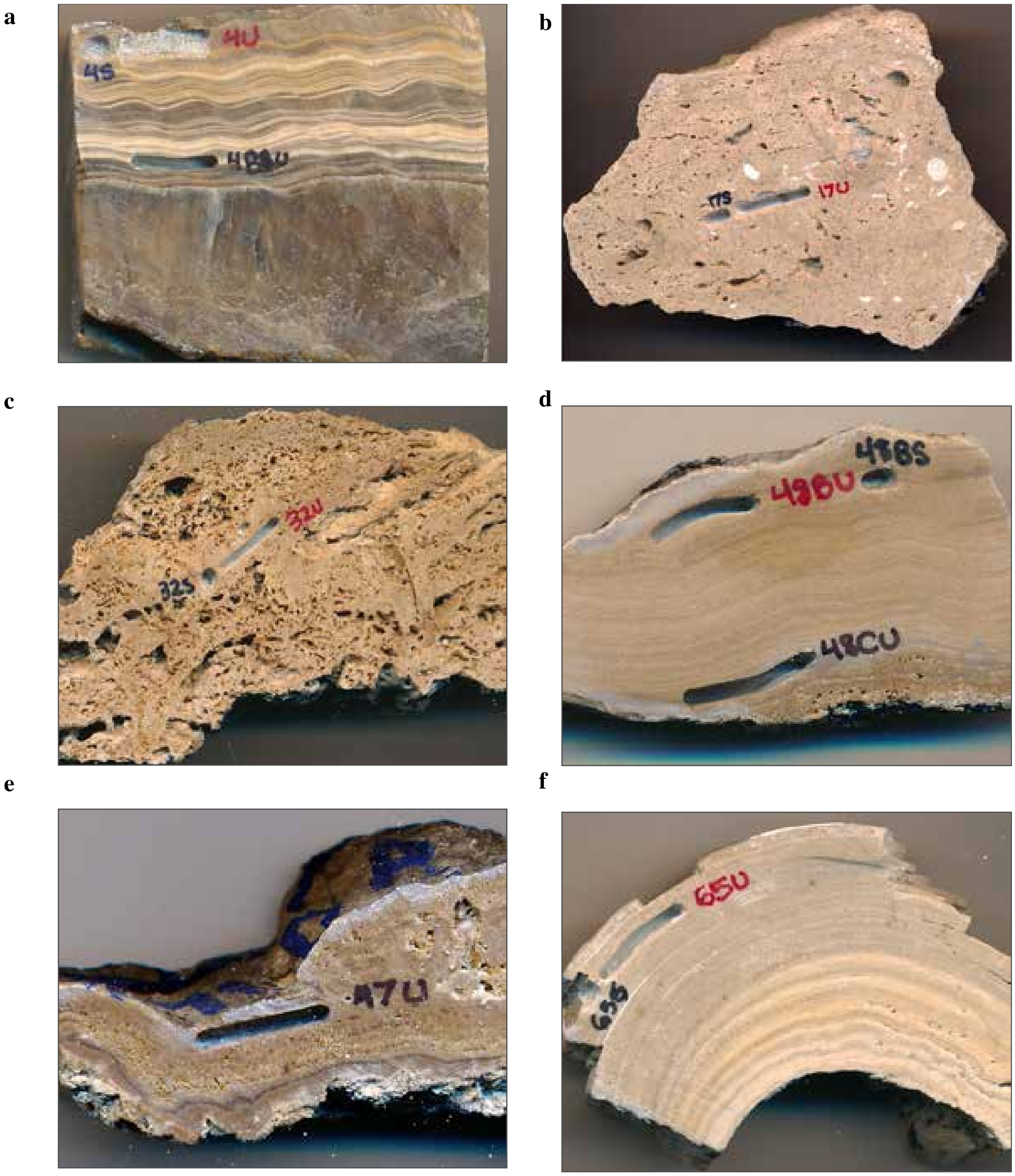

Figure 4. Scanned sample slabs showing several representative travertine textures (drill path is ~1.5 mm thick). a) Finely laminated flowstone from “groundwater speleothem” facies at Crystal Mountain. b) Dense micrite from a lakebed at Dakhla Oasis. c) Phytohermal layering from a paludal sequence at Refuf Pass. d) Finely laminated flowstone from a rimstone dam at Wadi Midauwara. e) Botryoidal coating from the bottom of a shelf at Wadi Midauwara. f) Large plant cast from paludal facies at Kurkur Oasis.

arcuate fluvial barrage dams, fissure ridges, and fluvially-reworked paludal facies (Ford and Pedley, 1996; Pentecost, 2005). Figure 4 shows examples of these textures in slabbed hand samples.

Crystal Mountain exhibits fluvial barrage and perched springline facies, including pourover dams, microterracettes, and dissolution caves (Figs. 3a and 4a; Ford and Pedley, 1996, Pentecost, 2005). Much of the travertine at Crystal Mountain showed evidence of recrystallization, with abundant sparite textures. We note that the lack of vegetative facies at Crystal Mountain could suggest high-temperature deposition, but further study would be required to confirm this. Previous attempts to date travertine at Crystal Mountain (Holzkamper, 2004) yielded ages out of U/Th range; to our knowledge, we have obtained the first date on Crystal Mountain travertine, of 523 ± 30 ka on a groundwater speleothem-type structure, which is interpreted to be the youngest carbonate in this deposit. We also obtained two $\delta^{234}U$ model ages in excess of 1 Ma (Table 1).

Travertine deposits occur in several different areas of Dakhla Oasis, from thin, widespread lacustrine deposits and ironstone spring mounds in the Kellis and Balat-Tineida basins south of the carbonate plateau (see Kieniewicz and Smith, 2009; Adelsberger and Smith, 2010), to colluvium-covered surfaces along the plateau escarpment to the north (Brookes, 1993; Kleindienst et al., 1999). Previous workers have successfully dated travertine float blocks from colluvium near the plateau escarpment, generating ages of 134 ± 12 ka, 170 ka ± 12 ka, and 176 ka ± 14 ka, which they extrapolated to the Dakhla paleolake (Kleindienst et al., 1999).

We report the first direct dates on the Dakhla paleolake beds: 349 ± 6 from the top and 292 ± 5 ka from the bottom of flat-lying, finely-layered lacustrine deposits composed of dense micritic mud, (see Figs. 3b and 4b; Table 1). These ages differ greatly from the previously assumed age of ~120 ka. Although the $^{230}Th/^{232}Th$ of the younger age we obtained indicates significant detrital contamination ($^{230}Th/^{232}Th$ activity of 10.42; Table 1), the older date is analytically sound, suggesting that both ages are reasonably accurate.

Travertine at Refuf Pass has been extensively studied; multiple levels of deposition above modern base height exist, which previous workers classified as “wadi” (meaning “wash,” closer to modern base level) and “plateau” (levels topographically higher in the landscape) (Caton-Thompson and Gardner, 1932; Smith et al., 2004a; Kieniewicz and Smith, 2007; Smith and Kieniewicz, 2006; Kleindienst et al., 2008). These facies are described by Caton-Thompson and Gardner (1932), and the results of more recent work summarized by Smith et al. (2004b). Our field observations are similar to theirs, with predominant fluvial barrage and perched springline facies, the latter having stick casts or vegetative textures indicative of paludal development (Figs. 3c, 3d). Our geochronology on these travertine differs from the prior division of travertine into young/wadi and old/plateau deposits. A wide range of U/Th dates has been reported for Refuf Pass travertine, mostly centering on ~130 ka (MIS 6/5e), as well as 170, 200, 240, and 300 ka (Kleindienst et al., 2008). In contrast, our U/Th dates from four different topographic levels corroborate deposition at ~130 ka but also show significant deposition from 450-600 ka (Table 1). Importantly, the lowest topographic level includes both young (130 ka) and old (450-600 ka) deposition.

Several travertine levels also exist at Wadi Midauwara. Again, our facies observations follow those of previous workers (Smith et al., 2004a; Smith et al., 2004b; Smith et al., 2007): fluvial barrage dams were common at the lowest topographic level (Fig. 3e), and paludal facies at higher levels, often with botryoidal coatings. Prior successful dates on Wadi Midauwara travertine have highlighted an important depositional episode at ~130 ka (Smith et al., 2007) and earlier deposition ~150 ka and 360 ka, as well as multiple ages out of U/Th analytical range (400 ka at the time; Smith et al., 2004b). We report several new depositional episodes, at ~100 ka, 160-180 ka, and ~550-600 ka; we also note significant earlier deposition, approximated to 700-900 ka with d^{234}U model ages (Table 1).

Travertine deposition at Kurkur also occurred at multiple stratigraphic levels, which have been described by Crombie et al. (1997). They followed the classification scheme previously established at Kharga Oasis (see above), designating a lowest level “inverted wadi,” followed by an intermediate “spring mound” level, and then a higher plateau level. We observed mixed fluvial facies at the lowest landscape levels, with travertine rubble and casts ranging up to palm trunk size surrounded by well-laminated botryoidal drapes (Fig. 3g, corresponding to Crombie et al.’s (1997) inverted wadi and spring mound levels); the highest stratigraphic level was predominantly composed of a paludal facies including small dissolution caves and one fissure ridge (Fig. 3f). Crombie et al. (1997) reported U/Th dates ranging from 68 ka to ~220 ka at lower landscape levels, and several ages out of U/Th analytical range for the higher plateau travertine. We obtained largely similar ages for the lower stratigraphic levels (~76 ka to 246 ka); for the higher levels, we found an age of ~514 ka, and d234U ages suggesting deposition between ~600 ka and 1 Ma. We dated the fissure ridge atop the highest landscape level to 191 ka (Table 1).

DISCUSSION

Episodicity and timing of travertine deposition

We synthesized our new geochronology with our parsed compilation of previously published dates in order to discern whether travertine deposition occurred in discrete intervals or continuously. Summarizing the resulting data compilation in a probability density plot (Fig. 5) shows multiple, distinct peaks in probability of travertine occurrence (note that $d^{234}U$ model ages from this study are not included in the analysis, as they did not meet our 20% error criterion; see Methods). This probability profile supports the idea that travertine deposition in the Western Desert was indeed episodic throughout the late Pleistocene, a conclusion generally shared by previous workers (e.g., Smith et al., 2004b; Kleindienst et al., 2008; Smith, 2012).

The episodicity of Western Desert travertine deposition suggests response to some intermittent forcing, possibly pluvial episodes. However, the spatial and temporal heterogeneity of travertine deposition warrants careful interpretation. In the discussion that follows, it should be stressed that caution is needed when considering peak amplitude in the probability density plot (Fig. 5): high probability in the plot largely reflects a greater number of samples from a given time interval and not necessarily absolute travertine volume, as well as lower analytical error on samples younger than ~400 ka. For example, high probability in the 100-200 ka range reflects several factors: first, technique advances since earlier studies (the inability to date samples older than ~350 ka lead authors to focus on younger, datable samples). Second, some studies described numerous,

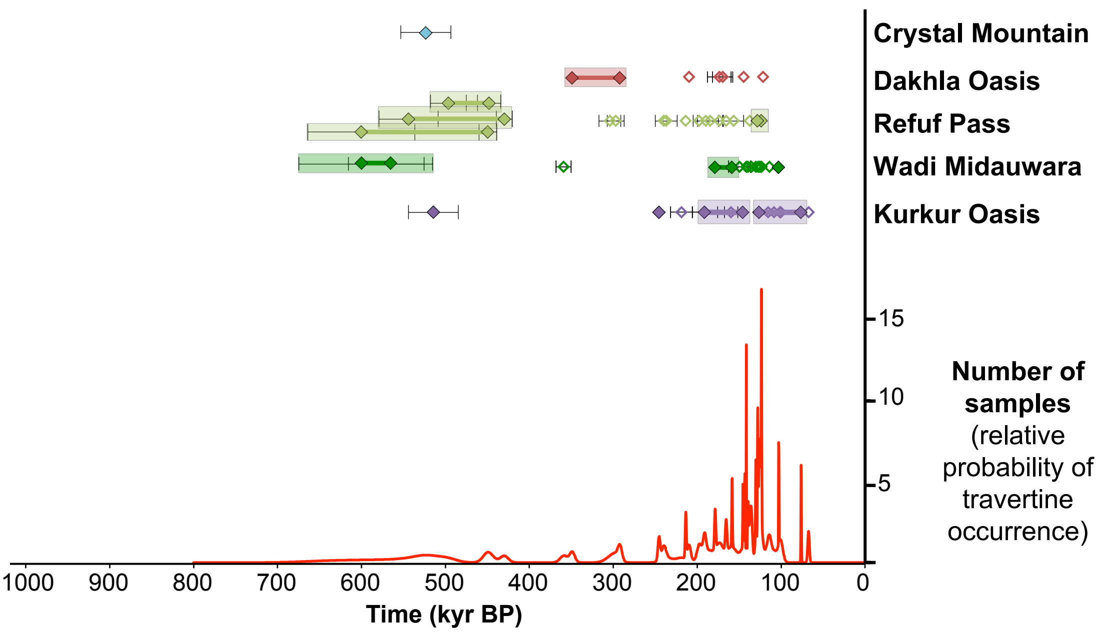

Figure 5. Top: compilation of travertine geochronology from the Western Desert, including ages from this study (filled diamonds; see Table 1) and parsed ages from previous studies (open diamonds; see Appendix 1). Colored rectangles indicate samples from this study inferred by stratigraphy to represent the beginning and end of a depositional episode; a probability density plot of all ages is shown below. Bottom: probability density plot of all ages.

roughly coeval samples from single locations, often for archaeological purposes. Finally, we note that determining the magnitude of a depositional episode is complicated by the uncertain volumetric significance of some ages from previous studies, as workers did not always give context for their ages in terms of travertine volume and facies.

A prominent characteristic of our travertine dataset is that, while two or more distinct episodes of travertine deposition occurred at every paleo-oasis area, these episodes were not synchronous across all Western Desert oasis areas. For example, deposition at ~130 ka episode occurred at every paleo-oasis except Crystal Mountain. Another example is that significant deposition ~75 and 100 ka is only documented at Kurkur Oasis. Sampling gaps could partially explain these inconsistencies: given the complexity of travertine stratigraphy throughout the Western Desert, accumulations representing some time periods may not have been sampled, by omission or because they were erased or covered by later deposition. However, it does seem likely that the spatial heterogeneity in the most significant travertine accumulations is real, as these large accumulations would probably have been targeted for sampling (by us or previous workers).

Another notable feature of our travertine compilation is that the depositional episodes we determined stratigraphically often span multiple peaks in the age probability diagram (Fig. 5). This suggests that deposition may have ceased and resumed in the same stratigraphic unit over two or more pluvial episodes.

Based on these depositional episodes, as well as peaks in probability of travertine occurrence, two depositional episodes stand out. First, our field observations of large-volume accumulation at ~130 ka, and the prevalence of samples at several oasis areas in this age range (Refuf Pass, Wadi Midauwara, and Kurkur Oasis) implies that this episode was likely very significant. Additionally, our new geochronology gives evidence for significant travertine accumulation at several paleo-oasis areas between ~450-600 ka (Refuf Pass, Wadi Midauwara, Kurkur Oasis, and to a lesser extent Crystal Mountain; Table 1). While differentiating episodes in this age range is difficult, as ages approaching the limit of U/Th dating are fairly imprecise, it is likely that more than one depositional episode occurred in this age range, and these episodes may have been synchronous across the various paleo-oases.

This study is the first to offer any temporal constraints for Western Desert travertine deposition older than ~400 ka. Although we can only constrain travertine deposition with any precision to ~650 ka, it is also noteworthy that significant travertine deposition occurred earlier in the Pleistocene in many oasis areas (Crystal Mountain, Wadi Midauwara, and Kurkur Oasis; Table 1). We suggest that Western Desert travertine-depositing systems have likely been active for at least the last 2 Ma.

It is interesting, though, that travertine is older and much less abundant in Farafra Oasis than in oases to the south, and may be entirely absent further north in Bahariya Oasis (Fig. 1). Our date of 523 ± 30 ka comes from the stratigraphically youngest unit we observed at Crystal Mountain, and $\delta^{234}U$ model ages suggest greater deposition earlier in the Pleistocene (Table 1). There is evidence for later-Pleistocene deposition at Farafra Oasis: Sultan et al. (1997) dated a sample from a dissolution cave near Farafra Oasis to 287 ± 67 ka. However, the only large-volume travertine accumulation in Farafra Oasis, Crystal Mountain, apparently ceased deposition much earlier than oases further to the south. It is conceivable that some geographic or hydrologic control may have restricted travertine deposition over a north to south spectrum.

One possibility is a decrease in water availability through the late Pleistocene. Travertine volume generally decreases in volume as well as elevation above modern base level throughout our record (see Table 1 and following section), and ceases across the Western Desert after ~70 ka. Travertine deposition also generally stops in the north first (Crystal Mountain ~520 ka), and the south last (Kurkur Oasis, ~70 ka). Szabo et al. (1989) suggested that water table levels declined over the Pleistocene, based on progressively lowering heights of calcium carbonate cemented terraces in southern Egypt and northern Sudan.

Age constraints for the Dakhla paleolake

Our new dates on the Dakhla lakebeds suggest that at least one phase of lacustrine deposition occurred much earlier than previously thought (~290-350 ka rather than 125-130 ka; Table 1). While the sequence of ages we report is puzzling—the older age is at the top of the lakebeds—it is possible that lowering lake level caused deposition of young material over original, older material, or dissolution and reprecipitation of old carbonate. Despite their puzzling stratigraphy, our dates certainly indicate significantly wet conditions from ~290-350 ka.

The only other direct dates on the Dakhla lakebeds come from the Dakhla Glass, a silicate glass probably formed from a meteorite impact, which has been found in several locations throughout Dakhla Oasis, either overlying or interbedded in calcareous lacustrine silts (Osinski et al., 2007). $^{40}Ar/^{39}Ar$ analysis yielded isochron ages ranging from 282 ± 121 ka to 119 ± 45 ka, from which Osinski et al. (2007) quote a weighted average age of 122 ± 40 ka, stressing its preliminary nature. In comparing these results to our direct dates, two points are noteworthy: first, the Dakhla Glass dates carbonate lake sediments that may be related to a different lake generation than our travertine lakebeds. Second, the large uncertainties in the $^{40}Ar/^{39}Ar$ dates on the Dakhla Glass admit the possibility that the Dakhla Glass was contemporaneous with or even older than the lakebeds we dated.

Thus, we stress that our dates are noteworthy in that they represent the first direct and precise dates on the Dakhla paleolake. These dates do not rule out the possibility of later lacustrine deposition ~130 ka, but at least call into question the assumption that the majority of the lakebeds date to this time. Also, the availability of water at Dakhla Oasis in a much older timeframe than previously supposed could have significant implications for the habitability of this area for hominids.

Controls on travertine deposition

Travertine deposition in tectonically-active, erosional regions such as the Western United States commonly shows inset relationships, with the oldest travertine occurring highest in the landscape and younger travertine depositing lower as the landscape level drops due to erosion. In contrast, if the landscape if stable and very slowly eroding, travertine age would have no relationship to its landscape height and variations in travertine landscape level would be due to fluctuating hydrologic head.

We suggest that travertine in Egypt's Western Desert follows the latter pattern, with travertine position in the landscape reflecting paleohydrologic variation rather than incision history. We investigated travertine deposition patterns by constructing schematic elevation transects of travertine deposition at Refuf Pass, Wadi Midauwara, and Kurkur Oasis (Fig. 6). For Wadi Midauwara and Kurkur Oasis, high-resolution profiles were not available, so we mapped our samples onto a low-resolution digital elevation model, which we refined based on field elevations and relationships. At Refuf Pass, samples were plotted on a surveyed profile (modified from Caton-Thompson and Gardner, 1932). We added dated samples published by other workers to the profiles at Refuf Pass (Kleindienst et al., 2008; with elevations extrapolated based on map location) and Kurkur Oasis (Crombie et al., 1997). We were unable to add previous workers' samples to our Wadi Midauwara profile; either they were collected far from our sample sites (Smith et al., 2007) or precise sample locations and elevations were not published (Smith et al., 2004b).

At every oasis area we studied, our geochronology compilation shows that travertine-depositing springs were recurrently active in the same places, and at the same elevations over time. This hints that spring sources were not responding to a lowering water table following gradual incision, but rather emerged at various landscape heights according to hydrologic head. Our new chronology at Wadi Midauwara shows

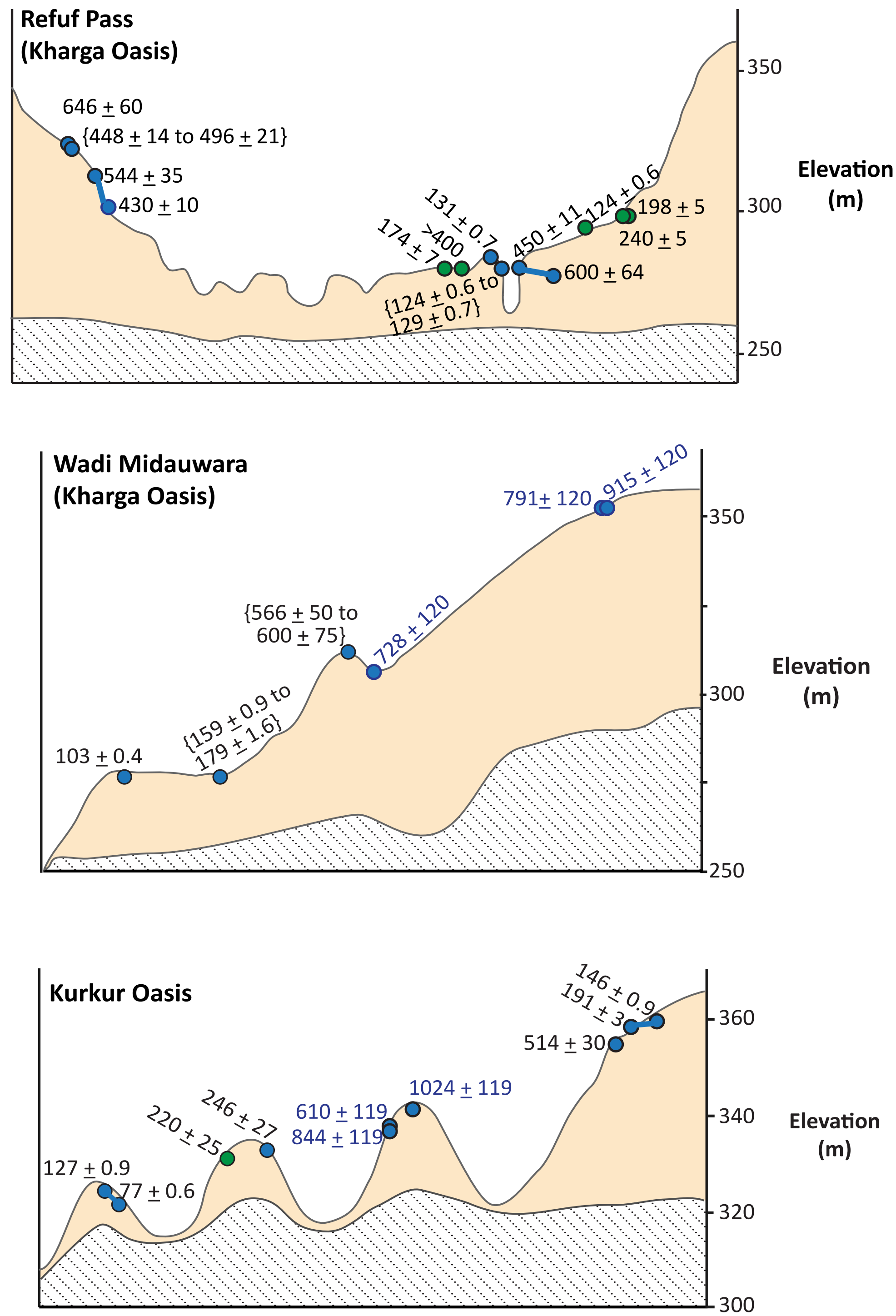

Fig. 6. Schematic elevation traverses from Refuf Pass, Wadi Midauwara, and Kurkur Oasis, with dated travertine sample locations and ages (blue dots indicate samples from this study, and green, literature samples; all ages are in ka). Episodes of deposition (i.e. constrained by samples in the same location, such as inner and outer bands of the same sample) are shown as bracketed durations or with a line connecting two samples. Blue lettering denotes $\delta^{234}U$ model ages (see Table 1). Areas hashed in gray show approximate modern base level; yellow denotes topography above base level (potentially including travertine, limestone bedrock, and/or wadi fill).

a pattern of travertine ages and landscape heights that resembles inset stratigraphy (young travertine low in the landscape and old travertine higher; Fig. 6). Although comparison of these dates to previous work is difficult because precise sample locations were not published, we note that Smith et al. (2004a) report ages of >350 ka for the stratigraphically lowest travertine they studied (Wadi Tufa 1). Thus, we suggest that stratigraphy at Wadi Midauwara is not actually inset. Similarly, at Refuf Pass, 450-600 ka travertine formed both high and low in the landscape (Fig. 6), and at Kurkur Oasis, ~146-190 ka travertine formed a fissure ridge/vein system at the highest landscape level, atop a ~500 ka travertine deposit.

Based on these findings, we suggest that changing hydrologic head generally controlled travertine position in the Western Desert landscape rather than landscape incision. This conclusion represents a significant departure from previous workers' assumptions that Western Desert travertine deposition represents inset stratigraphy (Caton-Thompson and Gardner, 1932; Smith et al., 2004b).

Stable isotopic geochemistry of Western Desert travertines and groundwaters

Travertine stable isotopic signatures preserve information about the source waters from which they precipitated, allowing comparison of paleo-groundwaters (as inferred from travertine) to modern groundwaters. Travertine samples from this study and previous literature are shown in Figure 7a. There is general coherence between travertine stable isotopic values measured in this study and by previous workers, with the possible exception of at Dakhla Oasis, where Kieniewicz and Smith (2009) reported travertines and lacustrine carbonate silts up to 4‰ more depleted in $\delta^{13}C$ than any samples we measured.

Western Desert travertines exhibit a wide range of stable isotopic signatures, with $\delta^{13}C$ ranging from -12 to 2‰ and $\delta^{18}O$ between -14 and -7‰ (Fig. 7a). One explanation for this range in geochemistry could be paleoclimatic, with the wide range in travertine signatures reflecting isotopic changes in source water, such as depleted values from the Indian monsoon (Smith et al., 2004a; Kieniewicz and Smith, 2007) or Atlantic-sourced precipitation depleted by rainout over the continent (Crombie et al., 1997; Sultan et al., 1997). A second, and not mutually exclusive, explanation is that travertine source waters began with a fairly consistent hydrochemistry, which then experienced a range of kinetic effects prior to precipitation, creating a wide spread in travertine stable isotopic signatures.

We assessed the problem of travertine source water by comparing travertine versus modern Nubian aquifer groundwater stable isotopic signatures. We converted

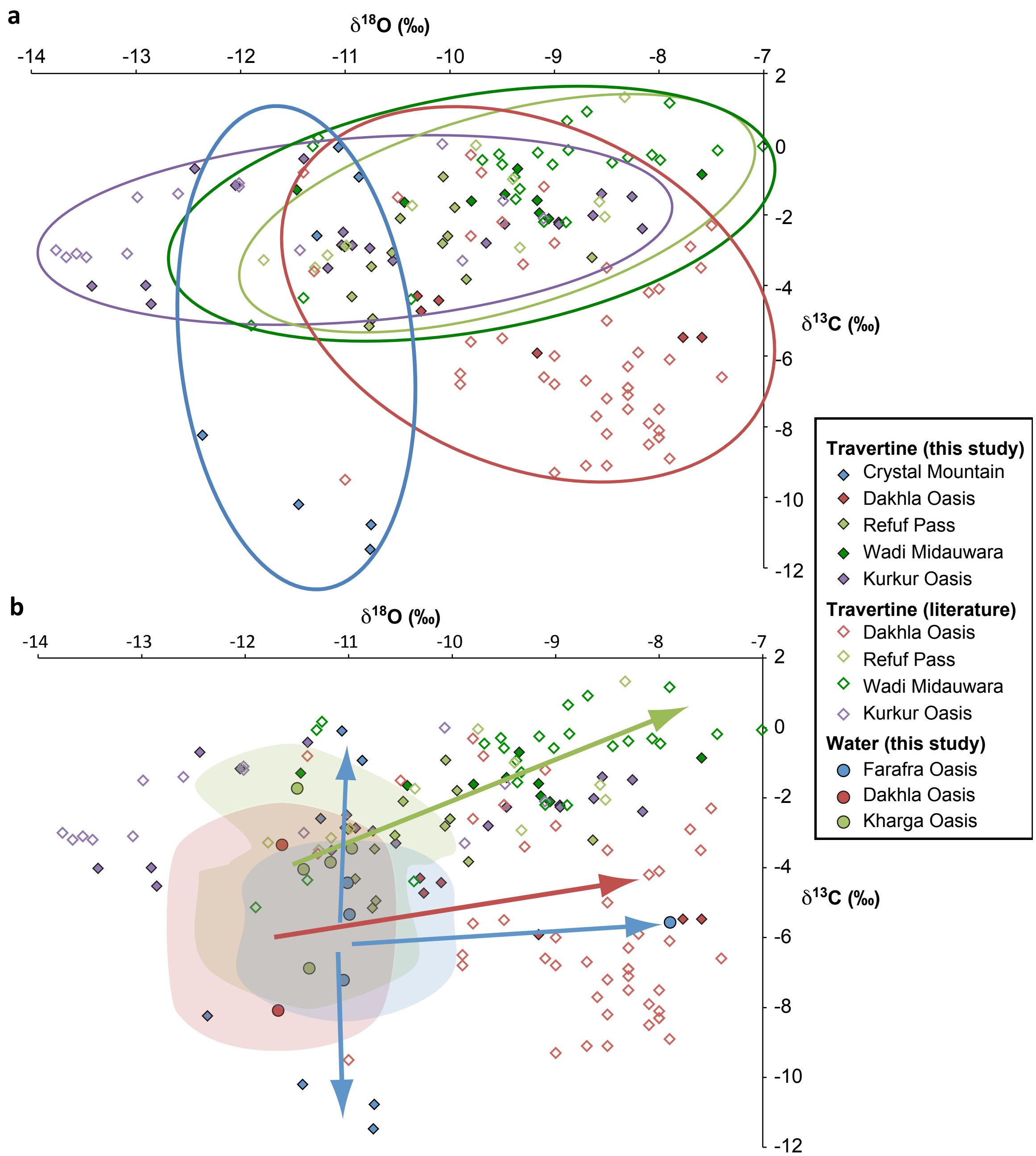

Figure 7. δ^{13}C versus δ^{18}O for travertine (diamonds) and water samples (circles) from the Western Desert (filled symbols indicate samples from this study and open, previous studies; see Table 2 and Appendix 2). a) Trends in stable isotopic composition of travertine samples. Colored ovals bound samples from each paleo-oasis area. Refuf Pass, Wadi Midauwara, and Kurkur Oasis share simliar geochemistry while Dakhla Oasis and Crystal Mountain form distinct groupings. b) The relationship between travertine geochemistry and modern water hydrochemistry is explored by extrapolating modern water isotopic signatures from Farafra, Dakhla, and Kharga Oases to calcite equivalents (shown as colored fields encompassing precipitation from 15-25˚C). Inferred calcite signatures are consistent with possible source water compositions for Dakhla, Kharga, and Farafra Oases; as indicated by colored arrows, these waters could evolve to the travertine compositions we measured via evaporation or degassing (see Talbot, 1990).

water stable isotopic signatures to calcite equivalents for water samples from Farafra, Dakhla, and Kharga Oases: using the equilibrium calcite precipitation equations of Demény et al. (2010; for δ18O) and Romanek et al. (1992; for δ13C), we calculated the stable isotopic signatures of calcite that would precipitate from a given water sample. We assumed a 15-25°C temperature range, since most artesian Western Desert springs are not thermal, having mean surface temperatures from 26-29°C (Swanberg et al., 1983). Our modern Western Desert groundwater $\delta^{18}O$ signatures (-10 to -11‰, VSMOW; Table 3) are similar to those reported by previous workers (Thorweihe, 1990; Sultan et al., 1997). One sample, from a heavily modified artesian spring in Farafra, has a much more positive $\delta^{18}O$ signature than the other waters, suggesting it may have experienced some evaporation prior to sampling; we therefore treated it as an outlier. The samples yield calcite-equivalent signatures of approximately -2 to -8‰ in $\delta^{13}C$ and -11‰ in $\delta^{18}O$ (Table 3, Fig. 7b).

These calculated calcite equivalents (Fig. 7b) roughly match the most depleted $\delta^{13}C$ and $\delta^{18}O$ signatures of Western Desert travertine samples. To a first-order analysis, this coherence suggests that modern groundwaters are indeed similar to past travertine source waters, which would have been fairly depleted before precipitating at the surface as travertine, at which point their isotopic signatures would tend to become enriched due to kinetic effects (evaporation and/or degassing). Thus, it is possible that travertines precipitated from Nubian aquifer groundwaters, and the range in travertine stable isotopic signatures predominantly derives from kinetic fractionation.

Examining the distribution of travertine stable isotopic signatures by oasis lends support the idea that kinetic effects dominate the spread in travertine values. A large proportion of Western Desert travertine groups together: Kharga Oasis areas (Refuf Pass and Wadi Midauwara) and Kurkur Oasis all have widely varying $\delta^{18}O$ values but a smaller range in $\delta^{13}C$. This pattern suggests the presence of an evaporation trend driving travertine $\delta^{18}O$ away from equilibrium precipitation values towards more positive signatures (Talbot, 1990; Li et al., 2008a).

Dakhla Oasis samples form a separate group (Fig. 7a), with a ~10‰ range in $\delta^{13}C$ and ~5‰ variation in $\delta^{18}O$. Dakhla's distinct geochemical signature probably derives in large part from sample deposition in a lacustrine (as opposed to spring-fed) environment, and lacustrine carbonate silt samples analyzed by Kieniewicz and Smith (2009) may be especially difficult to compare to spring-deposited travertine. However, once again, there are several processes that could modify an original, Nubian aquifer groundwater to create the observed spread in travertine stable isotopic signatures. Both degassing and equilibration with the atmosphere ($\delta^{13}C \approx -7‰$, so that water equilibrated with the atmosphere has $\delta^{13}C$ of 1-3‰) would enrich a water's $\delta^{13}C$ signature (Li et al., 2008a). In contrast, the presence of vegetation in the Dakhla paleolake could have driven water $\delta^{13}C$ in the opposite direction, to yield more depleted values.

Finally, at Crystal Mountain, samples form two groups; one, with groundwater speleothem-type samples, has similar $\delta^{13}C$ values to Kharga and Kurkur Oasis areas. The other group of Crystal Mountain samples includes perched springline facies that may have been deposited at high temperatures, and these have extremely depleted $\delta^{13}C$ values of -8 to -11‰. Given the lack of vegetated textures in Crystal Mountain travertine, as well as the possibility of hydrothermal deposition at that site, it is doubtful that the isotopically light $d^{13}C$ at Crystal Mountain originated from vegetation. However, some biological activity is implicated in order to achieve such low $d^{13}C$ values, perhaps bacterial respiration.

Given the resemblance between stable isotopic signatures of Western Desert travertine and modern groundwaters, we suggest that paleo-oasis areas share a similar, Nubian aquifer source water: most samples could plausibly evolve from a source water with $\delta^{18}O$ of -14 to -12‰ and $\delta^{13}C$ of -6 to -4 ‰ (Fig. 7b). If travertines do share a similar source water, then, kinetic effects are a simpler explanation for the variability in travertine signatures than changing source water.

$^{87}Sr/^{86}Sr$ geochemistry of Western Desert travertines and groundwaters

The idea that Western Desert travertines broadly share a source water similar to modern groundwaters is supported by $^{87}Sr/^{86}Sr$ analysis, as the $^{87}Sr/^{86}Sr$ value of groundwaters generally reflects the composition of aquifer host rocks (e.g. Dogramaci and Herczeg, 2002). The $^{87}Sr/^{86}Sr$ composition of Western Desert travertines is very consistent across space (paleo-oasis areas) and time (different episodes of deposition), implying hydrological similarity between travertine source waters over the Pleistocene (Fig. 8, Table 2).

$^{87}Sr/^{86}Sr$ values of travertine at Refuf Pass, Wadi Midauwara, and Kurkur Oasis range from 0.70782 to 0.70799, suggesting equilibration in a carbonate aquifer. The marine limestone El Rufuf and Thebes Groups that underlie the Western Desert are the most likely carbonate sources for travertine (Fig. 1b, Fig. 2); although $^{87}Sr/^{86}Sr$ signatures have not been quantified for these units, late Paleocene-early Eocene marine values would suggest a $^{87}Sr/^{86}Sr$ signature of 0.7077-0.7076 (reflecting late Paleocene-early Eocene marine values; Denison et al., 1993). These values are consistent with analysis of Paleocene limestones and shales in the Eastern Desert of Egypt, which showed highly invariant $^{87}Sr/^{86}Sr$ values of ~0.7077 (Charisi and Schmitz, 1995). If Paleocene-Eocene

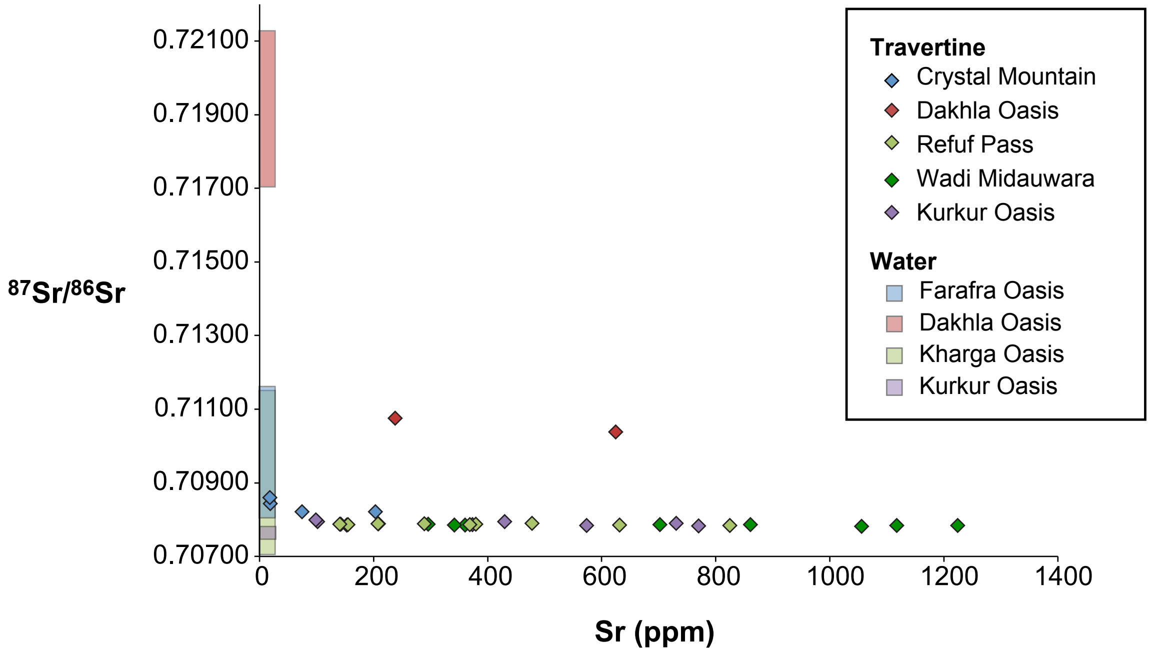

Figure 8. Sr concentrations plotted against $^{87}Sr/^{86}Sr$ values of Western Desert travertines; modern groundwater $^{87}Sr/^{86}Sr$ values are shown as rectangular fields along the vertical axis (Sr concentration in waters is very low in comparison to travertines). While travertine Sr concentrations vary widely over the Western Desert, $^{87}Sr/^{86}Sr$ values are remarkably constant over most paleo-oasis areas. Crystal Mountain samples are slightly radiogenic compared to most Western Desert samples, while Dakhla Oasis samples are markedly radiogenic. Modern water $^{87}Sr/^{86}Sr$ signatures are more variable than travertine signatures from the same oasis area, and tend to be higher; however, they show similar patterns, with very enriched values at Dakhla Oasis and more carbonate-like values at Farafra, Kharga, and Kurkur Oases.

limestone and shale units across the Western Desert have similarly monotonic $^{87}Sr/^{86}Sr$ signatures, then the consistency observed in $^{87}Sr/^{86}Sr$ of travertines would be expected. The slight enrichment in travertine $^{87}Sr/^{86}Sr$ compared to Paleocene-Eocene marine values could reflect the contributions of a deeper, more radiogenic component to the Nubian aquifer groundwater sourcing these travertines.

Samples from Crystal Mountain and Dakhla Oasis are enriched with respect to other paleo-oasis areas. Dakhla samples in particular have highly radiogenic $^{87}Sr/^{86}Sr$ signatures (0.71038 to 0.71076), suggesting a significant contribution of deep groundwater equilibrated with radiogenic crystalline basement rocks. An alternative hypothesis, that this signature is derived from interaction with sand at the surface of the Dakhla paleolake basin (0.716-0.7192 has been quoted as a value integrating modern Saharan dust; e.g., Box et al., 2011) seems unlikely given that spring and lake water geochemistry generally reflects source water, not basin characteristics (see Talbot, 1990; Li et al., 2008a). Additionally, modern Dakhla groundwaters pumped from depth have even more enriched $^{87}Sr/^{86}Sr$ signatures than their travertine counterparts, signifying that the radiogenic Sr is sourced at depth, not from the surface (Fig. 8). Crystal Mountain samples also show moderate $^{87}Sr/^{86}Sr$ enrichment (0.70821-0.70859), with more radiogenic signatures in samples from subaerial drapes than in groundwater speleothems (see Table 2).

The pattern of $^{87}Sr/^{86}Sr$ enrichment observed in travertine, with carbonate-like values at Kharga and Kurkur Oases, and more radiogenic values at Dakhla Oasis and Crystal Mountain (Farafra Oasis), is also present in modern groundwaters (Fig. 8). However, modern waters are generally more radiogenic than travertines, possibly because these waters are pumped from greater depth than past artesian flow, thus sourcing deeper groundwaters in contact with radiogenic crystalline rocks. Additionally, these deep waters would likely reside in the Nubian sandstone and have little time to acquire carbonate-like $^{87}Sr/^{86}Sr$ signatures by equilibration with shallower carbonate units.

The similarity in $^{87}Sr/^{86}Sr$ signatures between Western Desert travertines and modern Nubian groundwaters indicates that the Nubian aquifer could have been the primary groundwater source for these travertines. If travertine deposition were caused by precipitation recharging shallow aquifers at the paleo-oasis areas themselves, we might expect to see greater variation in $^{87}Sr/^{86}Sr$ over space or time. Finally, it is significant that Dakhla Oasis travertines and waters have far more radiogenic $^{87}Sr/^{86}Sr$ signatures than other areas, suggesting a distinct source water characterized by greater contributions from deep groundwater.

Groundwater sources for travertine

Together, stable isotope and $^{87}Sr/^{86}Sr$ data from travertines and modern groundwaters suggest that most Western Desert travertines are similar geochemically, and likely shared one groundwater source. Much of the variability in travertine stable isotopic signatures is probably attributable to kinetic effects as well as different systematics (spring systems versus lacustrine, subaerial samples versus dissolution caves, and ambient versus hydrothermal). Plotting $\delta^{13}C$ against $^{87}Sr/^{86}Sr$ illustrates this point well (Fig. 9); the majority of samples plot in one area, including Kharga and Kurkur Oasis samples as well as groundwater speleothem samples from Crystal Mountain, which have similar $\delta^{13}C$ but slightly higher $^{87}Sr/^{86}Sr$. This group of samples, which includes the majority of Western Desert travertines, has $^{87}Sr/^{86}Sr$ values slightly enriched with respect to Paleocene-Eocene seawater, and $\delta^{13}C$ signatures consistent with an endogenic CO_2 source (White et al., 1990; Zhang et al., 2008; Crossey et al., 2009), allowing for enrichment due to degassing in some samples. Drape samples from Crystal Mountain

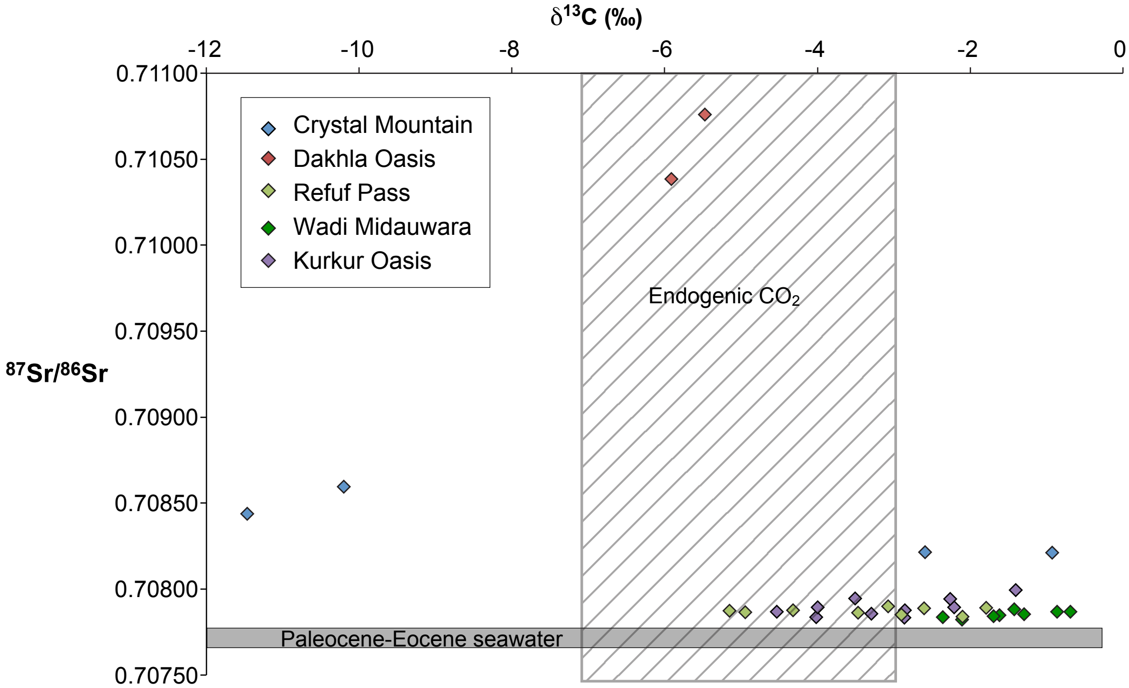

Figure 9. $\delta^{13}C$ versus $^{87}Sr/^{86}Sr$ of Western Desert travertine. Samples from Kharga and Kurkur Oases group with groundwater speleothem samples from Crystal Mountain; these samples resemble Paleocene-Eocene seawater in $^{87}Sr/^{86}Sr$ and have $\delta^{13}C$ signatures consistent with an endogenic CO_2 source. Dakhla Oasis samples form a distinct group that with very radiogenic $^{87}Sr/^{86}Sr$, although their $\delta^{13}C$ signatures are also endogenic. Drape samples from Crystal Mountain form a third group, with radiogenic $^{87}Sr/^{86}Sr$ values compared to the majority of Western Desert travertines, and extremely depleted $\delta^{13}C$ signatures.

and Dakhla Oasis samples form distinct groups, both depleted in $\delta^{13}C$ and enriched in $^{87}Sr/^{86}Sr$.

The geochemical characteristics of Western Desert travertine and modern groundwaters suggest that most of these travertines shared a consistent groundwater source, which likely had some deeply-derived component. These conclusions differ from those of previous researchers, however. Many authors argued that travertine table isotopic signatures were too depleted to have derived from a Nubian Aquifer source (Sultan et al., 1997; Smith et al., 2004a; Kieniewicz and Smith, 2007; Kieniewicz and Smith, 2009). Instead, Sultan et al. (1997) proposed that travertine source water came from westerly winds pushing Atlantic moisture over North Africa, while Smith et al. (2004) and Kieniewicz and Smith (2007; 2009) invoked a lighter Indian Ocean moisture source.

Consistency in $^{87}Sr/^{86}Sr$ and stable isotopic signatures across most oasis areas imply a similar source water for all paleo-oasis areas and over multiple episodes of travertine deposition. While there is evidence for direct precipitation over the Western

Desert, such as lakebeds requiring at least some meteoric precipitation at Dakhla Oasis (Kieniewicz and Smith, 2009) and buried drainage channels throughout Egypt implying significant drainage across the surface of the Western Desert (McCauley et al., 1982), we suggest that local meteoric recharge was not the most significant water source for Western Desert travertines. Nubian aquifer calcite-water equivalents are depleted in $\delta^{13}C$ and $\delta^{18}O$ in comparison to most Western Desert travertines, but these could plausibly evolve to the travertine values we measured via kinetic processes.

The suggestion that Western Desert oasis groundwater is primarily fed by deep, remote contributions is supported by previous research: comparing U concentration, ^{234}U excess, and $^{234}U/^{238}U$ activity ratios, Dabous and Osmond (2001) concluded that southern oases (including Dakhla and Kharga) had a very high proportion of deeply-sourced water. They estimated that local meteoric recharge accounted for only about 4% of groundwater at Kharga Oasis, and 8% at Dakhla Oasis; even at Farafra Oasis, further to the north, Dabous and Osmond calculated that ~26% of groundwater was derived from local recharge. Thus, other lines of evidence support the link between remote pluvial recharge feeding oasis springs.

Travertine as a pluvial indicator

Figure 10 shows our compilation of travertine geochronology (to 400 ka, which is the range within which U/Th dating precision allows for paleoclimate correlations), alongside marine pluvial indicators and potential forcings: glacial cycles, sapropels from the eastern Mediterranean Sea (Larrasoaña et al., 2003), and the monsoon index (calculated after Rossignol-Strick, 1983; Colleoni et al., 2012).

We note, first, that travertine deposition shows little association with glacial cycles, occurring across both odd and even MIS. This conclusion is contrary to many previous authors' conclusions that travertine tended to deposit during interglacial periods (Crombie et al., 1997; Smith et al., 2004b) and more generally that the terrestrial record of North African pluvial periods demonstrates glacial cycle control (Szabo et al., 1995; Kieniewicz and Smith, 2009). While the operation of high-latitude teleconnections has been postulated, and shown in model simulations (Tuenter et al., 2003; Bosmans et al., 2012), further work is necessary to investigate this possibility.

A second major result of our compilation of travertine geochronology is the apparent correlation between travertine deposition and sapropels, and thus pluvial episodes. Travertine accumulations do seem to occur synchronously with or shortly after sapropels in many instances (Fig. 10). The fact that travertine depositional episodes do not accompany every sapropel, especially before ~250 ka, is more likely related to gaps

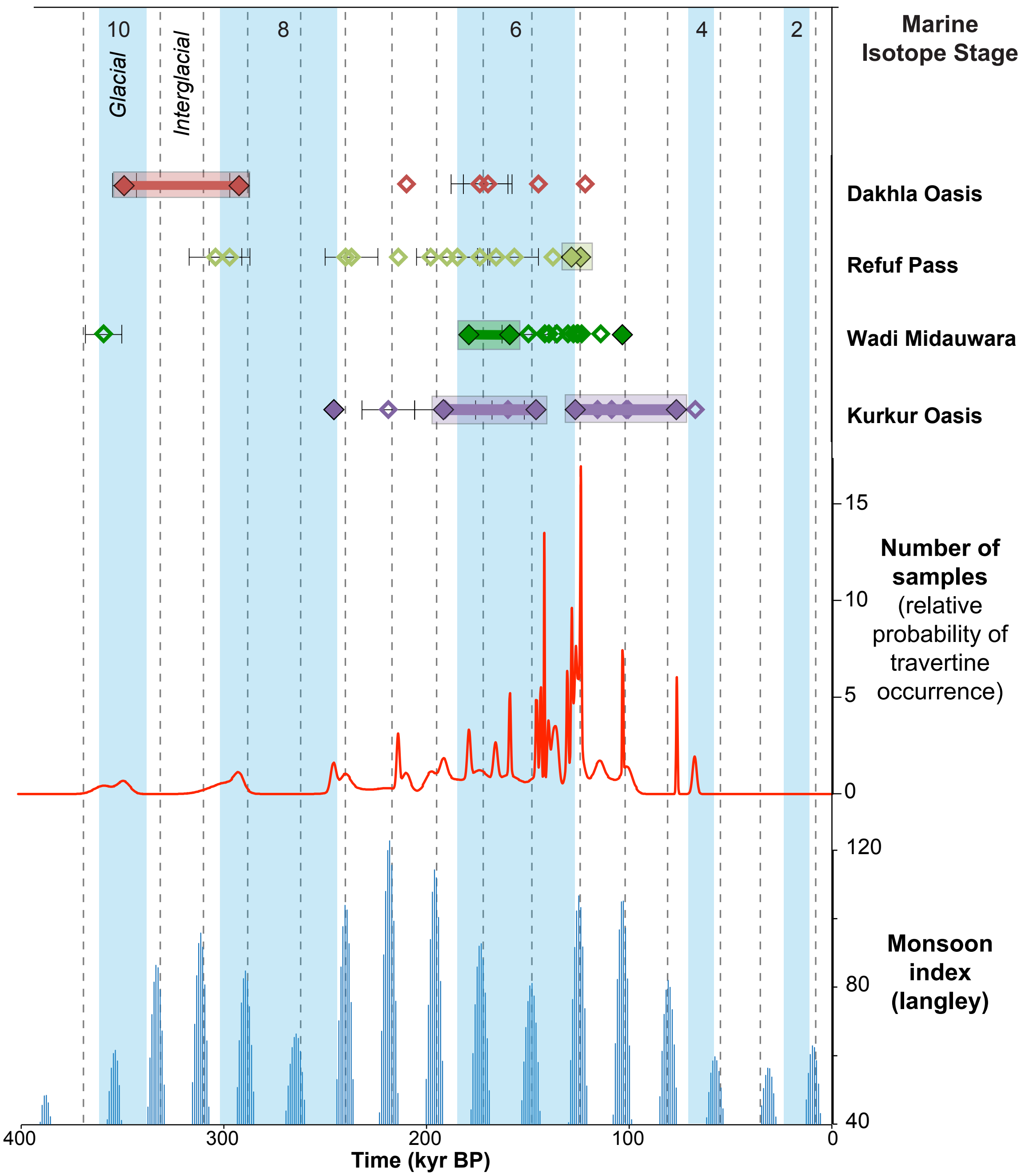

Figure 10. Travertine occurrence plotted against climatic forcings. From top to bottom: glacial marine isotope stages (MIS) are indicated in blue; compiled travertine geochronology by oasis area (error bars are shown unless they are smaller than data points); probability density graph of travertine samples; the African monsoon index (calculated after Rossignol-Strick, 1983, and Colleoni et al., 2012). Vertical dotted lines are sapropels from Site 967 in the eastern Mediterranean (Larrasoaña et al., 2003).

in travertine sampling than a fundamental change in the North African monsoon over land, or the relationship between travertine and pluvial forcing.

Some of the difference between timing of travertine deposition and sapropels may derive from each proxy's distinct response to monsoonal rains. First, Mediterranean sapropels have an error from 2000 to 5000 years, which includes some lag between monsoon initiation and the onset of Mediterranean deep water anoxia (Emeis et al., 2000; Lourens et al., 2001; Emeis et al., 2003; Rohling et al., 2002), so that the chronology has varying precision. In contrast, while U/Th dates on travertine are generally more precise, at least after ~300 ka, travertine would not deposit immediately after monsoon recharge occurred. Some lag time would be present, depending on the time necessary for transmission of higher pressure to Egyptian oasis areas; this lag time could vary depend on where recharge occurs in the Nubian basin.

Thus, although the rough correspondence in the timing of travertine deposition and sapropels suggests that both proxies respond to the same ultimate forcing, differences intrinsic to each record could cause variable offsets in timing. While the regularity of sapropels in the marine record is likely due to the integration of a large regional signal, that heterogeneity of monsoon rains on a smaller spatial scale could be more important for terrestrial proxies. The geographic extent of a given monsoon/pluvial episode could determine whether and when Nubian recharge areas received precipitation; the amount of precipitation could also impact whether travertine deposition occurred across all oasis areas or just those closest to recharge areas.

Lastly, we note that the presence of significant deposition between 650 ka and 1 Ma (based on δ^{234}U model ages ages), implies that significant pluvial episodes occurred over North Africa before and during the mid-Pleistocene transition, although the sapropel record is punctuated by gray intervals at this time (Almogi-Labin, 2011). Based on the significant deposition we observe earlier in the Pleistocene, relative to lesser deposition restricted to only some oasis areas later, we suggest that moisture availability declined throughout our record.

CONCLUSIONS

Our compiled dataset, including new, high-precision geochronology coupled to stratigraphic context and multi-tracer geochemistry, has significant implications for the timing and nature of travertine deposition in the Western Desert.

1) Travertines over most of the Western Desert share a consistent groundwater source similar to Nubian Aquifer groundwaters, depleted in δ^{13}C and δ^{18}O, and with a consistent, Paleocene to Eocene-like carbonate source based on ^{87}Sr/^{86}Sr.

We conclude, contrary to previous studies, that travertine deposition was fueled by remote recharge to the Nubian Aquifer, with only secondary contributions from local meteoric recharge.

2) Dakhla Oasis has distinct geochemical characteristics, with very enriched $^{87}Sr/^{86}Sr$ indicative of deep groundwater contributions. The presence of highly radiogenic signatures at Dakhla is suggestive, though, that the entire Nubian system may have fault-influenced hydrochemistry.

3) Travertine deposited episodically over the late Pleistocene in Egypt's Western Desert, with especially large episodes at approximately 130 ka and between 450-600 ka.

4) The first direct dates on the Dakhla paleolake deposits imply that the lake was much older than previously assumed, roughly 290-350 ka.

5) Travertine depositional peaks roughly coincide with sapropels, suggesting that travertine is indeed a record of pluvial episodes, and follows the same precessional forcing as marine records.

6) Travertine deposition occurs during both odd and even MIS stages, showing that it is likely oversimplistic to interpret Western Desert pluvials based on glacial cycles, a common practice in previous literature.

Travertine from Egypt's Western Desert constitutes a promising terrestrial paleohydrologic record which has the potential to offer paleoclimatic insight, as well as adding to an understanding of past North African hydroclimates, with implications for managing modern water resources. The improved chronology we report, and its link to regionally important and well-constrained climatic forcings, also helps to set the climatic backdrop of a key period in human history, potentially informing evolutionary theory and helping to identify the timing of migration corridors (deMenocal, 2004; Trauth et al., 2009; Blome et al., 2012).

LIST OF APPENDICES

Appendix 1
Geochronology and stratigraphic context of travertine samples from previous studies

Sample ID	Study	Site description	Sample description	Reported U/Th age	+/- error
Dakhla Oasis					
MRK1988-DAK-2a	Kleindienst et al., 2008	Wadi el-Ueb	travertine float block on P-III terraced gravels	122000	9000
MRK1988-DAK-2b	Kleindienst et al., 2008	Wadi el-Ueb	travertine float block on P-III terraced gravels	145000	6000
Churcher 1985 a	Kleindienst et al., 2008	N of Maohoub	travertine float block on scarp colluvium	170000	12000
Churcher 1985 b	Kleindienst et al., 2008	N of Maohoub	travertine float block on scarp colluvium	174000	14000
K. Nicoll Eg96-182	Kleindienst et al., 2008	E of Sheikh Muftah, on Tawil anticline	travertine float block	210000	4000
Kharga Oasis: Refuf Pass vicinity					
92 REF-2	Kleindienst et al., 2008	Railway km 147	Tufa #4	166000	2000
92 REF-3	Kleindienst et al., 2008	Railway km 148	Tufa #4	297000	10000
92 REF-6	Kleindienst et al., 2008	Railway km 148	Tufa #4	304000	13000
96 REF-3	Kleindienst et al., 2008	Railway km 148.5, Locus VII	Tufa #4	125000	1600
RP- 103 (1995)	Kleindienst et al., 2008	Railway km 148.5, Locus VII	Tufa #3/#4-intercalated	138000	2000
RP- 104 (1995)	Kleindienst et al., 2008	Railway km 148.5, Locus VII	Tufa #3	237000	13000
92 REF-9	Kleindienst et al., 2008	Railway km 148.6	Tufa #3	214000	1400
92 REF-8	Kleindienst et al., 2008	Railway cut km149	Tufa #3	124000	600
96 REF-4	Kleindienst et al., 2008	Railway km 149.8, Locus IV	Tufa #3	240000	5000
96 REF-5	Kleindienst et al., 2008	Railway km 149.8, Locus IV	Tufa #3	198000	5000
RP- 105 (1995)	Kleindienst et al., 2008	Railway km149	Tufa #2	174000	7000
NASTF-8	Sultan et al., 1997	Gebel El Yabisa (Refuf group)	travertine from mear top of escarpment	185000	15000
AT-3	Sultan et al., 1997	Gebel El Agouz (Refuf group)	travertine from dissolution cave	190000	15000
AT-5	Sultan et al., 1997	Gebel El Agouz (Refuf group)	travertine	157000	12000
Kharga Oasis: Wadi Midauwara vicinity					
WM033	Smith et al., 2004a	Wadi Midauwara	Wadi Tufa 3	136000	3000
WM010	Smith et al., 2004a	Wadi Midauwara	Wadi Tufa 2	126000	4000
WM045	Smith et al., 2004a	Wadi Midauwara	Wadi Tufa 2	140000	1200
MAT001T2	Smith et al., 2004a	Mata'na	Wadi Tufa 2	142000	300
WM035	Smith et al., 2004a	Wadi Midauwara	Scarp	150000	13000
WM049	Smith et al., 2004a	Wadi Midauwara	Plateau tufa	359000	9000
01-MAT-001G	Smith et al., 2007	Mata'na Site G	Wadi tufa	127892	1300
NB-01-03B (KH/BQ-04)	Smith et al., 2007	Bulaq, Wadi 3 Locus 1	Wadi tufa	114395	4193
WM-037B	Smith et al., 2007	Wadi Midauwara	Wadi tufa	125665	2500
WM-037Ba	Smith et al., 2007	Wadi Midauwara	Wadi tufa	123840	3645
WM-E10	Smith et al., 2007	Wadi Midauwara	Wadi tufa	136039	2200
WM-E10a	Smith et al., 2007	Wadi Midauwara	Wadi tufa	130532	2832
Kurkur Oasis					
E95-10	Crombie et al., 1997	---	wadi travertine (north)	68000	2000
E95-20	Crombie et al., 1997	---	wadi travertine (north)	102000	6000
E95-11	Crombie et al., 1997	---	wadi travertine (north)	101000	5000
E95-7B	Crombie et al., 1997	---	wadi travertine (north)	109000	6000
E95-13	Crombie et al., 1997	---	wadi travertine (south)	116000	6000
E95-12	Crombie et al., 1997	---	wadi travertine (south)	160000	8000
E95-14A	Crombie et al., 1997	---	wadi travertine (south)	219000	13000
E95-4	Crombie et al., 1997	---	mound travertine	191000	15000

Notes:
-Sample and site descriptions are from the original authors, as is reported U/Th age. Errors are 2σ.

Appendix 2
Geochemistry of travertine samples from previous studies

Sample ID	Study	Site description	Sample description	$\delta^{13}C$ (‰)	$\delta^{18}O$ (‰)
Dakhla Oasis					
B20-121	Kienewicz and Smith, 2009	Balat	carbonate sediment	-6	-9
B20-197	Kienewicz and Smith, 2009	Balat	carbonate sediment	-6.6	-9.1
B20-76	Kienewicz and Smith, 2009	Balat	carbonate sediment	-5	-8.5
B35-50	Kienewicz and Smith, 2009	Balat	carbonate sediment	-2.9	-7.7
B4-143	Kienewicz and Smith, 2009	Balat	carbonate sediment	-3.5	-7.6
B4-203	Kienewicz and Smith, 2009	Balat	carbonate sediment	-2.3	-7.5
B4-260	Kienewicz and Smith, 2009	Balat	carbonate sediment	-6.1	-7.9
B4-390	Kienewicz and Smith, 2009	Balat	carbonate sediment	-6.6	-7.4
B4-445	Kienewicz and Smith, 2009	Balat	carbonate sediment	-6.2	-6.4
B4-73	Kienewicz and Smith, 2009	Balat	carbonate sediment	-3.5	-8.5
B28-198	Kienewicz and Smith, 2009	Balat	carbonate sediment	-5.6	-9.8
B28-50	Kienewicz and Smith, 2009	Balat	carbonate sediment	-5.5	-9.5
B28-95	Kienewicz and Smith, 2009	Balat	carbonate sediment	-6.8	-9.9
B28-145	Kienewicz and Smith, 2009	Balat	carbonate sediment	-6.5	-9.9
B15-146	Kienewicz and Smith, 2009	Balat	carbonate sediment	-6.3	-8.3
B15-246	Kienewicz and Smith, 2009	Balat	carbonate sediment	-6.7	-8.7
B15-66	Kienewicz and Smith, 2009	Balat	carbonate sediment	-2.6	-9.8
B15-96	Kienewicz and Smith, 2009	Balat	carbonate sediment	-4.2	-8.1
D11-115	Kienewicz and Smith, 2009	Kellis	carbonate sediment	-3.4	-9.3
D11-215	Kienewicz and Smith, 2009	Kellis	carbonate sediment	-2.8	-9
D11-265	Kienewicz and Smith, 2009	Kellis	carbonate sediment	-0.8	-9.7
D11-315	Kienewicz and Smith, 2009	Kellis	carbonate sediment	-0.3	-9.8
D11-387	Kienewicz and Smith, 2009	Kellis	carbonate sediment	-4.1	-8
D11-407	Kienewicz and Smith, 2009	Kellis	carbonate sediment	-6.9	-8.3
D11-427	Kienewicz and Smith, 2009	Kellis	carbonate sediment	-7.2	-8.5
D11-467	Kienewicz and Smith, 2009	Kellis	carbonate sediment	-6.8	-9
D11-477	Kienewicz and Smith, 2009	Kellis	carbonate sediment	-5.9	-8.2
D11-482	Kienewicz and Smith, 2009	Kellis	carbonate sediment	-8.1	-8
D11-495	Kienewicz and Smith, 2009	Kellis	carbonate sediment	-8.2	-8.5
D11-504	Kienewicz and Smith, 2009	Kellis	carbonate sediment	-7.5	-8
D11-509	Kienewicz and Smith, 2009	Kellis	carbonate sediment	-8.5	-8.1
D11-519	Kienewicz and Smith, 2009	Kellis	carbonate sediment	-9.1	-8.5
D11-524	Kienewicz and Smith, 2009	Kellis	carbonate sediment	-8.3	-8
D11-574	Kienewicz and Smith, 2009	Kellis	carbonate sediment	-9.1	-8.7
D11-589	Kienewicz and Smith, 2009	Kellis	carbonate sediment	-7.1	-8.3
D11-594	Kienewicz and Smith, 2009	Kellis	carbonate sediment	-6.9	-8.3
D11-604	Kienewicz and Smith, 2009	Kellis	carbonate sediment	-7.9	-8.1
D11-614	Kienewicz and Smith, 2009	Kellis	carbonate sediment	-7.5	-8.3
D11-634	Kienewicz and Smith, 2009	Kellis	carbonate sediment	-7.7	-8.6
D11-644	Kienewicz and Smith, 2009	Kellis	carbonate sediment	-8.9	-7.9
D11-654	Kienewicz and Smith, 2009	Kellis	carbonate sediment	-8.3	-8
D11-664	Kienewicz and Smith, 2009	Kellis	carbonate sediment	-9.3	-9
Y2K DOP1	Kienewicz and Smith, 2009		escarpment tufa	-3.6	-11.3
Y2K DOP2	Kienewicz and Smith, 2009		escarpment tufa	-1.2	-9.1
JS DOPT2	Kienewicz and Smith, 2009		escarpment tufa	-1.5	-10.5
JS DOPT3	Kienewicz and Smith, 2009		escarpment tufa	-0.8	-11.4
JS DOPT4	Kienewicz and Smith, 2009		escarpment tufa	-9.5	-11
JS Y2K6	Kienewicz and Smith, 2009		escarpment tufa	-2.2	-9.5
Kharga Oasis: Refuf Pass and vicinity					
unknown	Smith et al., 2004	Rizeikat/ Matana	travertine	-3.28	-11.78
unknown	Smith et al., 2004	Rizeikat/ Matana	travertine	-0.99	-9.4
unknown	Smith et al., 2004	Rizeikat/ Matana	travertine	1.33	-8.33

unknown	Smith et al., 2004	Rizeikat/ Matana	travertine	-2.87	-10.99
unknown	Smith et al., 2004	Rizeikat/ Matana	travertine	-3.49	-11.29
unknown	Smith et al., 2004	Rizeikat/ Matana	travertine	-3.15	-11.17
unknown	Smith et al., 2004	Rizeikat/ Matana	travertine	-0.03	-9.75
unknown	Smith et al., 2004	Rizeikat/ Matana	travertine	-1.63	-8.57
unknown	Smith et al., 2004	Bulaq	travertine	-2.06	-8.52
unknown	Smith et al., 2004	Bulaq	travertine	-2.93	-9.33
unknown	Smith et al., 2004	Bulaq	travertine	-1.74	-10.36
Kharga Oasis: Wadi Midauwara					
unknown	Smith et al., 2004	Wadi Midauwara	travertine	-0.58	-9.5
unknown	Smith et al., 2004	Wadi Midauwara	travertine	0.66	-8.88
unknown	Smith et al., 2004	Wadi Midauwara	travertine	-0.45	-9.69
unknown	Smith et al., 2004	Wadi Midauwara	travertine	-0.18	-7.44
unknown	Smith et al., 2004	Wadi Midauwara	travertine	-0.29	-9.53
unknown	Smith et al., 2004	Wadi Midauwara	travertine	-1.56	-9.37
unknown	Smith et al., 2004	Wadi Midauwara	travertine	-1.27	-9.33
unknown	Smith et al., 2004	Wadi Midauwara	travertine	-0.58	-9.02
unknown	Smith et al., 2004	Wadi Midauwara	travertine	-2.2	-9.1
unknown	Smith et al., 2004	Wadi Midauwara	travertine	-0.06	-11.31
unknown	Smith et al., 2004	Wadi Midauwara	travertine	0.92	-8.69
unknown	Smith et al., 2004	Wadi Midauwara	travertine	0.18	-11.26
unknown	Smith et al., 2004	Wadi Midauwara	travertine	-4.35	-11.4
unknown	Smith et al., 2004	Wadi Midauwara	travertine	-4.39	-10.37
unknown	Smith et al., 2004	Wadi Midauwara	travertine	-0.24	-9.16
unknown	Smith et al., 2004	Wadi Midauwara	travertine	1.17	-7.9
unknown	Smith et al., 2004	Wadi Midauwara	travertine	-5.13	-11.9
unknown	Smith et al., 2004	Wadi Midauwara	travertine	-2.21	-8.89
unknown	Smith et al., 2004	Wadi Midauwara	travertine	-0.93	-9.38
unknown	Smith et al., 2004	Wadi Midauwara	travertine	-0.45	-7.99
unknown	Smith et al., 2004	Wadi Midauwara	travertine	-0.06	-7.01
unknown	Smith et al., 2004	Wadi Midauwara	travertine	0.04	-5.8
unknown	Smith et al., 2004	Wadi Midauwara	travertine	0.71	-6.29
unknown	Smith et al., 2004	Wadi Midauwara	travertine	-0.3	-8.07
unknown	Smith et al., 2004	Wadi Midauwara	travertine	-0.38	-8.3
unknown	Smith et al., 2004	Wadi Midauwara	travertine	-0.17	-8.87
unknown	Smith et al., 2004	Wadi Midauwara	travertine	-0.52	-8.45
Kurkur Oasis					
E95-10	Crombie et al., 1997	Kurkur	wadi travertine (north)	-1.5	-12.99
E95-20	Crombie et al., 1997	Kurkur	wadi travertine (north)	-3	-13.76
E95-11	Crombie et al., 1997	Kurkur	wadi travertine (north)	-3.2	-13.47
E95-7B	Crombie et al., 1997	Kurkur	wadi travertine (north)	-3.2	-13.67
E95-13	Crombie et al., 1997	Kurkur	wadi travertine (south)	-3.1	-13.08
E95-12	Crombie et al., 1997	Kurkur	wadi travertine (south)	-3.1	-13.57
E95-14A	Crombie et al., 1997	Kurkur	wadi travertine (south)	-3	-11.43
E95-4	Crombie et al., 1997	Kurkur	mound travertine	-1.2	-12.02
E95-5	Crombie et al., 1997	Kurkur	mound travertine	0	-10.07
E95-9	Crombie et al., 1997	Kurkur	plateau travertine	-1.4	-12.60
E95-15A	Crombie et al., 1997	Kurkur	plateau travertine	-3.3	-9.88
E95-17	Crombie et al., 1997	Kurkur	plateau travertine	-2.1	-9.10
E95-8	Crombie et al., 1997	Kurkur	plateau travertine	-1.6	-9.49
E95-19	Crombie et al., 1997	Kurkur	plateau travertine	-1.1	-12.02

Notes:
-Stable isotopic ratios are reported relative to VPDB.

Appendix 3
List of samples (this study)

Sample ID	Geochronology	Geochemistry	Latitude	Longitude
Crystal Mountain				
K11E-CRYS-3	---	C,O	27.661122	28.431196
K11E-CRYS-4	U/Th	C,O; Sr	27.661122	28.431196
K11E-CRYS-4B	model age	C,O; Sr	27.661122	28.431196
K11E-CRYS-5	secular equilibrium	C,O; Sr	27.661122	28.431196
K11E-CRYS-6	---	C,O	27.661122	28.431196
K11E-CRYS-7A	model age	C,O; Sr	27.660527	28.431939
K11E-CRYS-7B	---	C,O	27.660527	28.431939
Dakhla Oasis				
K12E-DAK-14	---	C,O	25.475119	29.110658
K12E-DAK-15A	---	C,O	25.474572	29.111047
K12E-DAK-15B	---	C,O	25.474572	29.111047
K12E-DAK-17	U/Th	C,O; Sr	25.51423	29.178466
K12E-DAK-18A	---	C,O	25.507979	29.182392
K12E-DAK-18B	U/Th	C,O; Sr	25.507979	29.182392
Kharga Oasis: Refuf Pass				
K12E-KHAR-20	U/Th	C,O; Sr	25.679802	30.812764
K12E-KHAR-21	U/Th	C,O; Sr	25.679811	30.812803
K12E-KHAR-22	---	C,O	25.680063	30.816365
K12E-KHAR-23	---	C,O	25.67845	30.817719
K12E-KHAR-24	---	C,O	25.676673	30.818389
K12E-KHAR-30	U/Th	C,O; Sr	25.677807	30.821197
K12E-KHAR-31	U/Th	C,O; Sr	25.678347	30.821665
K12E-KHAR-32	U/Th	C,O; Sr	25.678912	30.822033
K12E-KHAR-33	U/Th	C,O; Sr	25.682876	30.822121
K12E-KHAR-34	U/Th	C,O; Sr	25.683026	30.821949
K12E-KHAR-35	U/Th	C,O; Sr	25.684433	30.822451
K12E-KHAR-36	U/Th	C,O; Sr	25.684398	30.822501
K12E-KHAR-37	U/Th	C,O; Sr	25.684398	30.822501
Kharga Oasis: Wadi Midauwara				
K12E-MIDA-40	U/Th	C,O; Sr	24.960771	31.060566
K12E-MIDA-41	---	C,O	24.958262	31.068934
K12E-MIDA-42	---	C,O	24.95817	31.06952
K12E-MIDA-43	model age	C,O; Sr	24.958458	31.0701
K12E-MIDA-44	---	C,O	24.958206	31.070163
K12E-MIDA-45	model age	C,O; Sr	24.958257	31.069914
K12E-MIDA-46	model age	C,O; Sr	24.959642	31.065347
K12E-MIDA-47	U/Th	C,O; Sr	24.96034	31.064881
K12E-MIDA-47B	U/Th	C,O; Sr	24.96034	31.064881
K12E-MIDA-48	U/Th	C,O; Sr	24.959873	31.062333
K12E-MIDA-48C	U/Th	C,O; Sr	24.959873	31.062333
Kurkur Oasis				
K12E-KUR-50	---	C,O	23.888176	32.323048
K12E-KUR-51	---	C,O	23.888304	32.32342
K12E-KUR-52	U/Th	C,O; Sr	23.892264	32.322398
K12E-KUR-53	U/Th	C,O; Sr	23.892352	32.325983
K12E-KUR-54	---	C,O	23.892352	32.325983
K12E-KUR-55	U/Th	C,O; Sr	23.891957	32.326397
K12E-KUR-56	U/Th	C,O; Sr	23.891957	32.326397
K12E-KUR-58	U/Th	C,O; Sr	23.898155	32.32496
K12E-KUR-59	model age	C,O; Sr	23.905869	32.325107
K12E-KUR-60	model age	C,O; Sr	23.905869	32.325107
K12E-KUR-61	---	C,O	23.905617	32.325226
K12E-KUR-62	model age	C,O; Sr	23.905671	32.325295
K12E-KUR-63	U/Th	C,O; Sr	23.906209	32.324388
K12E-KUR-64	---	C,O	23.906191	32.324349
K12E-KUR-65	U/Th	C,O; Sr	23.906145	32.324212
K12E-KUR-65B	---	C,O	23.880896	32.298913
K12E-KUR-66	---	C,O	23.880758	32.298295
K12E-KUR-67	---	C,O	23.887198	32.292533
K12E-KUR-68	---	C,O	23.88699	32.292348
K12E-KUR-69	---	C,O	23.886437	32.293932

Sample site locations

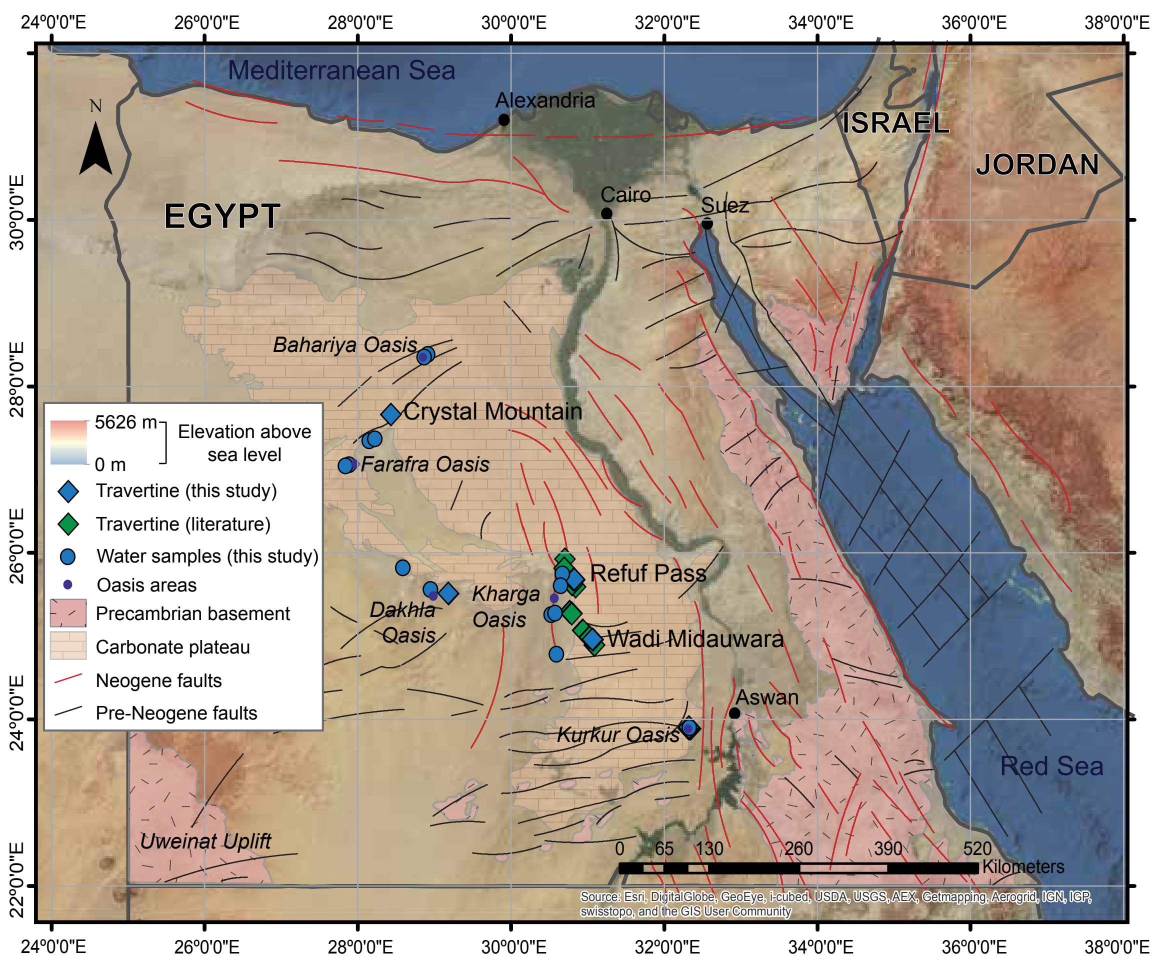

Crystal Mountain

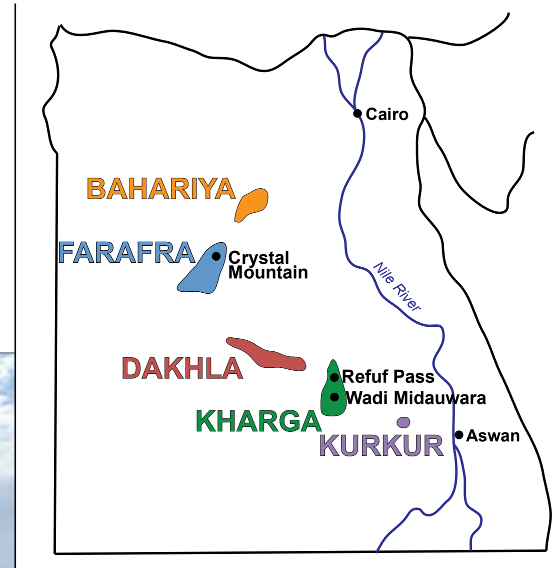

Crystal Mountain

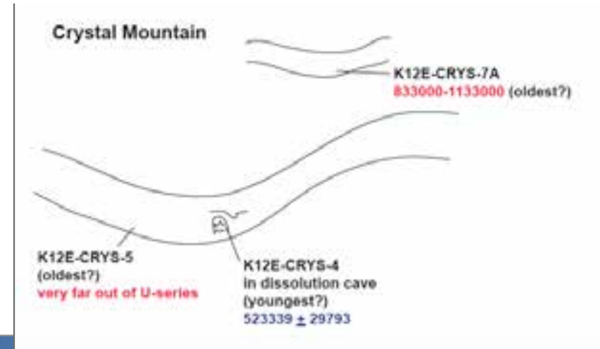

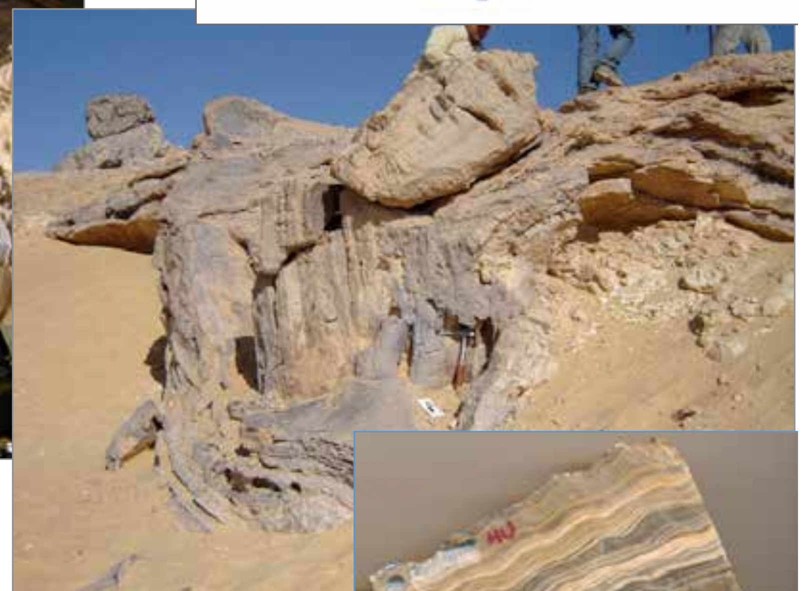

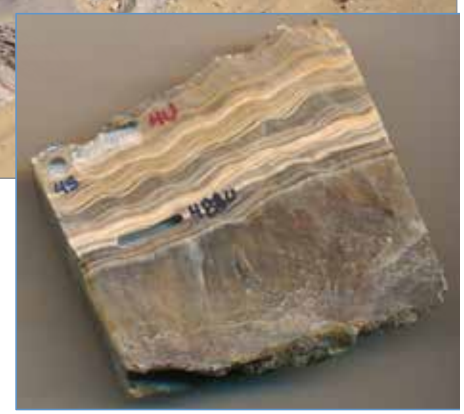

K12E-CRYS-4 (523339 ± 29793)
Exterior bands of flowstone rind w/sparry core; youngest travertine?

K12E-CRYS-4B (1397 ± 181 ka)
Interior bands of flowstone rind

Crystal Mountain

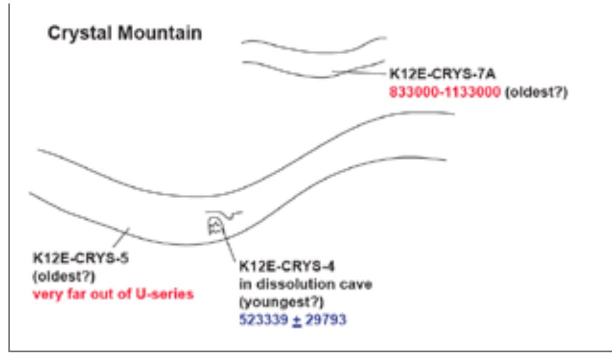

K12E-CRYS-5 (secular equilibrium)

Fine sparry layer just above contact w/Tarawan chalk; probably the oldest travertine.

Crystal Mountain

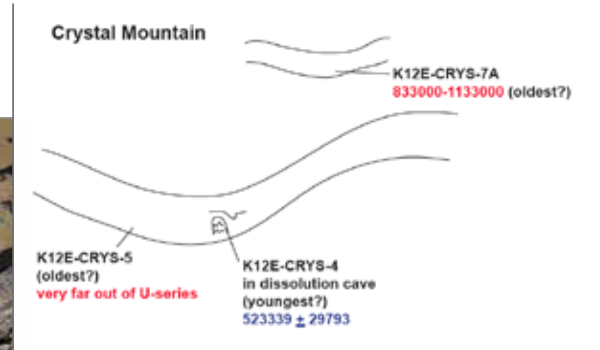

K12E-CRYS-7A (1014 ± 119 ka)

drape in hillside (uphill from previous samples).

Crystal Mountain—not dated

K12E-CRYS-3, 6, 7B

Dakhla Oasis

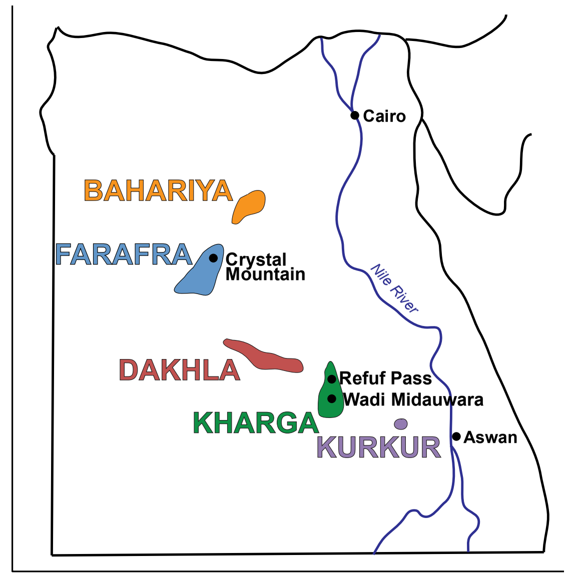

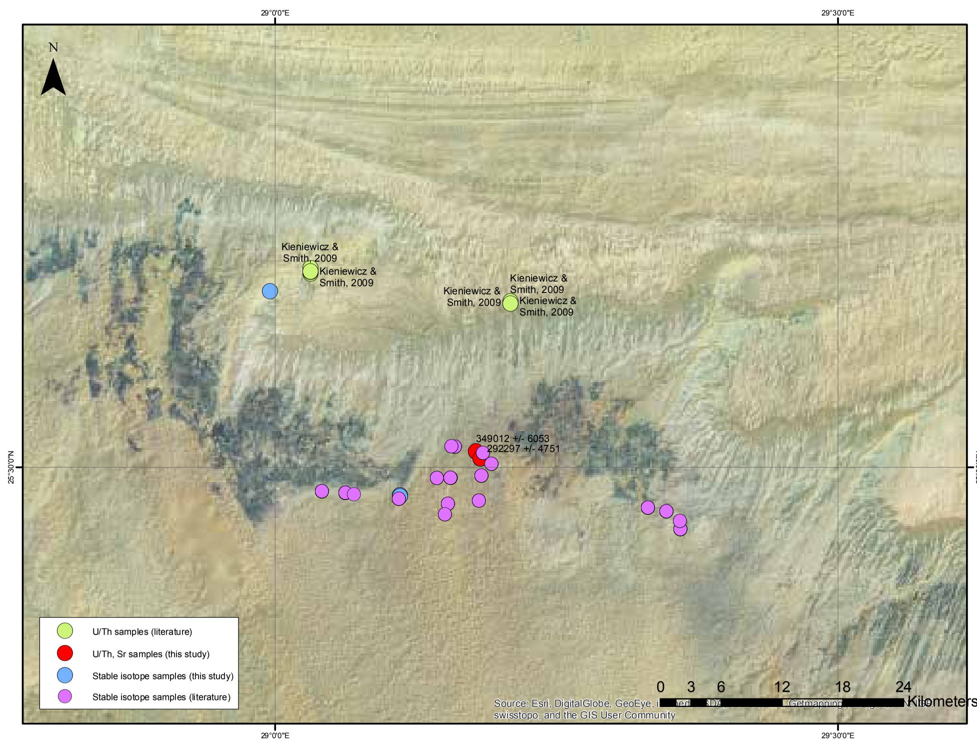

Dakhla

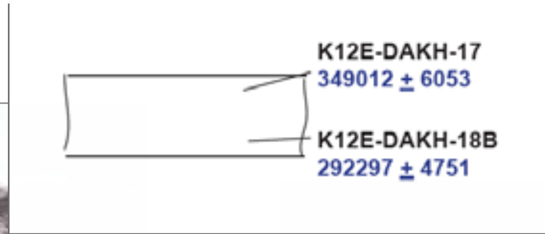

K12E-DAKH-17U (349012 ± 6053)

micritic layer at top of lakebeds

Dakhla

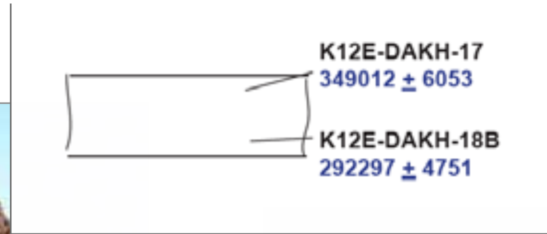

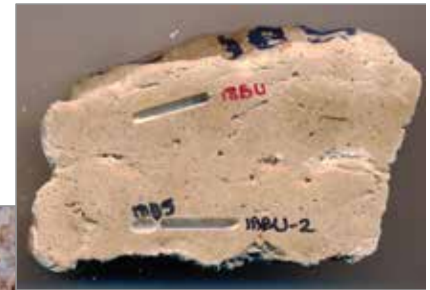

K12E-DAKH-18BU (292297 ± 4751)

~3cm layer at bottom of lakebeds overlying shale

Dakhla Oasis—not dated

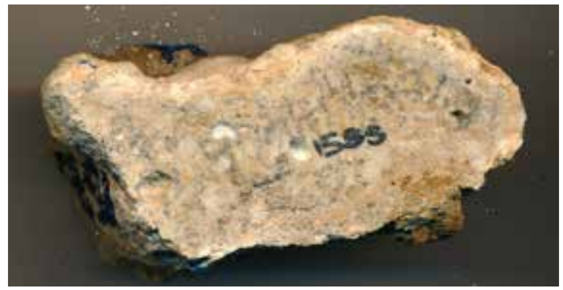

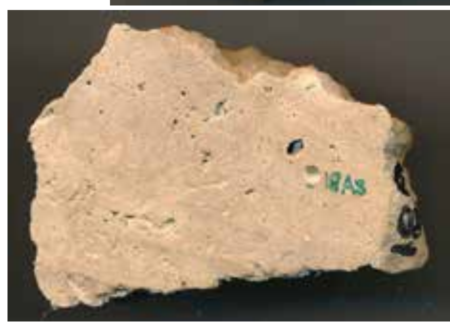

K12E-DAKH-14, 15A, 15B, 18A

Refuf Pass

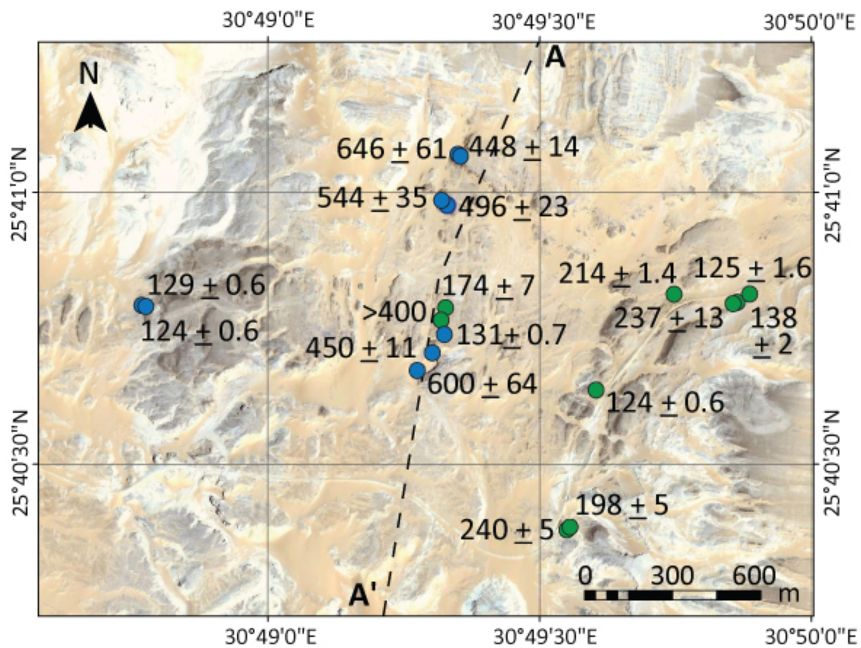
30°49'0"E
30°49'30"E
30°50'0"E
25°41'0"N
25°40'30"N
N
A
A'
646 ± 61
448 ± 14
544 ± 35
496 ± 23
129 ± 0.6
124 ± 0.6
174 ± 7
>400
131± 0.7
450 ± 11
600 ± 64
214 ± 1.4
125 ± 1.6
237 ± 13
138
± 2
124 ± 0.6
198 ± 5
240 ± 5
0 300 600 m

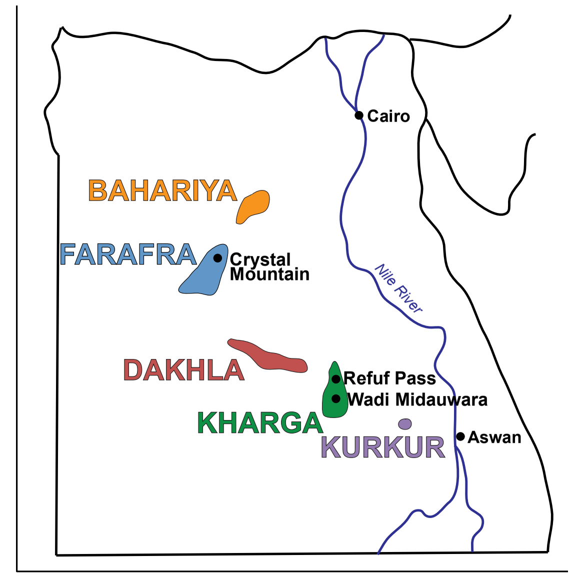
Cairo
BAHARIYA
FARAFRA
Crystal Mountain
Nile River
DAKHLA
Refuf Pass
Wadi Midauwara
KHARGA
KURKUR
Aswan

Refuf Pass- 1

K12E-KHAR-30U (600220 ± 63819)
base of Level 1, sitting atop gravels

Refuf Pass- 1

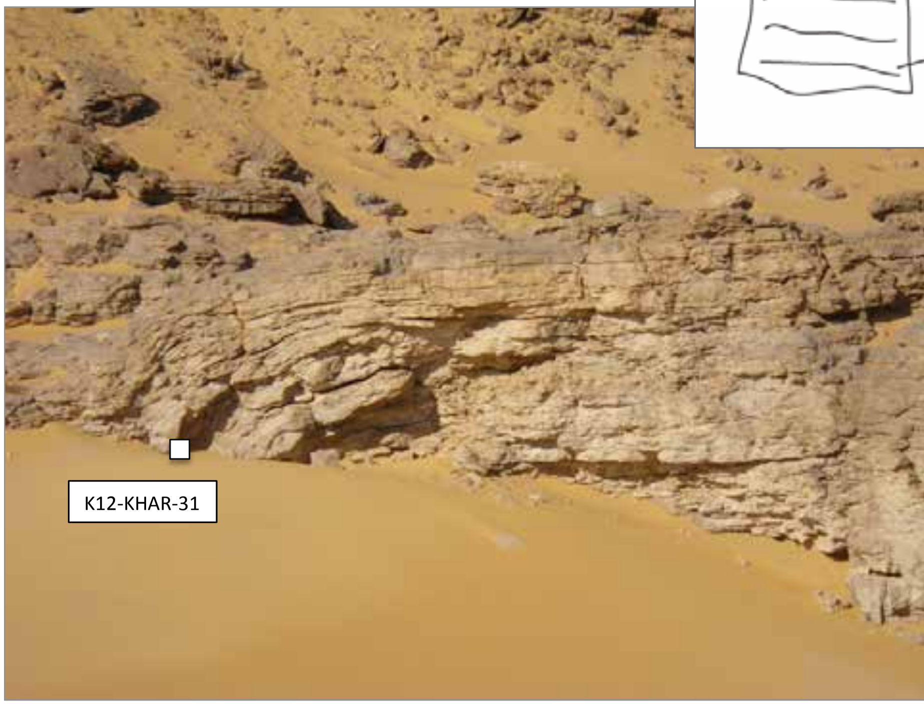

K12E-KHAR-31U (449554 ± 10520)

~1m from top of large drape in 4m section of Level 1

Refuf Pass-2

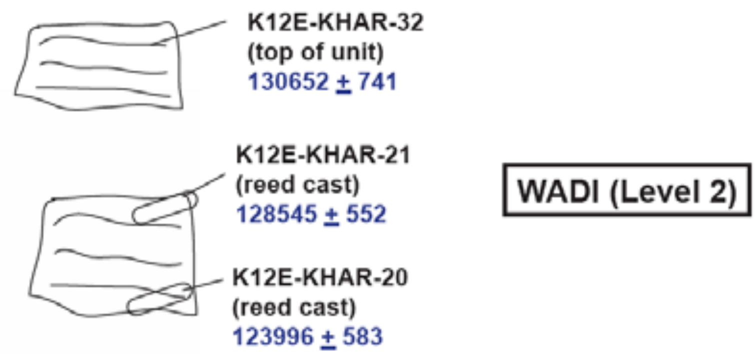

K12E-KHAR-20U (123996 ± 583)

large root cast at bottom of mid-level outcrop

Refuf Pass-2

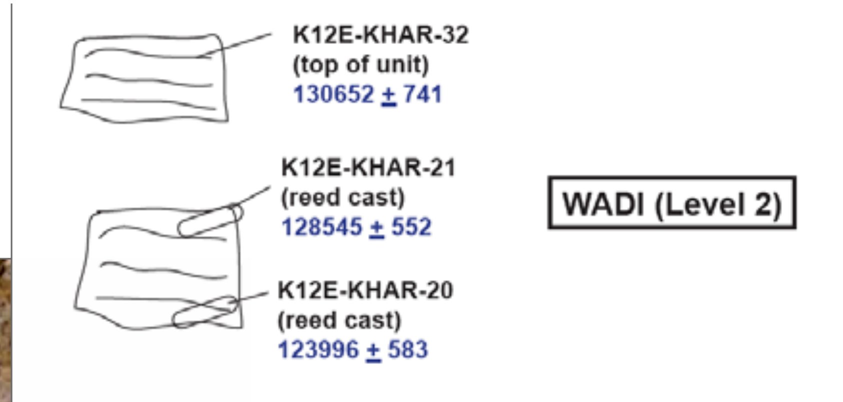

K12E-KHAR-21U (128545 ± 552)

large root cast towards top of Level 2; in spongy, porous travertine

Refuf Pass-2

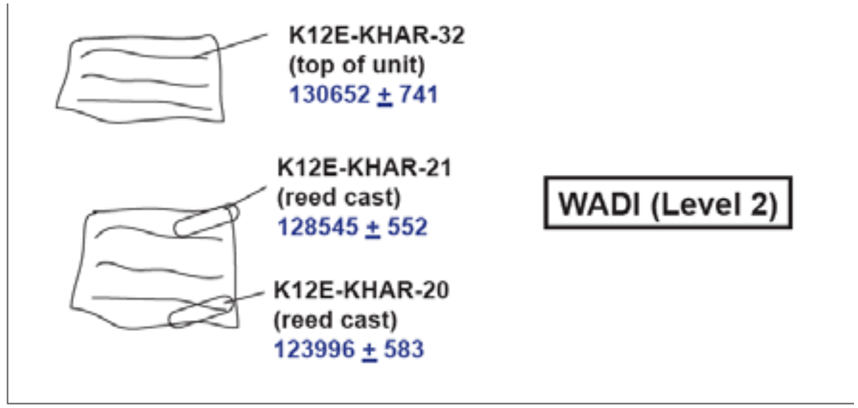

K12E-KHAR-32U (130652 ± 741)
top of Level 2

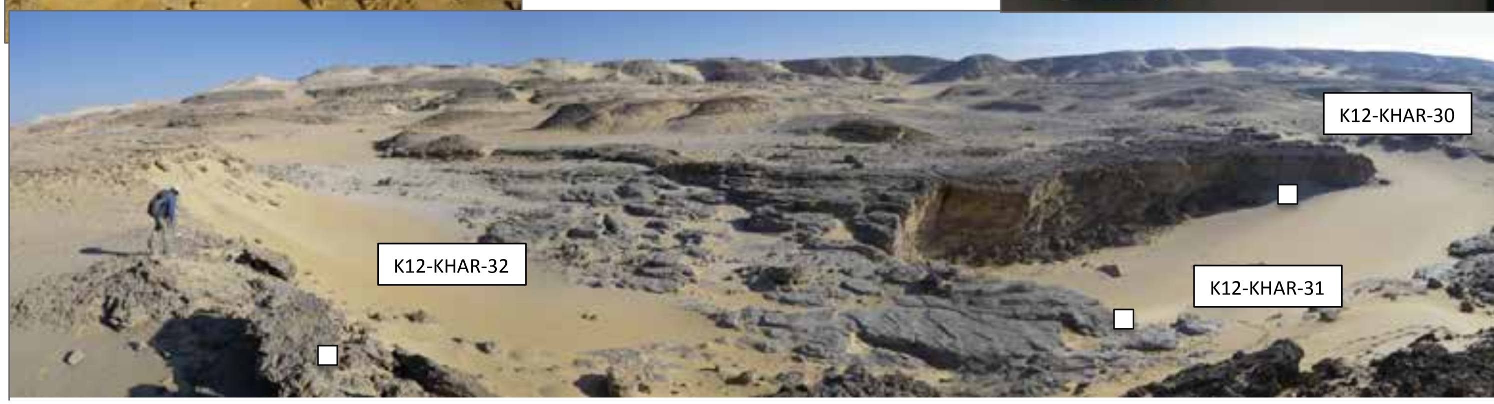

Refuf Pass-3

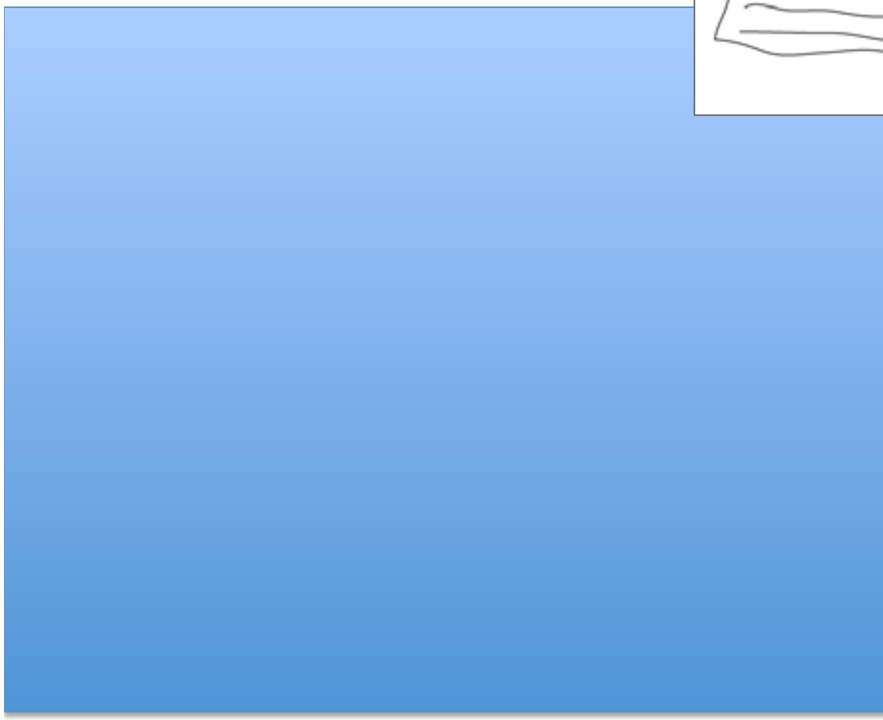

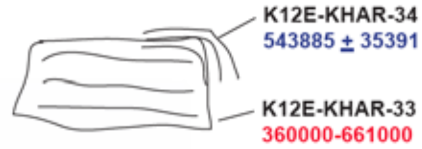

PLATEAU (Level 3)

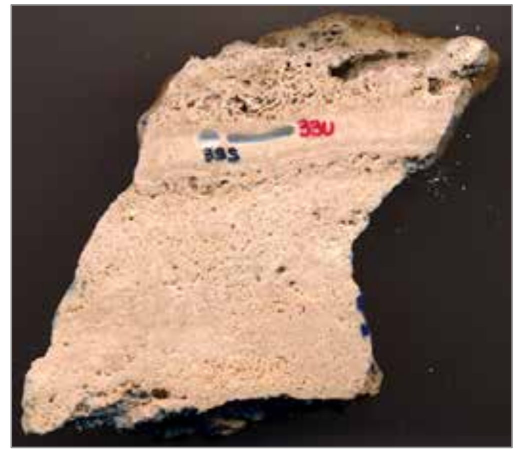

K12E-KHAR-33U (429895 ± 9565)
base of Level 3

Refuf Pass-3

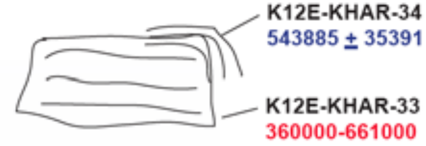

PLATEAU (Level 3)

K12E-KHAR-34U (543885 ± 35391)
Drape at top of level 3

Refuf Pass-4

K12E-KHAR-35U (645793 ± 60676)
base of Level 4; bottom/interior of drape

Refuf Pass-4

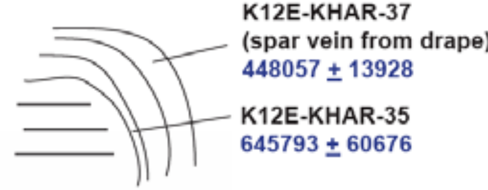

PLATEAU (Level 4)

K12E-KHAR-36U (496495 ± 22947)
root cast in small cave, ~1m from outside of drape

Refuf Pass-4

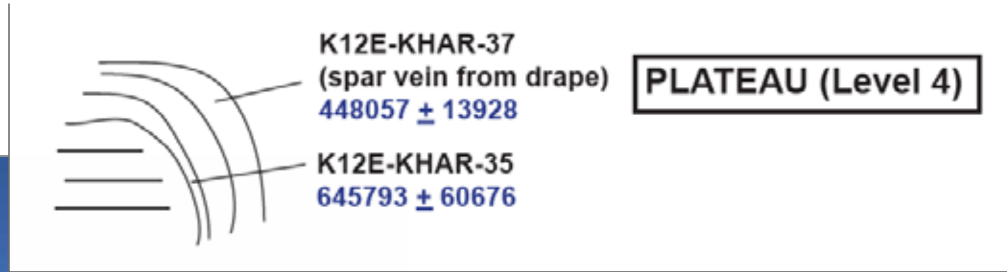

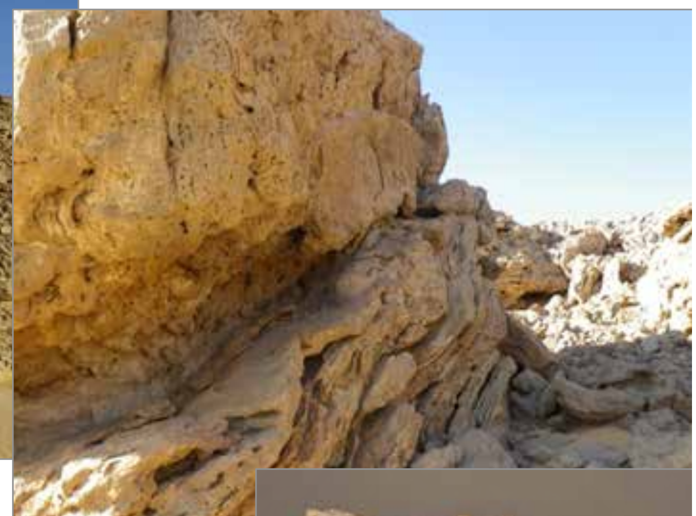

K12E-KHAR-37U (448057 ± 13928)
top of Level 4, exterior/top of drape; sparry vein

Refuf Pass—not dated

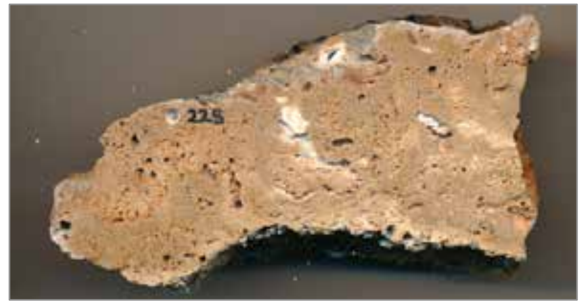

K12E-KHAR-19 (gastropods), 22, 23, 24

Wadi Midauwara

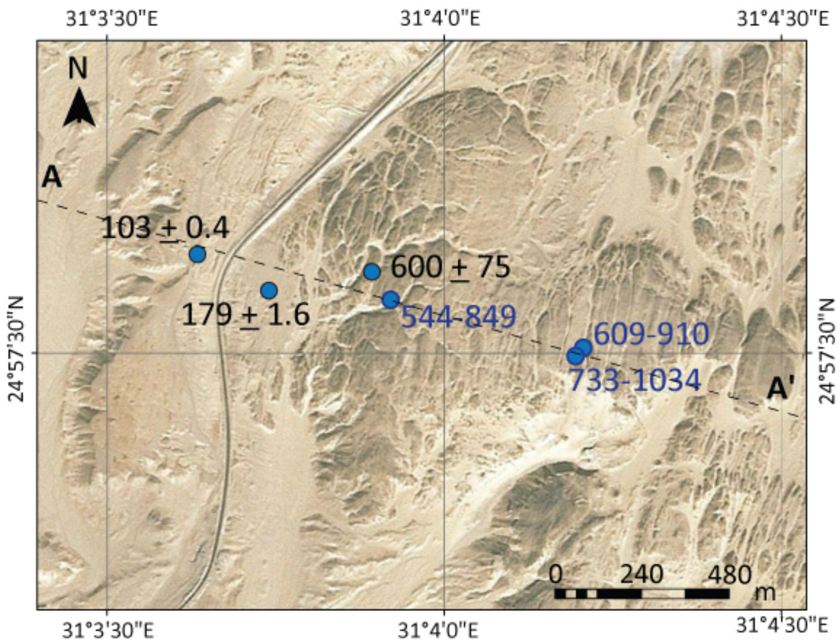

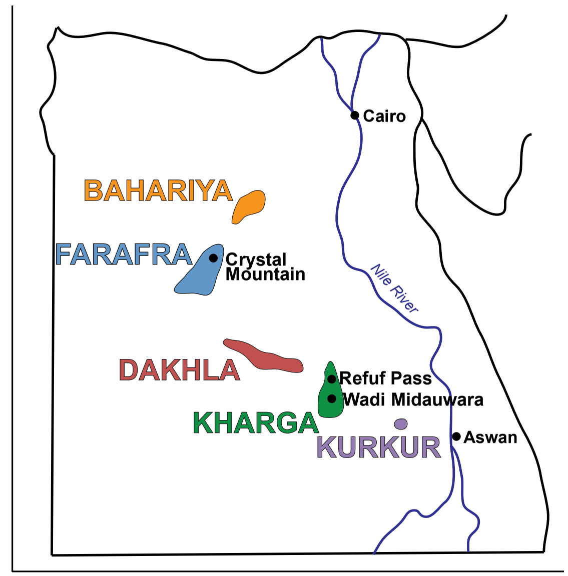

Midauwara-1

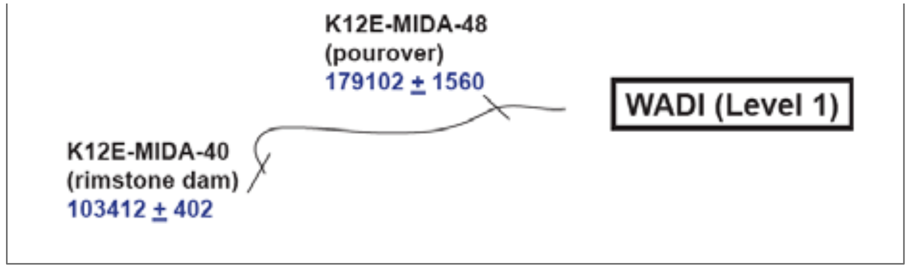

K12E-MIDA-40U (103412 ± 402)
rind from pourover in level 1; youngest travertine?

Midauwara-1

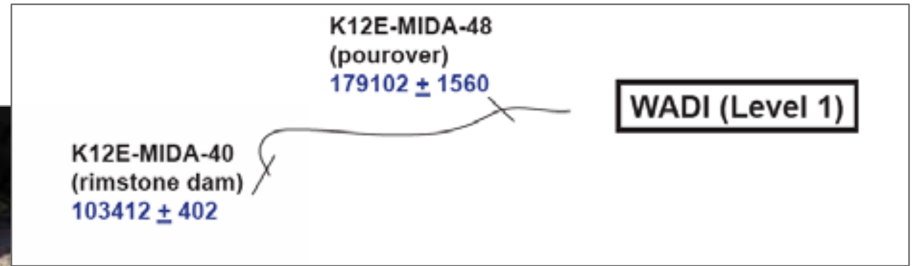

K12E-MIDA-48B (179102 + 1560)
outer bands of laminated rimstone, level 1; top?

K12E-MIDA-48C (158949 + 872)
inner bands of laminated rimstone, level 1; top?

Midauwara-2

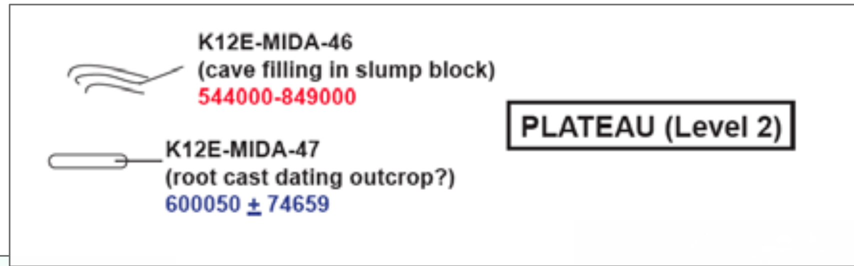

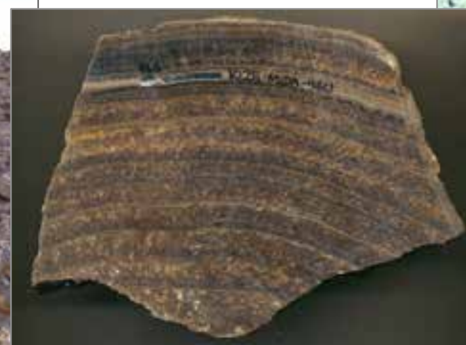

K12E-MIDA-46 (728 ± 120 ka)

Large, well-laminated; probably not in place; bottom of level 2

Midauwara-2

K12E-MIDA-46
(cave filling in slump block)
700794 ± XXX

K12E-MIDA-47
(root cast dating outcrop?)
600050 ± 74659

PLATEAU (Level 2)

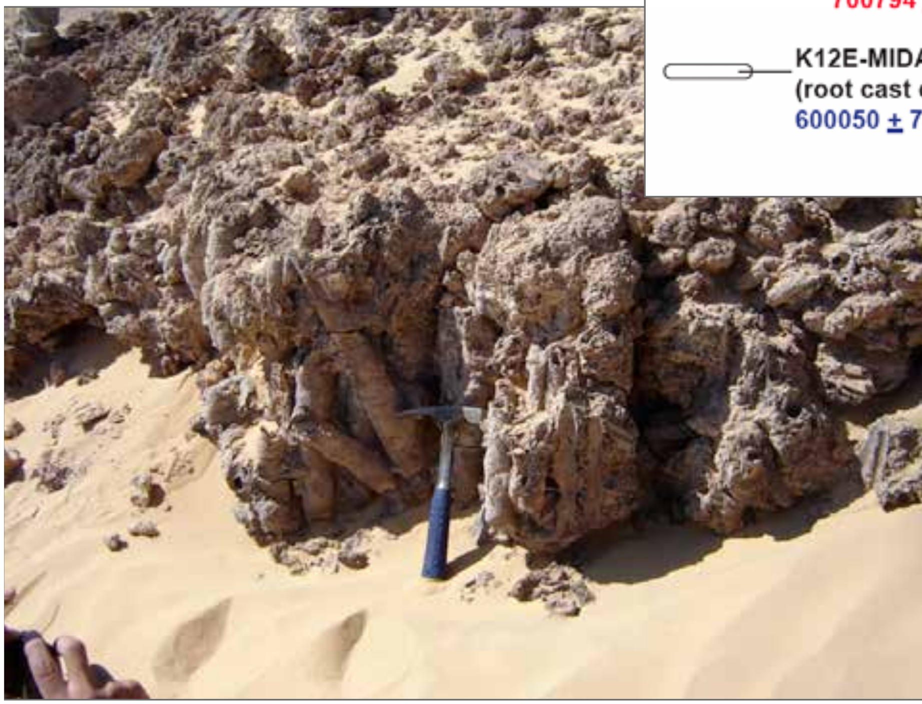

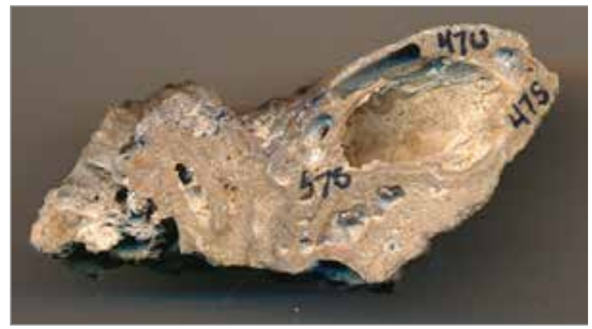

K12E-MIDA-47 (600050 ± 74659)

Root cast (dating outcrop itself?)

Midauwara-2

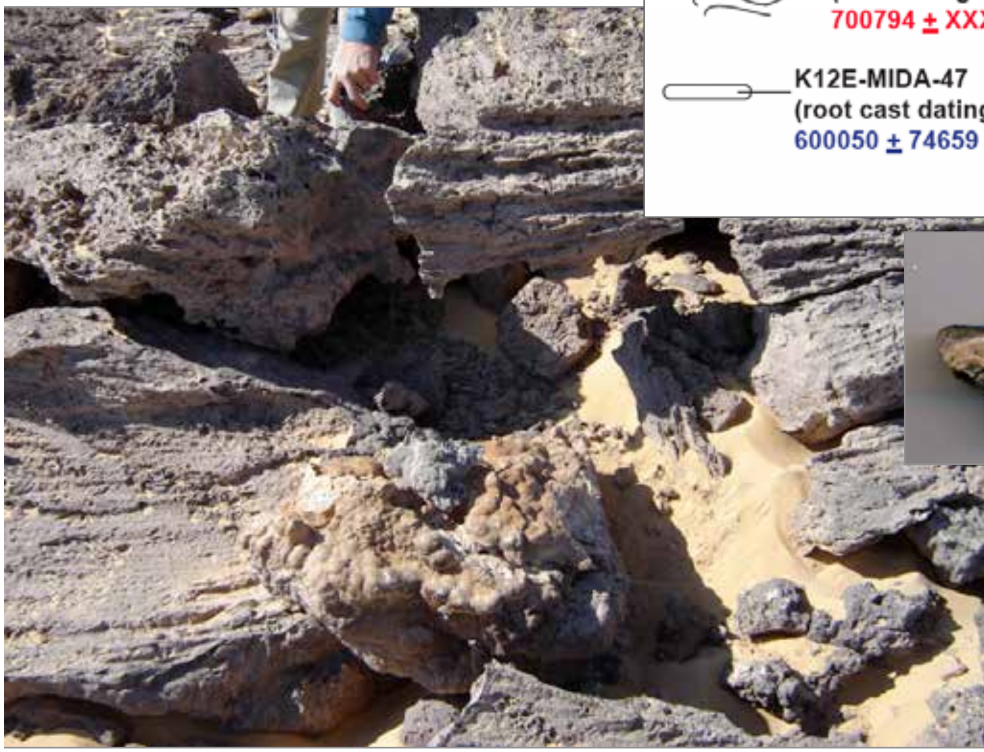

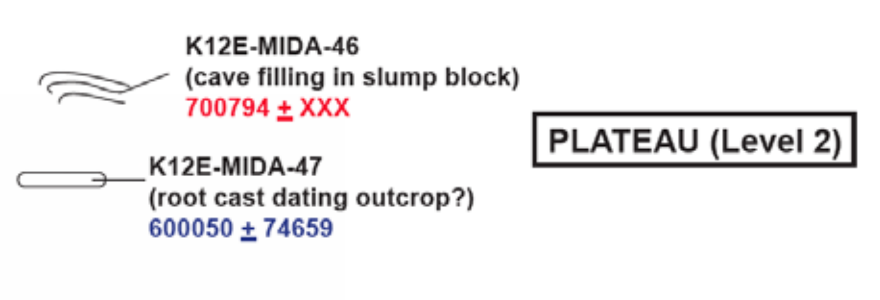

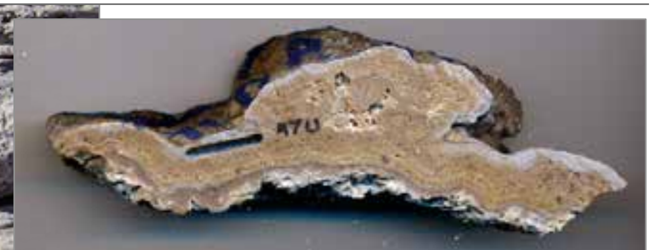

K12E-MIDA-47B (565518 ± 50194)

Botryoidal coating on bottom of shelf; close to 47 (root cast) but younger?

Midauwara-3

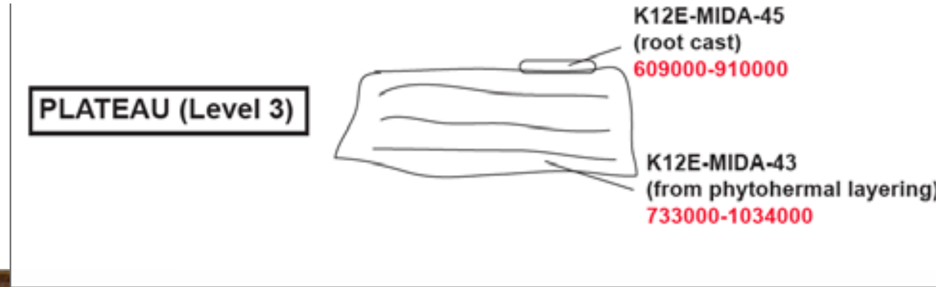

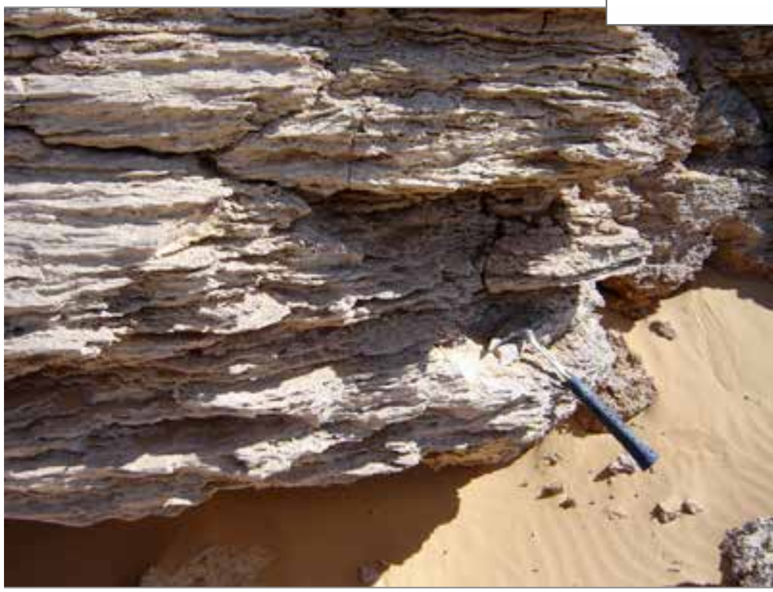

K12E-MIDA-43 (791 ± 120 ka)

From bottom of level 3; mixed phytohermal/flow layering, w/crinkled "mini-dams"

Midauwara-3

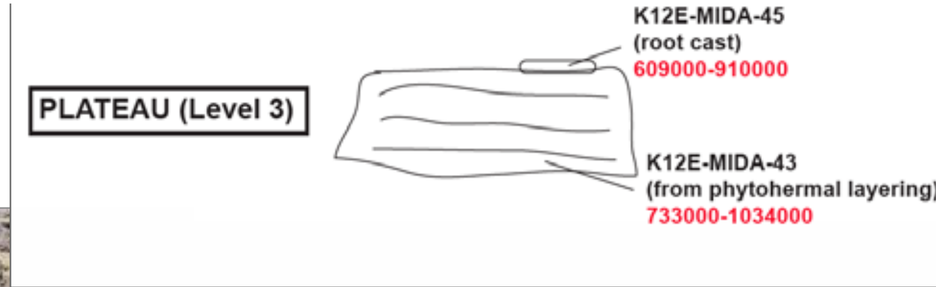

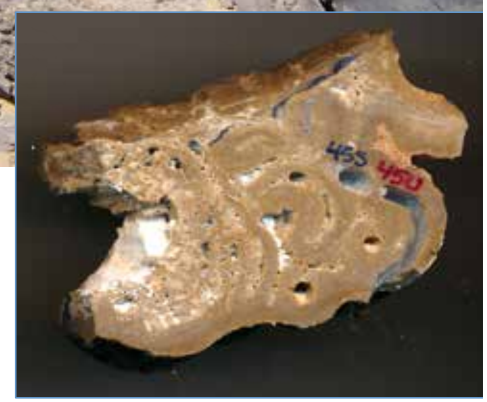

K12E-MIDA-45 (915 ± 120)

finely laminated root casts on pourover feature; top of Level 3

Wadi Midauwara—not dated

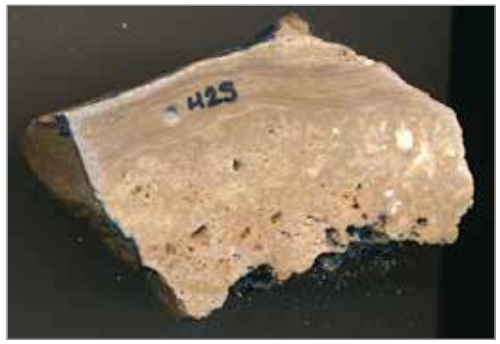

K12E-MIDA-41, 42, 44

Kurkur Oasis

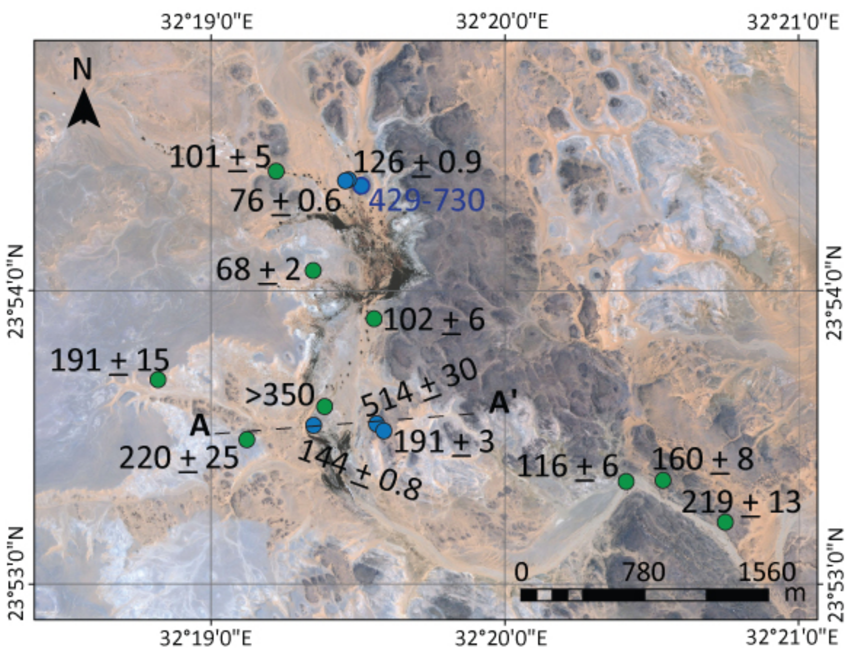

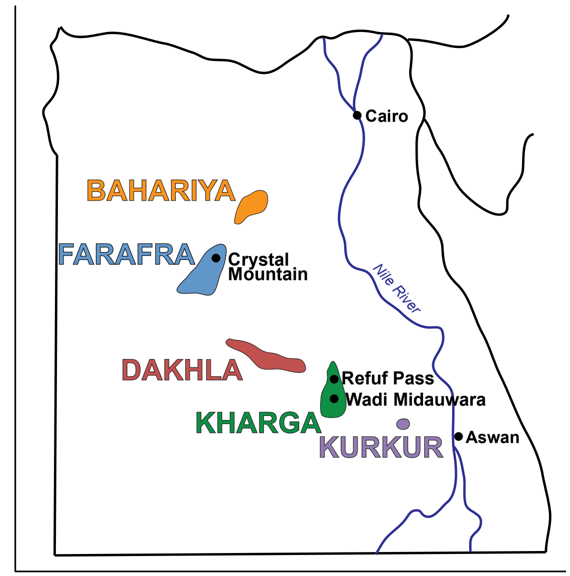

Kurkur-1

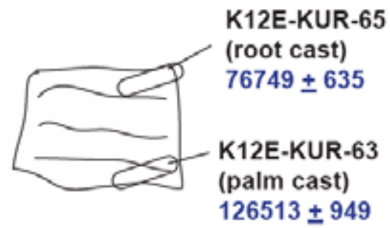

WADI (Level 1)

K12E-KUR-63 (126513 ± 949)
stick cast just above modern wadi level (bottom level 1)

Kurkur-1

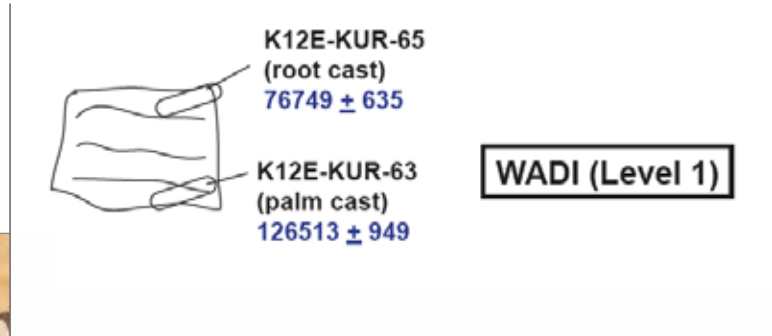

K12E-KUR-65 (76749 ± 635)
Root cast near deposit top, 7.5 m above modern wadi

Kurkur-1

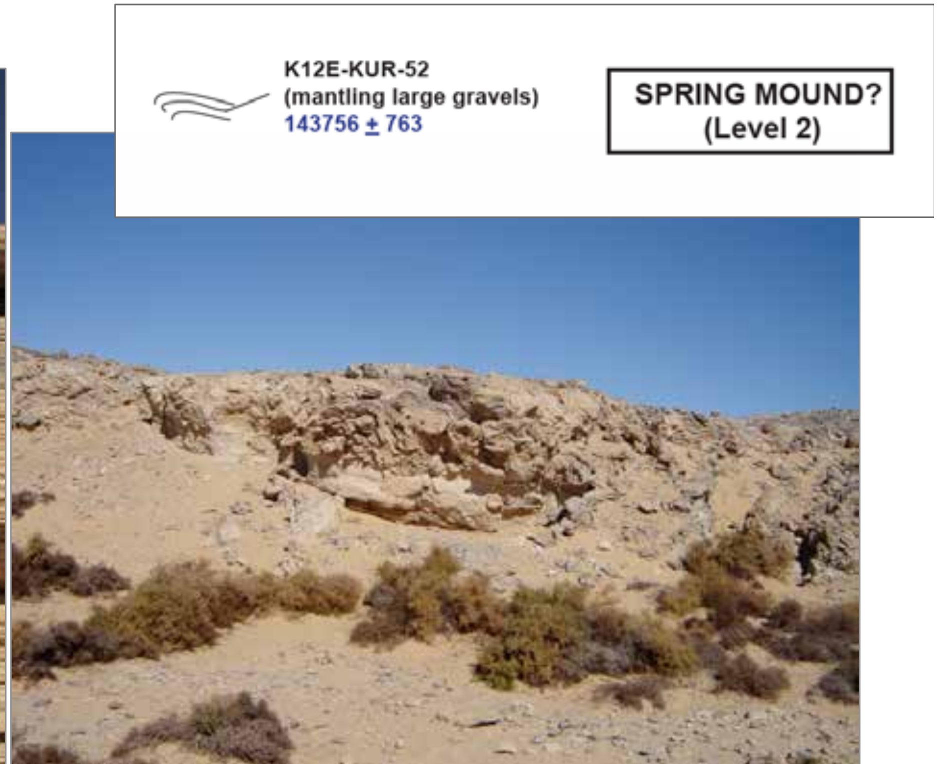

K12E-KUR-52 (143756 ± 763)

Banded rind in mound cementing gravels; spring mound layer?

Kurkur-2

K12E-KUR-58 (245825 ± 2665)
lowest level travertine, at level of modern wadi, atop gravel; big cast among botryoidal drapes on boulders (some transported but many grew in place?; horizontal continuity apparent)

Kurkur-3

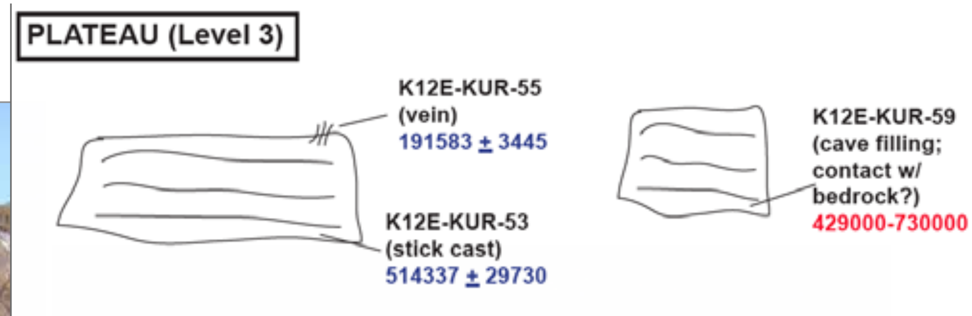

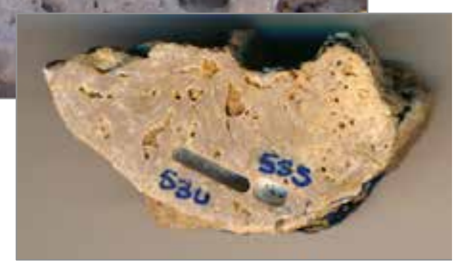

K12E-KUR-53 (514337 ± 29730)

Stick cast from bottom of slumped but intact? Level 3 (non-slumped equivalent 42m above wadi)

Kurkur-3V

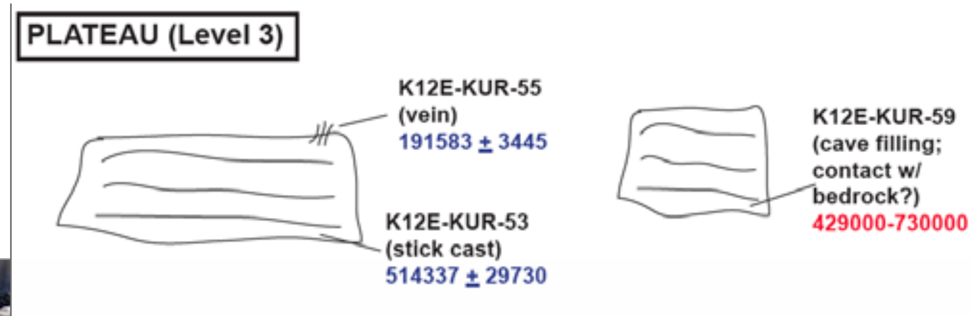

K12E-KUR-55 (191583 ± 3445)
Micrite vein at top of plateau (level 3); culmination of 9m strat section

Kurkur-3V

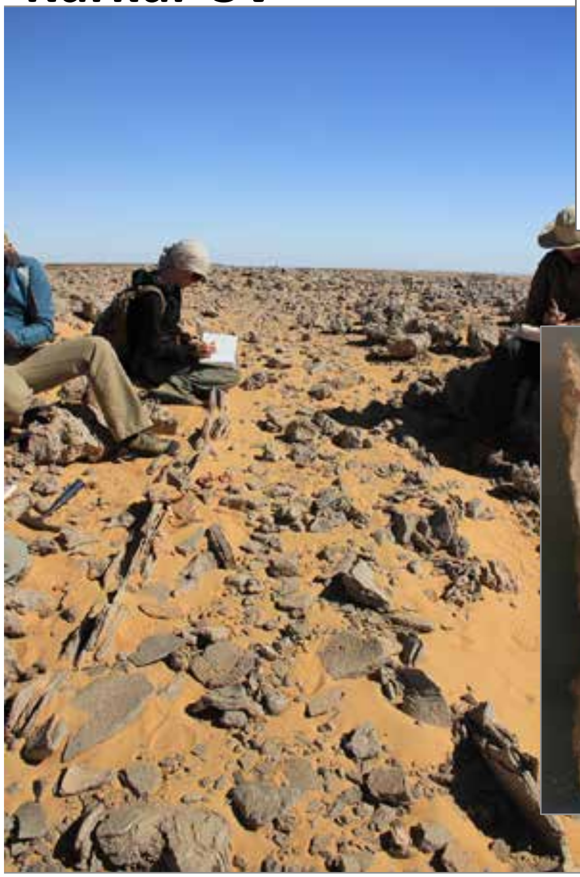

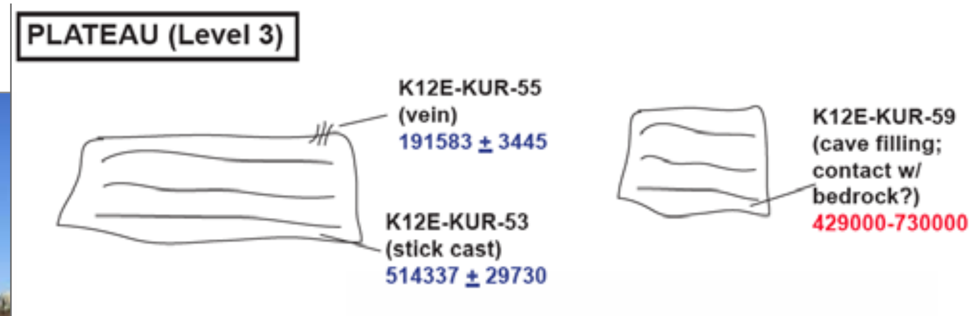

K12E-KUR-56 (145803 ± 894)

At top of plateau (level 3)—fed by vein (55)?; culmination of 9m strat section

Kurkur-3

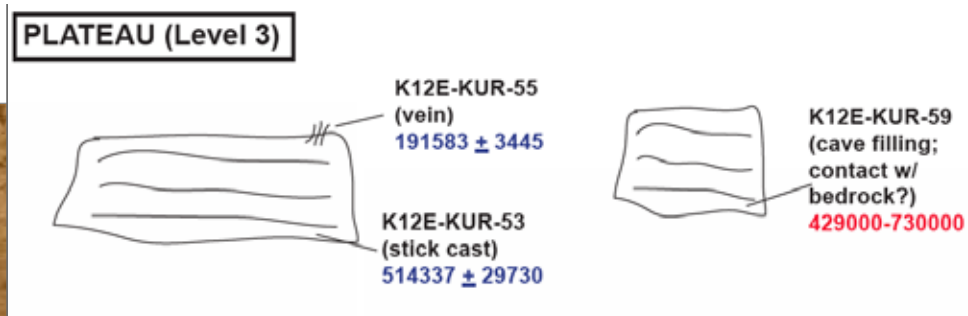

K12E-KUR-59 (610 ± 119 ka)
botryoidal cave filling; at base of plateau (level 3) near contact with bedrock

Kurkur-3

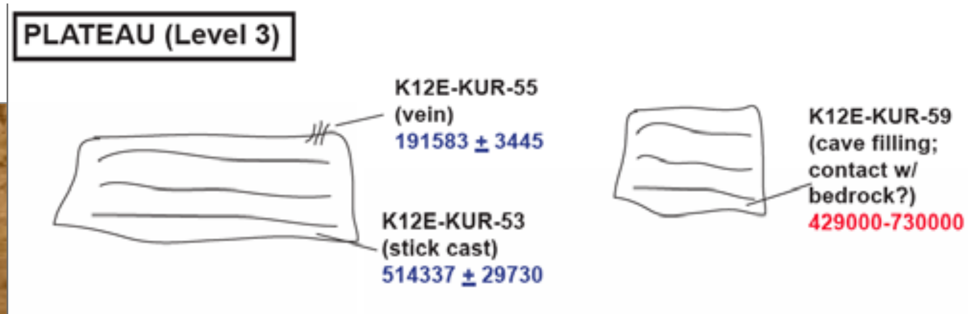

K12E-KUR-60 (844 ± 119 ka)

Micrite ledge/cave filling at base of plateau (level 3) just below 59

Kurkur-3

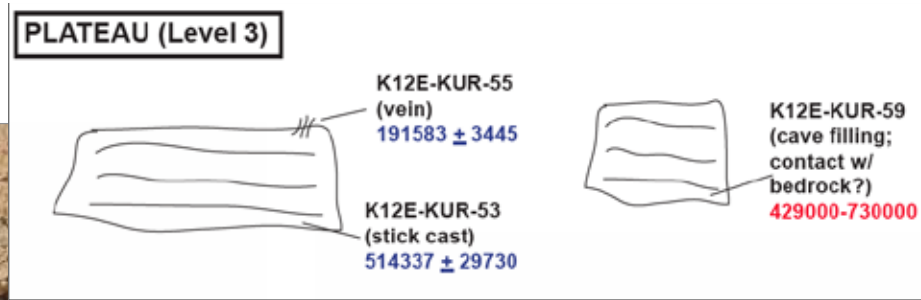

K12E-KUR-62 (1024 ± 119 ka)
stick cast at bottom of small cave w/ good banding (cave filling also collected but not drilled); 21m above wadi

Kurkur Oasis—not dated

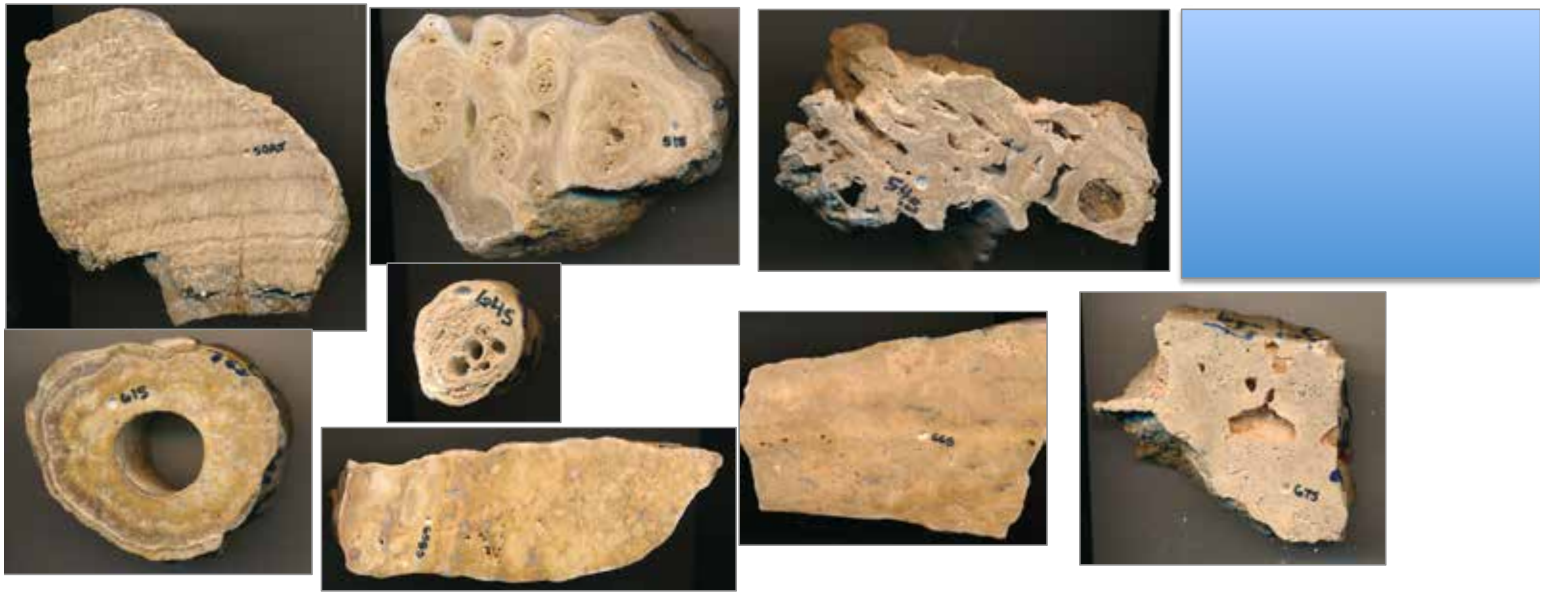

K12E-KUR-50A, 51, 54, 57-missing,
61, 64, 65B, 66, 67, 68, 69

REFERENCES

Adelsberger, K.A., and Smith, J.R., 2010, Paleolandscape and paleoenvironmental interpretation of spring-deposited sediments in Dakhleh Oasis, Western Desert of Egypt: Catena, v. 83, no. 1, p. 7–22, doi: 10.1016/j.catena.2010.06.009.

Almogi-Labin, A., 2011, The paleoclimate of the Eastern Mediterranean during the transition from early to mid Pleistocene (900 to 700ka) based on marine and non-marine records: An integrated overview: Journal of Human Evolution, v. 60, no. 4, p. 428–436, doi: 10.1016/j.jhevol.2010.03.007.

Andersen, M.B., Stirling, C.H., Potter, E.-K., Halliday, A.N., Blake, S.G., McCulloch, M.T., Ayling, B.F., and O'Leary, M., 2008, High-precision U-series measurements of more than 500,000 year old fossil corals: Earth and Planetary Science Letters, v. 265, no. 1-2, p. 229–245, doi: 10.1016/j.epsl.2007.10.010.

Andrews, J.E., 2006, Palaeoclimatic records from stable isotopes in riverine tufas: synthesis and review: Earth-Science Reviews, v. 75, no. 1, p. 85–104, doi: 10.1016/j.earscirev.2005.08.002.

Asmerom, Y., Polyak, V.J., and Burns, S.J., 2010, Variable winter moisture in the southwestern United States linked to rapid glacial climate shifts: Nature Geoscience, v. 3, no. 2, p. 1–4, doi: 10.1038/ngeo754.

Auler, A.S., and Smart, P.L., 2001, Late Quaternary Paleoclimate in Semiarid Northeastern Brazil from U-Series Dating of Travertine and Water-Table Speleothems: Quaternary Research, v. 55, no. 2, p. 159–167, doi: 10.1006/qres.2000.2213.

Bischoff, J.L., and Fitzpatrick, J.A., 1991, U-Series Dating of Impure Carbonates: An Isochron Technique Using Total-Sample Dissolution: Geochimica et Cosmochimica Acta, v. 55, no. 2, p. 543–554, doi: 10.1016/0016-7037(91)90011-S.

Blome, M.W., Cohen, A.S., Tryon, C.A., Brooks, A.S., and Russell, J., 2012, The environmental context for the origins of modern human diversity: A synthesis of regional variability in African climate 150,000-30,000 years ago: Journal of Human Evolution, v. 62, no. 5, p. 563–592, doi: 10.1016/j.jhevol.2012.01.011.

Bosmans, J.H.C., Drijfhout, S.S., Tuenter, E., Lourens, L.J., Hilgen, F.J., and Weber, S.L., 2012, Monsoonal response to mid-holocene orbital forcing in a high resolution GCM: Climate of the Past, v. 8, no. 2, p. 723–740, doi: 10.5194/cp-8-723-2012.

Box, M.R., Krom, M.D., Cliff, R.A., Bar-Matthews, M., Almogi-Labin, A., Ayalon, A., and Paterne, M., 2011, Response of the Nile and its catchment to millennial-scale climatic change since the LGM from Sr isotopes and major elements of East Mediterranean sediments: Quaternary science reviews, v. 30, no. 3-4, p. 431–442, doi: 10.1016/j.quascirev.2010.12.005.

Brook, G.A., Embabi, N.S., Ashour, M.M., Edwards, R.L., Cheng, H., Cowart, J.B., and Dabous, A.A., 2002, Djara Cave in the Western Desert of Egypt: Morphology and evidence of Quaternary climatic change: Cave and Karst Science, v. 29, no. 2, p. 57–66.

Brookes, I.A., 1993, Late Pleistocene basinal sediments, Dakhla Oasis region, Egypt: A non-interglacial pluvial: Geoscientific research in northwest Africa,, p. 627–633.

Carucci, V., Petitta, M., and Aravena, R., 2012, Interaction between shallow and deep aquifers in the Tivoli Plain (Central Italy) enhanced by groundwater extraction: A multi-isotope approach and geochemical modeling: Applied Geochemistry, v. 27, no. 1, p. 266–280, doi: 10.1016/j.apgeochem.2011.11.007.

Caton-Thompson, G., and Gardner, E.W., 1932, The prehistoric geography of Kharga Oasis: The Geographical Journal.

Charisi, S.D., and Schmitz, B., 1995, Stable (δ13C, δ18O) and strontium (87Sr/86Sr) isotopes through the Paleocene at Gebel Aweina, eastern Tethyan region: Palaeogeography, Palaeoclimatology, Palaeoecology, v. 116, no. 1, p. 103–129.

Cheng, H., Edwards, R.L., Hoff, J., Gallup, C.D., Richards, D.A., and Asmerom, Y., 2000, The half-lives of uranium-234 and thorium-230: Chemical Geology, v. 169, no. 1, p. 17–33.

Colleoni, F., Masina, S., Negri, A., and Marzocchi, A., 2012, Plio–Pleistocene high–low latitude climate interplay: A Mediterranean point of view: Earth and Planetary Science Letters, v. 319-320, p. 35–44, doi: 10.1016/j.epsl.2011.12.020.

Crombie, M.K., Arvidson, R.E., Sturchio, N.C., Alfy, El, Z., and Zeid, K.A., 1997, Age and isotopic constraints on Pleistocene pluvial episodes in the Western Desert, Egypt: Palaeogeography, Palaeoclimatology, Palaeoecology, v. 130, no. 1, p. 337–355.

Crossey, L.J., Karlstrom, K.E., Newell, D.L., Kooser, A., and Tafoya, A., 2011, The La Madera travertines, Rio Ojo Caliente, northern New Mexico: investigating the linked system of CO2-rich springs and travertines as neotectonic and paleoclimate indicators: Geology of the Tusas Mountains and Ojo Caliente Area, New Mexico Geological Society, Guidebook, v. 62, p. 301–316.

Crossey, L.J., Karlstrom, K.E., Springer, A.E., Newell, D., Hilton, D.R., and Fischer, T., 2009, Degassing of mantle-derived CO2 and He from springs in the southern Colorado Plateau region--Neotectonic connections and implications for groundwater systems: Geological Society of America Bulletin, v. 121, no. 7-8, p. 1034–1053, doi: 10.1130/B26394.1.

Dabous, A.A., and Osmond, J.K., 2000, U/Th isotopic study of speleothems from the

Wadi Sannur Cavern, Eastern Desert of Egypt: Carbonates and Evaporites, v. 15, no. 1, p. 1–6.

Dabous, A.A., and Osmond, J.K., 2001, Uranium isotopic study of artesian and pluvial contributions to the Nubian Aquifer, Western Desert, Egypt: Journal of Hydrology.

Dabous, A.A., Osmond, J.K., and Dawood, Y.H., 2002, Uranium/Thorium isotope evidence for ground-water history in the Eastern Desert of Egypt: Journal of Arid Environments, v. 50, no. 2, p. 343–357, doi: 10.1006/jare.2001.0861.

Darling, W.G., Bath, A.H., Gibson, J.J., and Rozanski, K., 2005, Isotopes in water (M. J. Leng, Ed.): Isotopes in Palaeoenvironmental Research,, p. 1–66.

deMenocal, P.B., 2004, African climate change and faunal evolution during the Pliocene–Pleistocene: Earth and Planetary Science Letters, v. 220, no. 1-2, p. 3–24, doi: 10.1016/S0012-821X(04)00003-2.

Demény, A., Kele, S., and Siklósy, Z., 2010, Empirical equations for the temperature dependence of calcite-water oxygen isotope fractionation from 10 to 70°C: Rapid Communications in Mass Spectrometry, v. 24, no. 24, p. 3521–3526, doi: 10.1002/rcm.4799.

Denison, R.E., Koepnick, R.B., Fletcher, A., Dahl, D.A., and Baker, M.C., 1993, Reevaluation of early Oligocene, Eocene, and Paleocene seawater strontium isotope ratios using outcrop samples from the US Gulf Coast: Paleoceanography, v. 8, no. 1, p. 101–126.

Dogramaci, S.S., and Herczeg, A.L., 2002, Strontium and carbon isotope constraints on carbonate-solution interactions and inter-aquifer mixing in groundwaters of the semi-arid Murray Basin, Australia: Journal of Hydrology, v. 262, no. 1, p. 50–67.

Edwards, R.L., Gallup, C.D., and Cheng, H., 2003, Uranium-series dating of marine and lacustrine carbonates: Reviews in Mineralogy and Geochemistry, v. 52, no. 1, p. 363–405.

Emeis, K.-C., Sakamoto, T., Wehausen, R., and Brumsack, H.-J., 2000, The sapropel record of the eastern Mediterranean Sea — results of Ocean Drilling Program Leg 160: Palaeogeography, Palaeoclimatology, Palaeoecology, v. 158, no. 3-4, p. 371–395, doi: 10.1016/S0031-0182(00)00059-6.

Emeis, K.-C., Schulz, H., Struck, U., Rossignol-Strick, M., Erlenkeuser, H., Howell, M.W., Kroon, D., Mackensen, A., Ishizuka, S., and Oba, T., 2003, Eastern Mediterranean surface water temperatures and δ18O composition during deposition of sapropels in the late Quaternary: Paleoceanography, v. 18, no. 1, p. 1005, doi: doi:10.1029/2000PA000617.

Ford, T.D., and Pedley, H.M., 1996, A review of tufa and travertine deposits of the world:

Earth-Science Reviews, v. 41, no. 3, p. 117–175.

Hermina, M., 1990, The surroundings of Kharga, Dakhla, and Farafra oases, *in* The geology of egypt.

Hesse, K.H., Hissene, A., Kheir, O., and Schnäcker, E., 1987, Hydrogeological investigations in the Nubian Aquifer System, Eastern Sahara: Berliner Geowiss Abh A.

Holzkamper, S., 2004, Dating and Interpretation of Secondary Carbonate Deposits from the Last Interglacial: 1 p.

Kieniewicz, J.M., and Smith, J.R., 2007, Hydrologic and climatic implications of stable isotope and minor element analyses of authigenic calcite silts and gastropod shells from a mid-Pleistocene pluvial lake, Western Desert, Egypt: Quaternary Research, v. 68, no. 3, p. 431–444, doi: 10.1016/j.yqres.2007.07.010.

Kieniewicz, J.M., and Smith, J.R., 2009, Paleoenvironmental reconstruction and water balance of a mid-Pleistocene pluvial lake, Dakhleh Oasis, Egypt: Geological Society of America Bulletin, v. 121, no. 7-8, p. 1154–1171.

Kleindienst, M.R., Churcher, C.S., McDonald, M.M., and Schwarcz, H.P., 1999, Geography, geology, geochronology and geoarchaeology of the Dakhleh Oasis region: An interim report: OXBOW MONOGRAPH,, p. 1–54.

Kleindienst, M.R., Schwarcz, H.P., Nicoll, K., Churcher, C.S., Frizano, J., Giegengack, R., and Wiseman, M.F., 2008, Water in the desert: First report on Uranium-series dating of Caton-Thompson's and Gardner's "classic" Pleistocene sequence at Refuf Pass, Kharga Oasis:, p. 25–54.

Larrasoaña, J.C., Roberts, A.P., Rohling, E.J., Winklhofer, M., and Wehausen, R., 2003, Three million years of monsoon variability over the northern Sahara: Climate Dynamics, v. 21, no. 7-8, p. 689–698.

Li, H.-C., Xu, X.-M., Ku, T.-L., You, C.-F., Buchheim, H.P., and Peters, R., 2008a, Isotopic and geochemical evidence of palaeoclimate changes in Salton Basin, California, during the past 20 kyr: 1. δ18O and δ13C records in lake tufa deposits: Palaeogeography, Palaeoclimatology, Palaeoecology, v. 259, no. 2-3, p. 182–197, doi: 10.1016/j.palaeo.2007.10.006.

Li, H.-C., You, C.-F., Ku, T.-L., Xu, X.-M., Buchheim, H.P., Wan, N.-J., Wang, R.-M., and Shen, M.-L., 2008b, Isotopic and geochemical evidence of palaeoclimate changes in Salton Basin, California, during the past 20 kyr: 2. 87Sr/86Sr ratio in lake tufa as an indicator of connection between Colorado River and Salton Basin: Palaeogeography, Palaeoclimatology, Palaeoecology, v. 259, no. 2-3, p. 198–212, doi: 10.1016/j.palaeo.2007.10.007.

Lourens, L.J., Wehausen, R., and Brumsack, H.J., 2001, Geological constraints on tidal dissipation and dynamical ellipticity of the Earth over the past three million years: Nature, v. 409, no. 6823, p. 1029–1033.

Luo, W., Arvidson, R.E., Sultan, M., Becker, R., Crombie, M.K., Sturchio, N., and Alfy, El, Z., 1997, Ground-water sapping processes, western desert, Egypt: Geological Society of America Bulletin, v. 109, no. 1, p. 43–62.

McCauley, J.F., Schaber, G.G., Breed, C.S., Grolier, M.J., Haynes, C.V., Issawi, B., Elachi, C., and Blom, R., 1982, Subsurface valleys and geoarcheology of the eastern Sahara revealed by shuttle radar: Science, v. 218, no. 4576, p. 1004–1020.

Neymark, L.A., 2011, Potential effects of alpha-recoil on uranium-series dating of calcrete: Chemical Geology, v. 282, no. 3-4, p. 98–112, doi: 10.1016/j.chemgeo.2011.01.013.

Osinski, G.R., Schwarcz, H.P., Smith, J.R., Kleindienst, M.R., Haldemann, A.F.C., and Churcher, C.S., 2007, Evidence for a ~200–100 ka meteorite impact in the Western Desert of Egypt: Earth and Planetary Science Letters, v. 253, no. 3-4, p. 378–388, doi: 10.1016/j.epsl.2006.10.039.

Osmond, J.K., and Dabous, A.A., 2004, Timing and intensity of groundwater movement during Egyptian Sahara pluvial periods by U-series analysis of secondary U in ores and carbonates: Quaternary Research, v. 61, no. 1, p. 85–94, doi: 10.1016/j.yqres.2003.09.004.

Osmond, J.K., Dabous, A.A., and Dawood, Y.H., 1999, U series age and origin of two secondary uranium deposits, central Eastern Desert, Egypt: Economic Geology and the Bulletin of the Society of Economic Geologists, v. 94, no. 2, p. 273–279, doi: 10.2113/gsecongeo.94.2.273.

Patterson, L.J., Sturchio, N.C., Kennedy, B.M., van Soest, M.C., Sultan, M., Lu, Z.-T., Lehmann, B., Purtschert, R., Alfy, El, Z., Kaliouby, El, B., Dawood, Y., and Abdallah, A., 2005, Cosmogenic, radiogenic, and stable isotopic constraints on groundwater residence time in the Nubian Aquifer, Western Desert of Egypt: Geochemistry, Geophysics, Geosystems, v. 6, no. 1, p. n/a–n/a, doi: 10.1029/2004GC000779.

Pentecost, A., 2005, Travertine: Springer-Verlag, Berlin.

Placzek, C., Patchett, P.J., Quade, J., and Wagner, J.D., 2006, Strategies for successful U-Th dating of paleolake carbonates: An example from the Bolivian Altiplano: Geochemistry, Geophysics, Geosystems, v. 7, no. 5.

Railsback, L.B., Dabous, A.A., Osmond, J.K., and Fleisher, C.J., 2002, Petrographic and geochemical screening of speleothems for U-series dating: an example from recrystallized speleothems from Wadi Sannur Cavern, Egypt: Journal of Cave and Karst Studies, v. 64, no. 2, p. 108–116.

Rohling, E.J., Cane, T.R., Cooke, S., Sprovieri, M., Bouloubassi, I., Emeis, K.-C., Schiebel, R., Kroon, D., Jorissen, F.J., and Lorre, A., 2002, African monsoon variability during the previous interglacial maximum: Earth and Planetary Science Letters, v. 202, no. 1, p. 61–75.

Romanek, C.S., Grossman, E.L., and Morse, J.W., 1992, Carbon isotopic fractionation in synthetic aragonite and calcite: Effects of temperature and precipitation rate: Geochimica et Cosmochimica Acta, v. 56, no. 1, p. 419–430, doi: 10.1016/0016-7037(92)90142-6.

Rossignol-Strick, M., 1983, African monsoons, an immediate climate response to orbital insolation: Nature, v. 304, no. 5921, p. 46–49.

Rossignol-Strick, M., 1985, Mediterranean Quaternary sapropels, an immediate response of the African monsoon to variation of insolation: Palaeogeography, Palaeoclimatology, Palaeoecology, v. 49, no. 3-4, p. 237–263, doi: 10.1016/0031-0182(85)90056-2.

Salem, O., and Pallas, P., 2004, The Nubian Sandstone Aquifer System (NSAS).

Smith, J.R., 2012, Spatial and temporal variation in the nature of Pleistocene pluvial phase environments across North Africa: Modern Origins,, doi: 10.1007/978-94-007-2929-2_3.

Smith, J.R., and Kieniewicz, J.M., 2006, Reconstructing Pleistocene pluvial phase environments, Western Desert, Egypt, from the geochemistry of authigenic water-lain deposits: Geochimica et …, v. 70, no. 18, p. A599, doi: 10.1016/j.gca.2006.06.1113.

Smith, J.R., Giegengack, R., and Schwarcz, H.P., 2004a, Constraints on Pleistocene pluvial climates through stable-isotope analysis of fossil-spring tufas and associated gastropods, Kharga Oasis, Egypt: Palaeogeography, Palaeoclimatology, Palaeoecology, v. 206, no. 1-2, p. 157–175, doi: 10.1016/j.palaeo.2004.01.021.

Smith, J.R., Giegengack, R., Schwarcz, H.P., McDonald, M., Kleindienst, M.R., Hawkins, A.L., and Churcher, C.S., 2004b, A reconstruction of Quaternary pluvial environments and human occupations using stratigraphy and geochronology of fossil-spring tufas, Kharga Oasis, Egypt: Geoarchaeology, v. 19, no. 5, p. 407–439, doi: 10.1002/gea.20004.

Smith, J.R., Hawkins, A.L., Asmerom, Y., Polyak, V., and Giegengack, R., 2007, New age constraints on the Middle Stone Age occupations of Kharga Oasis, Western Desert, Egypt: Journal of Human Evolution, v. 52, no. 6, p. 690–701, doi: 10.1016/j.jhevol.2007.01.004.

Sturchio, N.C., 2004, One million year old groundwater in the Sahara revealed by krypton-81 and chlorine-36: Geophysical Research Letters, v. 31, no. 5, p. L05503, doi: 10.1029/2003GL019234.

Sultan, M., Sturchio, N., Hassan, F.A., Hamdan, M.A.R., Mahmood, A.M., Alfy, Z.E., and Stein, T., 1997, Precipitation source inferred from stable isotopic composition of Pleistocene groundwater and carbonate deposits in the Western desert of Egypt: Quaternary Research, v. 48, no. 1, p. 29–37.

Swanberg, C.A., Morgan, P., and Boulos, F.K., 1983, Geothermal potential of Egypt: Tectonophysics, v. 96, no. 1, p. 77–94.

Szabo, B.J., Haynes, C.V., Jr, and Maxwell, T.A., 1995, Ages of Quaternary pluvial episodes determined by uranium-series and radiocarbon dating of lacustrine deposits of Eastern Sahara: Palaeogeography, Palaeoclimatology, Palaeoecology, v. 113, no. 2, p. 227–242.

Szabo, B.J., McHugh, W.P., Schaber, G.G., and Haynes, C.V., 1989, Uranium-series dated authigenic carbonates and Acheulian sites in southern Egypt: Science,, doi: 10.1126/science.243.4894.1053.

Talbot, M.R., 1990, A review of the palaeohydrological interpretation of carbon and oxygen isotopic ratios in primary lacustrine carbonates: Chemical Geology: Isotope Geoscience Section, v. 80, no. 4, p. 261–279.

Thorweihe, U., 1990, Nubian Aquifer system, *in* The geology of egypt.

Trauth, M.H., Larrasoaña, J.C., and Mudelsee, M., 2009, Trends, rhythms and events in Plio-Pleistocene African climate: Quaternary science reviews, v. 28, no. 5-6, p. 399–411, doi: 10.1016/j.quascirev.2008.11.003.

Tuenter, E., Weber, S.L., Hilgen, F.J., and Lourens, L.J., 2003, The response of the African summer monsoon to remote and local forcing due to precession and obliquity: Global and Planetary Change, v. 36, no. 4, p. 219–235, doi: 10.1016/S0921-8181(02)00196-0.

Tzedakis, P.C., 2007, Seven ambiguities in the Mediterranean palaeoenvironmental narrative: Quaternary science reviews, v. 26, no. 17-18, p. 2042–2066, doi: 10.1016/j.quascirev.2007.03.014.

White, A.F., Peterson, M.L., Wollenberg, H., and Flexser, S., 1990, Sources and fractionation processes influencing the isotopic distribution of H, O and C in the Long Valley hydrothermal system, California, U.S.A.: Applied Geochemistry, v. 5, no. 5-6, p. 571–585, doi: 10.1016/0883-2927(90)90057-C.

Zhang, T., Zhang, M., Bai, B., Wang, X., and Li, L., 2008, Origin and accumulation of carbon dioxide in the Huanghua depression, Bohai Bay Basin, China: AAPG Bulletin, v. 92, no. 3, p. 341–358, doi: 10.1306/10230706141.